UNIVERSIDADE FEDERAL DO CEARÁ
CENTRO DE TECNOLOGIA
DEPARTAMENTO DE ENGENHARIA DE TELEINFORMÁTICA
PROGRAMA DE PÓS-GRADUAÇÃO EM ENGENHARIA DE TELEINFORMÁTICA

SAMUEL TUMELERO VALDUGA

TRANSCEIVER DESIGN FOR MASSIVE MIMO SYSTEMS: APPROACHES BASED ON MATRIX COMPLETION, BEAM SELECTION AND RANDOM PILOTS

FORTALEZA
2018

SAMUEL TUMELERO VALDUGA

TRANSCEIVER DESIGN FOR MASSIVE MIMO SYSTEMS: APPROACHES BASED ON MATRIX COMPLETION, BEAM SELECTION AND RANDOM PILOTS

Tese apresentada ao Curso de Doutorado em Engenharia de Teleinformática da Universidade Federal do Ceará, como parte dos requisitos para obtenção do Título de Doutor em Engenharia de Teleinformática. Área de concentração: Sinais e Sistemas

Orientador: Prof. Dr. André Lima Férrer de Almeida

Coorientador: Prof. Dr. Luc Deneire

FORTALEZA
2018

Dados Internacionais de Catalogação na Publicação
Universidade Federal do Ceará
Biblioteca Universitária
Gerada automaticamente pelo módulo Catalog, mediante os dados fornecidos pelo(a) autor(a)

V237t Valduga, Samuel Tumelero.
Transceiver Design for Massive MIMO Systems: Approaches Based on Matrix Completion, Beam Selection and Random Pilots / Samuel Tumelero Valduga. – 2018.
111 f. : il. color.

Tese (doutorado) – Universidade Federal do Ceará, Centro de Tecnologia, Programa de Pós-Graduação em Engenharia de Teleinformática, Fortaleza, 2018.
Orientação: Prof. Dr. André Lima Férrer de Almeida.

1. Wireless Communications . 2. Massive MIMO. 3. Matrix Completion. 4. Beamforming. 5. Pilot Contamination. I. Título.

CDD 621.38

SAMUEL TUMELERO VALDUGA

TRANSCEIVER DESIGN FOR MASSIVE MIMO SYSTEMS: APPROACHES BASED ON MATRIX COMPLETION, BEAM SELECTION AND RANDOM PILOTS

Presented Thesis for the Post-graduate Program in Teleinformatics Engineering of Federal University of Ceará as a partial requisite to obtain the Ph.D. degree in Teleinformatics Engineering.

Approved at: 21-02-2018.

EXAMINATION BOARD

Prof. Dr. André Lima Férrer de Almeida (Orientador)
Universidade Federal do Ceará

Prof. Dr. Luc Deneire (Coorientador)
Universidade Côte d'Azur

Prof. Dr. Tarcisio Ferreira Maciel
Universidade Federal do Ceará

Prof. Dr. João César Moura Mota
Universidade Federal do Ceará

Prof. Dr. Gustavo Fraidenraich
Universidade de Campinas

Prof. Dr. Richard Demo
Universidade Federal do Paraná

To my family, my fiancée, all professors, colleagues, friends, and all whose taught me essential lessons for achieving this dream.

AGRADECIMENTOS

Primeiramente eu gostaria de agradecer aos meus pais, Antônio e Izabete, pelo suporte, motivação, por acreditarem sempre em mim, por me darem a oportunidade de estudar e nunca me deixarem desistir. Agradeço também as minhas irmãs, Elisa e Samira, pela paciência, suporte, auxílio, carinho e motivação. Não menos importante, gostaria de agradecer a minha noiva Tatiele, pelo auxílio e a participação em todos os momentos dessa jornada, pelo carinho e amor, pelas inúmeras discussões e horas de dedicação, pela paciência e por ter me ajudado a me encontrar.

Gostaria de agradecer meu orientador, Prof. André pela paciência e lições, por me ajudar em tudo que precisei, pela oportunidade de mostrar meu potencial e me trazer para o GTEL. Agradeço ao Prof. João César pela oportunidade de fazer o doutorado sanduíche na França e todas as proveitosas discussões que tivemos. O meu agradecimento também ao Profs. Luc e Ramon que durante todo o ano que estive na França me proporcionaram ensinamentos e afortunadas discussões. Gostaria de agradecer também ao Prof. Tarcisio pela paciência, discussões e auxílio na pesquisa e também ao Gtel pela estrutura que nesse último ano foi minha casa. Aos colegas do Gtel: Igor, Daniel, Carlos, Khaled, Hugo, Rafael, Eduardo, Weskley, Darlan, Laslon, Asim, Lucas, Raphael, Diego, João, Alexandre, Maírton, Marciel, Márcio, Yosbel, Victor, Paulo, Yuri, Carlos Igor, Roberto, Lívia, Isabel, Dona Vera, Thiago, Gadelha pelo auxílio e aos colegas da I3S, Henrique, Fernando, Sérgio, Jean Marie, Leslie, Myriana, Howard, Arnould, Youssef pela ajuda na França.

Principalmente agradeço ao Prof. Renato por me colocar no caminho da pesquisa e me dar suporte em tudo que precisei. Gostaria de agradecer a oportunidade de trabalhar nos projetos da Ericsson, aos Profs. Rodrigo, Charles, Yuri, Walter, pelo auxílio na pesquisa. Finalmente, meu agradecimento a UFC, CAPES e ao CNPq pela estrutura e suporte financeiro durante o período do doutorado.

“Persistence is the shortest path to success!”
(Charles Chaplin)

“Whether you think you can, or you think you can not – you are right!”
(Henry Ford)

“Vai dar certo!”
(Unknown)

RESUMO

A tecnologia usando um número massivo de antenas é a chave para alcançar os potenciais ganhos de capacidade em sistemas 5G. Sistemas MIMO (do inglês, *multiple-input-multiple-output*) massivo consistem na exploração de um grande número de antenas na estação base para servir a vários usuários simultaneamente. Para alcançar a capacidade total do sistemas MIMO, o conhecimento do estado do canal na estação base é desejável. Em sistemas operando em duplexação por divisão em frequência ((FDD) do inglês, *frequency division duplexing*), o problema está na carga do canal de realimentação aumentar linearmente com o número de antenas. Então, para canais de realimentação realistas, o *overhead* para a obtenção de informação de canal total se torna proibitivo devido à quantidade massiva de elementos de antena. Assim, o design eficiente na transmissão depende da informação do estado do canal, e consequentemente a falta da informação completa emerge como um gargalo dos sistemas baseados em FDD com MIMO massivo. Neste contexto, primeiramente desenvolvemos um arcabouço que usa a técnica de compleção matricial para reduzir a carga do canal de realimentação explorando a estrutura da matriz do canal com baixo posto. O arcabouço proposto é avaliado em dois cenários: comunicações sem fio em *backhaul* e com múltiplos usuários. Além disso, mostramos que o erro de reconstrução do canal está relacionado com o número de antenas da estação base e discutimos o desempenho em relação à taxa de erro de bit e à capacidade do canal.

Quando o número de antenas na estações base é moderado, o problema de interferência entre usuários alocados com o mesmos recursos de tempo-frequência precisa ser controlado eficientemente. A formatação de feixes (do inglês, *beamforming*) na transmissão é uma das técnicas para lidar com a interferência entre múltiplos usuários. Assumindo o conhecimento do estado do canal no domínio de feixes em sistemas MIMO massivos esparsos, propomos o projeto de um pré-codificador baseado em máxima razão de transmissão ((MRT) do inglês, *maximum ratio transmission*) que consiste em selecionar e otimizar os feixes dirigidos para os usuários no intuito de maximizar a razão sinal-ruído mais interferência ((SINR) do inglês, *signal-to-interference-plus-noise ratio*) no usuário. Consideramos dois diferentes modelos de canal baseados em variáveis independente e identicamente distribuídas e no modelo estocástico-geométrico, apresentamos heurísticas de baixa complexidade para a seleção de feixes e adaptação de taxa, e mostramos uma solução ótima para este problema. Resultados de simulação mostram que a solução ótima pode alcançar um desempenho melhor que o esquema de *beamforming* com forçagem a zero ((ZFBF) do inglês, *zero-forcing beamforming*). Além disso, comparado com o pré-codificador MRT, as heurísticas propostas melhoram o desempenho do sistema em um cenário esparso, que pode ser o caso nos canais MIMO com ondas milimétricas.

Finalmente, sob a perspectiva de um cenário com múltiplas células, propomos uma técnica de transmissão espaço-temporal de pilotos baseado em seleção aleatória que mitiga ou elimina o efeito da contaminação de pilotos em sistema MIMO massivo. O método espaço-temporal de

transmissão de pilotos utiliza a distribuição de Bernoulli para decidir a transmissão. Apesar da simplicidade do esquema proposto, resultados de simulação mostram que a estimação do canal é melhorada.

Palavras-chave: MIMO Massivo, Compleção Matricial, Realimentação, Múltiplos Usuários, FDD, MRT, ZFBF, Estimação de Canal, Beamforming, MILP, Contaminação Piloto.

ABSTRACT

Massive multiple-input-multiple-output (MIMO) technology is a key to achieve the promised capacity gains in 5G systems. Massive MIMO systems consist in the simultaneous deployment of a large number of antennas in a base station (BS) to serve many user equipments (UEs). For achieving the full potential capacity of MIMO, accurate knowledge of the channel state information (CSI) at the BS is essential. In frequency division duplexing (FDD) systems, the problem is that the channel feedback load grows linearly with the number of antennas. Then, for practical feedback channels, the overhead to obtain full CSI becomes prohibitively large due to the massive number of antenna elements. Thus, relying on CSI to design the downlink transmission emerges as a bottleneck in FDD-based massive MIMO systems. In this context, first, we develop a framework that uses the matrix completion (MC) technique to reduce the uplink feedback channel overhead exploiting the low-rank channel structure of the channel matrix. The proposed framework is evaluated in two application scenarios: wireless backhauling communications and a multi-user (MU) scenario. Furthermore, we show that the decrease of the reconstruction error is related to the number of BS antennas, and discuss the performance in terms of bit error rate (BER) and goodput.

When the number of BS antennas is moderate, an interference problem among UEs allocated for the same time-frequency resource has to be effectively handled. Transmit beamforming is one of the techniques to deal with MU interference. Assuming knowledge of the beamspace channel in a sparse massive MIMO system, we propose a precoder design based on the maximum ratio transmission (MRT) that consists of selecting and optimizing the power of the beams steered to the UEs in order to maximize the signal-to-interference-plus-noise ratio (SINR) at the UE. Considering two different sparse channel models based on independent identically distributed (i.i.d.) and geometric-stochastic beam domain representations, we propose low-complexity heuristics to beam selection and rate adaptation, and discuss the optimal solution for this problem. Simulation results show that our optimal solution can achieve a better performance than the zero-forcing beamforming (ZFBF) scheme. Besides, compared to the linear MRT precoder, the proposed low-complexity heuristics improve the performance of the system in a scenario with channel sparsity, which may be the case in millimeter-wave MIMO channels.

Finally, under a multi-cell perspective, we propose a space-time pilot transmission technique based on the space-time random pilot selection (ST-RPS) that mitigates or eliminates the effect of pilot contamination in massive MIMO system. The space-time pilot transmission method uses Bernoulli distribution to decide the transmission. Despite the conceptual simplicity of the ST-RPS scheme, simulation results show that it improves the channel estimation accuracy.

Keywords: Wireless Communications, Massive MIMO, Matrix Completion, Feedback, Multi-

User, FDD, MRT, ZFBF, Channel Estimation, Beamforming, Mixed Integer Linear Programming, Pilot Contamination.

LIST OF FIGURES

LIST OF TABLES

LIST OF ABBREVIATIONS AND ACRONYMS

3GPP	3rd Generation Partnership Project
AGB	antenna group beamforming
AoA	angle of arrival
AoD	angle of departure
BDMA	beam domain multiple access
BER	bit error rate
BILP	binary integer linear programming
BLER	block error rate
BnB	branch-and-bound
BPSK	binary phase shift keying
BS	base station
CS	compressed sensing
CSI	channel state information
D2D	device-to-device
DDU	direct data undersampling
DFT	discrete fourier transform
ECU	estimated channel undersampling
FDD	frequency division duplexing
FHT	fast numerical hard threshold algorithm
FPC	fixed point continuation
FST	fast numerical soft threshold algorithm
Grouse	grassman rank-one update subspace estimation
i.i.d.	independent identically distributed
ILP	integer linear programming
LA	Lagrangean relaxation
LMUI	limited multi-user interference
LOS	line-of-sight
LP	linear programming
LTE	long-term evolution
LTE-A	long-term evolution advanced
MAC	media access control
MC	matrix completion
MCS	modulation and coding scheme
MILP	mixed integer linear programming
MIMO	multiple-input-multiple-output
MISO	multiple-input-single-output

MMSE	minimum mean square error
MRT	maximum ratio transmission
MSB	minimization split bregman
MU	multi-user
MUI	multi-user interference
NCon	non-convex algorithm
NMSE	normalized mean square error
OFDM	orthogonal frequency division multiplexing
OptSpace	spectral matrix completion
p.d.f.	probability density function
QoS	quality of service
RF	radio frequency
Rx	receiver side
SDP	semidefinite programming
SIC	successive interference cancellation
SINR	signal-to-interference-plus-noise ratio
SIR	signal-to-interference ratio
SNR	signal-to-noise ratio
ST-RPS	space-time random pilot selection
SVD	singular value decomposition
SVT	singular value thresholding
TDD	time division duplexing
Tx	transmitter side
UE	user equipment
ULA	uniform linear array
UPA	uniform planar array
ZFBF	zero-forcing beamforming

LIST OF SYMBOLS

ϵ	Tolerance
ν	Number of bits
C	Set of complex-value number
$\mathcal{N}$	Normal distribution
$\mathcal{R}$	Set of real-value number
θ	Angle of arrival
ϑ	Angle of departure
$\mathbf{G}$	Beam domain channel matrix
L	Number of cells
C	Constant
δ	Data rate
n	Dimension
α	Fading amplitude
μ	Incoherency parameter
ξ	Wavelength
λ	Lagrange multiplier
m	Total number of the observed entries
C_l	Number of MU clusters
$\mathbf{N}$	Noise matrix
$\mathbf{S}$	Symbol matrix
σ_n^2	Noise variance
ω_1	Parameter of the algorithms
ρ	Transmit power
p_r	Probability
r	Rank
M_R	Number of receive antennas
P	Number of specular multipaths
$\mathbf{H}$	Channel matrix
$\mathbf{Y}$	Received signal matrix
τ	Number of pilot sequences
σ_a^2	Angle variance
σ	Singular value
γ	Minimum SINR
ds	Inter-element antenna spacing
χ	Sparsity level
τ_1	Singular value thresholding

T_f	Feedback data time
T_{us}	Time required to begin the undersampling
T	Time required to read the preamble
M_T	Number of transmit antennas
$\mathbf{\Omega}$	Set of the known entries
$P_{\mathbf{\Omega}}$	Sampling operator
Po	Transmit power
$\mathbf{Q}$	Target matrix
$\mathbf{X}$	Matrix of variables
N_T	Number of transmit signal
K	Number of users
σ_e^2	Error variance

NOTATIONS

In this thesis the following conventions are used. Italic represents scalar quantities, boldface lower-case letters indicate vectors, and boldface upper-case letters express matrices.

$\mathcal{R}^{i\times j}$	set of real-values numbers $(i\times j)$ matrix dimensions
$C^{i\times j}$	set of complex-values numbers $(i\times j)$ matrix dimensions
x_i	i-th vector element
$\lvert x_i\rvert$	modulus of i-th vector element
$\mathbf{x}^T$	transpose of vector $\mathbf{x}$
$\mathbf{x}^H$	Hermitian transpose of vector $\mathbf{x}$
$\mathbf{x}^*$	conjugate of vector $\mathbf{x}$
$\lVert\mathbf{x}\rVert$	ℓ_2 norm of vector $\mathbf{x}$
$X_{i,j}$	(i, j)-th matrix element
$\mathbf{X}^{-1}$	inverse of matrix $\mathbf{X}$
$\mathbf{I}_N$	$N\times N$ identity matrix
$\mathbf{1}_N$	"all ones" vector of dimensions N
$\lVert\mathbf{X}\rVert_p$	norm p of matrix $\mathbf{X}$
$\lVert\mathbf{X}\rVert_2$	spectral norm of matrix $\mathbf{X}$
$\lVert\mathbf{X}\rVert_\mathrm{F}$	Frobenius norm of matrix $\mathbf{X}$
$\lVert\mathbf{X}\rVert_*$	nuclear norm of matrix $\mathbf{X}$
$\lvert\langle\mathbf{A}, \mathbf{B}\rangle\rvert$	$\mathrm{tr}\left(\mathbf{A}^H\mathbf{B}\right)$
$\odot$	Hadamard product
$\otimes$	Kronecker product
$\langle.\rangle$	inner product
$\lVert.\rVert_\infty$	ℓ_∞ norm of a vector
vec	vectorization operator
diag	the diagonal operator
$O(.)$	big O notation
$\geq$	greater than or equal
$\mathbb{E}\{.\}$	the expectation operator

The collection of vectors $\mathbf{u}_k \in \mathbb{R}^n$ for $1 \leq k \leq d$, denote u_{ik} is the i-th vector element, $[\mathbf{u}_1, \ldots, \mathbf{u}_d]$ is a matrix dimension $n\times d$ where the k-th column is $\mathbf{u}_k$.

TABLE OF CONTENTS

1 INTRODUCTION

This thesis is inspired by the problems in the recent technology termed 5G or fifth-generation. In this introductory chapter, the main motivation and objectives of this thesis are presented in Sections 1.1 and 1.2, respectively. Section 1.3 describes the main assumption about the channel. Section 1.4 depicts the thesis organization, and, finally, publications are listed in Sections 1.5.2 and 1.5.3.

The world has seen four generations of mobile communications; the first (1G) in 1980s supported only voice; the second (2G) in 1990s added data transmission to voice; the third generation (3G) in 2001 extended the foundation of broadband data communication to support basic Internet services; the fourth generation (4G) in 2009 added the long-term evolution (LTE) system to achieve higher data rates paving the path for the future fifth generation (5G) of mobile communications which is the focus of our work.

The 5G is under development, promising higher data rates and even higher efficiency to mobile broadband communications [1]. However, the scope of 5G is much broader than just further an enhanced mobile broadband communication. Instead, 5G is commonly described as a platform that should enable wireless connectivity for mostly any kind of device or application as presented in Figure 1.1. These are vehicle-to-vehicle (connected cars), massive machine type, device-to-device (D2D), millimeter wave, long-term evolution advanced (LTE-A)/Wi-Fi integration and micro-BS communications. Furthermore, the 5G is assumed to enable connectivity for a much more extensive range of new cases. For example, wireless connectivity for remote control of machinery, wireless connectivity for traffic safety and control, and monitor/control of infrastructure, virtual and augmented reality, tree dimension and ultra-high dimension video and haptic feedback applications, industrial automation and applications in health, such as remote surgery, smart cities, data from multiple domains (transportation, public administration, emergency services and weather sensing), and others [2].

The vast range of use cases in 5G means that the capabilities in this generation have to extend far beyond that previous ones. The 5G should support high peak data rates of 10 Gbits/s. In urban and suburban environments, the forecast considers 100 Mbit/s, which means an increase of factor 10 compared to what can be provided with current technologies. Another aspect is the lower latency, where the order of 1 ms is often mentioned. The extreme reliability is also considered. It means very different things, for instance, an extremely low error rate (below 10^{-9}), or the ability to retain connectivity even in cases of unexpected events including natural disaster. The energy efficiency is an emerging requirement where the cost of energy needed to operate the network is a significant and operational expense part for many operators [2].

Figure 1.1 – Deployment scenario envisioned for 5G cellular system.

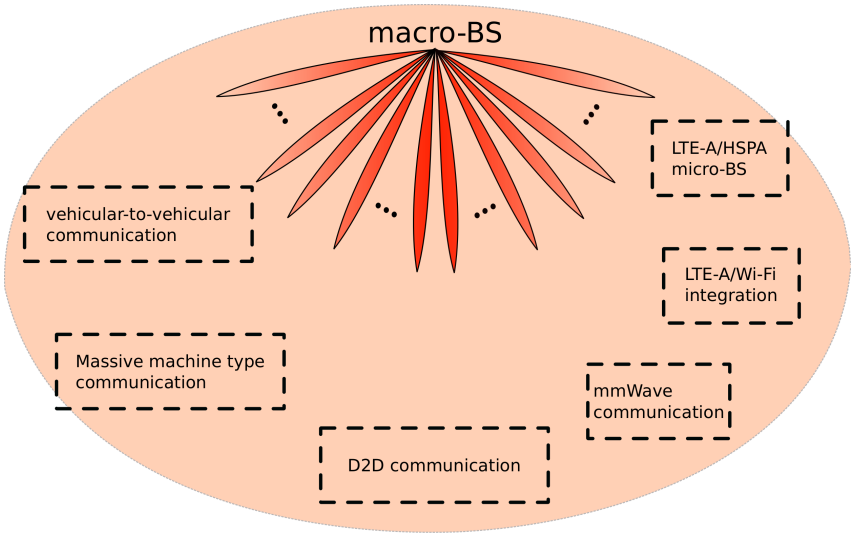

Source: Created by the author.

1.1 Motivation

Consider the 4G and 5G networks showed in Figure 1.2. Note that the 4G system can serve one UE[1] with a broad beam, while the 5G network has narrow beams which can give support to more than one UE simultaneously These beams are provided by the increase on the number of antenna elements at the BS. Thereby, the BS with a large number of antennas is named as massive MIMO BS. It means a large number of antennas is generating narrow beams with potential to light UEs in distinct regions, configuring a MU massive MIMO scenario.

Figure 1.2 – Evolution of a 4G network into 5G Massive MIMO with active phased-array antennas (APAA) with massive antenna elements network.

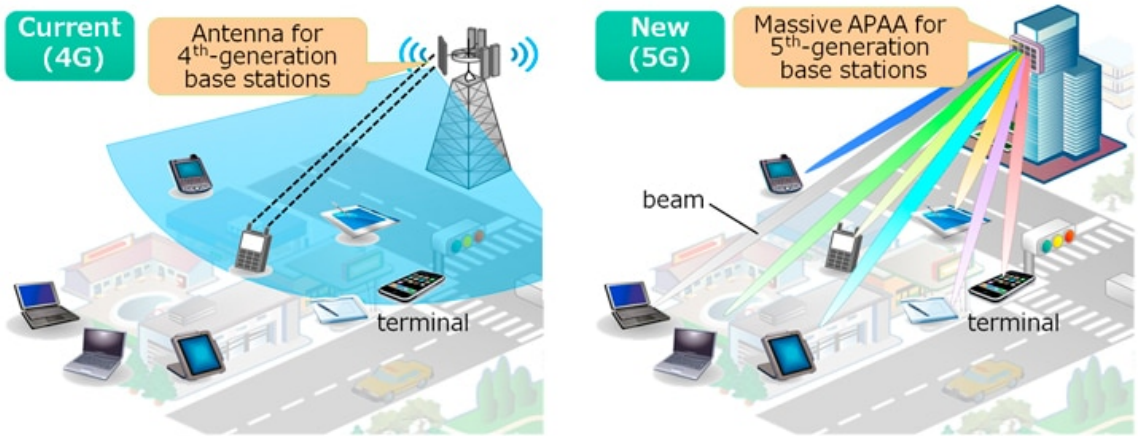

Source: [3].

Massive MIMO is one of the key technologies for the 5G wireless communication

[1] The UE is any device used directly by an end-user to communicate.

systems due to its potential to achieve high data rates and its robustness against interference, fading, hardware imperfections and failure [4]. In his seminal paper, Marzetta [5] showed that when the number of antennas grows very large, the effect of additive noise decreases, as well as the required transmitted energy per bit. The development of the new systems with massive MIMO can work in two operation modes, one based on time operation called time division duplexing (TDD) and another based on frequency operation called FDD. In TDD systems, the uplink and downlink transmissions are carried out using same frequency band, but separated in the time. Therefore, one can offer rely on channel reciprocity to acquire the CSI. However, the channel reciprocity may not hold, in practice, due to the calibration error between the uplink and downlink radio frequency (RF) chains [6, 7].

On the other hand, the uplink and downlink in the FDD systems utilize different frequencies. It is considered to be more effective under symmetric traffic and delay-sensitive applications due to small latency, continuous channel estimation, and backward compatibility. Moreover, the FDD operation mode is employed in most wireless systems of nowadays. However, FDD has a problem related with the channel feedback overhead that grows linearly with the number of BS (transmit) antennas [8]. Then, for practical feedback channels with limited transmission rate, the overhead to obtain the full CSI becomes prohibitively large due to the massive number of antenna elements. Thus, relying on CSI to design the downlink transmission emerges as a bottleneck in FDD systems. Furthermore, to fully utilize the spatial multiplexing and array gains expected for such promising technology, an accurate knowledge of CSI at the BS is essential to apply linear precoders as MRT or ZFBF.

Massive MIMO systems have potential to achieve high data rates mainly when more UEs are allocated the same frequency resource. Under this MU perspective, the systems have a huge potential to decrease the power consumption and to improve the communication system performance [9]. However, when the number of BS antennas is moderate, intra-cell interference among UEs appears and has to be effectively handled. Transmit beamforming is one of the techniques that achieves enhanced performance in MU massive MIMO systems, determining the complex antenna gains that optimize some performance criterion, e.g., the sum rate. The beamforming means that each data signal is sent from all antennas, but with different amplitude and phase to direct the signal spatially as shown in Figure 1.2 (right).

Under a multi-cell perspective, the massive number of antennas and more supported UEs intensify the problem for every UE and BSs to have orthogonal sequences in order to estimate the channel coefficients. This means that in the channel estimation stage, the performance is decreased since the interference is an extra problem. The inter-cell interference problem between any ordinary interfering BS of a mobile network is known as pilot contamination in the literature [5], which occurs when two pairs UE-BS use the same pilot sequence (also known as a reference signal). However, under a strictly coordinated control, it can be suppressed by using different pilots in adjacent cells in the conventional system with a small number of UEs (e.g., two). Meanwhile, the massive MIMO is supposed to have ten times more active UEs at

the same time/frequency resource than conventional systems which leads to more severe pilot contamination [10].

1.2 Main Contributions

This thesis deals with three key problems of 5G deployment, namely channel feedback in FDD systems, beamforming design, and pilot contamination. The main contributions of the work can be summarized as follows:

- A general framework for reducing the feedback load in FDD systems using matrix completion;
- A precoder design based on the beam domain channel representation to deal with the intra-cell interference;
- A space-time random pilot selection scheme for minimizing the pilot contamination in a multi-cell scenario.

1.3 Main Assumptions

Many discussions about the wireless channel were raised over the last years. This thesis relies on the assumption of poor scattering channel, where the number of dominant multipaths is much smaller compared to the number of antennas. Finite scattering models are usually adopted for millimeter-wave (mmWave) scenarios [11]. For example, of 60 GHz with massive MIMO, the high path loss will lead the primary propagation paths to be only the line-of-sight (LOS) or the first and second order reflections [12, 13].

Other scenarios also present a low number of scatterers. For example, in a scenario where the BS is equipped with a large number of antennas located in an elevated position with few scatterers around (e.g., on the top of a high building, a dedicated tower, or a unmanned aerial vehicle platform), and mainly characterized by rich local scatterers around the UE (e.g., the classical one-ring model [14, 15]). Meanwhile, for arrays with small aperture, antennas are highly directive, further reducing the number of surrounding scatterers. Hence, the angular spread seen by the BS is quite small and the number of incoming signal paths is also limited.

Moreover, several related works assume similar insights [7, 16, 17, 18, 19, 20, 21, 22, 23, 24, 25, 26, 27]. Thereby, for the considered scenarios in this work, the channel matrix is assumed to have low-rank or at least have deficient rank.

1.4 Thesis Organization

This thesis is organized as follows:

Chapter 1 presented an introduction about the next generation of mobile communications considering the massive MIMO system and raised some problems related with this new technology.

Chapter 2 presents the use of MC technique to reduce the FDD uplink feedback channel overhead exploiting the low-rank structure in the channel matrix for its accurate reconstruction from a few feedback information. In this context, a general framework which uses a matrix completion technique is proposed as a solution to the CSI feedback and reconstruction problem. The proposed framework is evaluated in two application scenarios: wireless backhauling communications and a clustered MU scenario uplink scenario.

Chapter 3 describes a formulation of a precoder design that exploits the geometric sparsity of the MU massive MIMO channel considering a practical rate assignment based on the modulation and coding scheme (MCS) of the LTE table, beam selection, and power optimization. An optimal solution to capacity following the MRT principle is shown. A heuristic based on Lagrangean relaxation and three additional simple heuristics are presented.

Chapter 4 describes a scheme based on a space-time pilot transmission, named ST-RPS, to mitigate the destructive effect of pilot contamination. The space-time pilot method uses Bernoulli distribution to decide about the transmission. The obtained simulation results show that the scheme leads to improved channel estimation accuracy due the reduction of pilot contamination.

Chapter 5 concludes this thesis by summarizing the main conclusions and listing some perspectives for future work.

The organization of the thesis is illustrated in Figure 1.3.

Figure 1.3 – Organization of the thesis in a block-diagram.

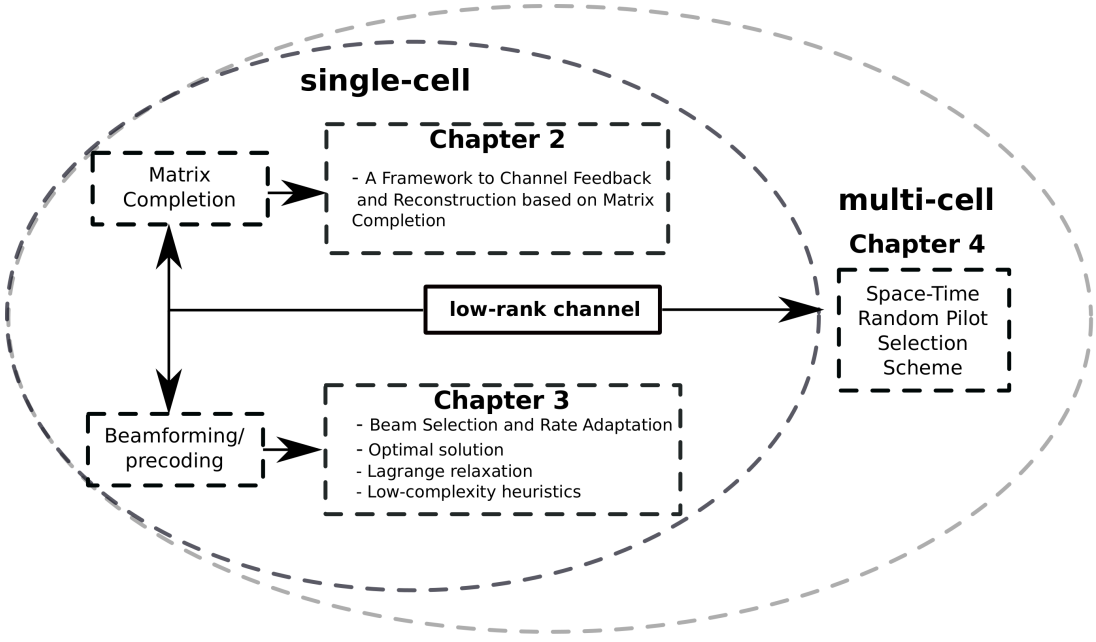

Source: Created by the author.

1.5 Scientific Production

The publications produced during the thesis period are listed below. Those publications may be divided into two general categories: main and related publications. The main publications served as the basis for this thesis, while the related ones are about correlated topics.

1.5.1 Technical Reports

These are the reports that served as the basis for some problems addressed in this thesis. The first and third parts of this thesis which are related to Chapters 2 and 4, respectively, were developed under the context of Ericsson/UFC technical cooperation projects:

- UFC. 34: *Transceiver Design in MIMO Communication Systems: Distributed Processing and Very-Large-Scale Approaches*, February/2014 - August/2014;
- UFC. 41: *Distributed Optimization and Very Large-MIMO Transceivers for 5G Wireless Communication Systems*, October/2014 - May/2016,

in which a number of four technical reports, one in UFC.34 and three in UFC.41 were delivered:

- VALDUGA, S. T.; ALMEIDA, A. L. F. de. **Fourth Technical Report UFC/Ericsson - Channel Estimation in Very-Large Scale MIMO**. GTEL-UFC, July 2014;
- VALDUGA, S. T.; ALMEIDA, A. L. F. de. **First Technical Report UFC/Ericsson - CSI Feedback and Reconstruction Using Matrix Completion for Massive MIMO Systems**. GTEL-UFC, Mar. 2015;
- VALDUGA, S. T.; ALMEIDA, A. L. F. de. **Second Technical Report UFC/Ericsson - Feedback Signaling and CSI Reconstruction Using Completion Techniques**. GTEL-UFC, Oct. 2015;
- VALDUGA, S. T.; ALMEIDA, A. L. F. de. **Third Technical Report UFC/Ericsson - CSI Feedback and Reconstruction Using Matrix Completion and Tensor Completion for FDD Uplink Multi User Massive MIMO**. GTEL-UFC, Feb. 2016.

Also, a request for a patent application named *Reduced feedback data using matrix completion for CSI acquisition* was performed.

1.5.2 Main Publications

The following journal paper and a letter were produced:

- VALDUGA, S. T. et al. A Framework to Channel Feedback and Reconstruction using Matrix Completion in Massive MIMO Systems, **Journal of Communication and Information Systems - JCIS**, Oct. 2017. Under review.

- VALDUGA, S. T. et al. Minimization of Pilot Contamination Effect with Space-Time Pilot Transmission Scheme, 2018. To be submitted.

The second part of this thesis is related to Chapter 3 which includes a one-year internship at the I3S Laboratory, CNRS, France, under the context of the following I3S/UFC technical cooperation project:

- *Massive MIMO Systems: Project and Modeling of the Large Scale MIMO Systems*, February/2016 - February/2017.

As a result of this internship, a conference and a journal paper were produced:

- VALDUGA, S. T. et al. **Low complexity beam selection for sparse massive MIMO systems**. In: PROC. Int. Symp. Wireless Communication Systems (ISWCS). Italy: [s.n.], Aug. 2017. p. 414–419. DOI: 10.1109/ISWCS.2017.8108150;

- VALDUGA, S. T. et al. Low-Complexity Heuristics to Beam Selection and Rate Adaptation in Sparse Massive MIMO Systems. **Transactions on Emerging Telecommunications Technologies - ETT**, Feb. 2018. Submitted.

1.5.3 Related Publications

Some works were produced during the last years of this doctoral thesis, in the context of codebooks for MIMO systems:

- VALDUGA, S. T. et al. **Low-Complexity Codebook-Based Beamforming with Four Transmit Antennas and Quantized Feedback Channel**. In: 2014 IEEE Wireless Communications and Networking Conference (WCNC). [S.l.: s.n.], Apr. 2014. p. 1212–1217. DOI: 10.1109/WCNC.2014.6952322;

- VALDUGA, S. T. et al. **Esquema MIMO Beamforming Otimizado para Canal de Retorno de Baixa Taxa de Transmissão**. In: XXXIII Simpósio Brasileiro de Telecomunicações, 2015, Juiz de Fora, Anais do XXXIII SBrT. [S.l.: s.n.], 2015. p. 1–5;

- VALDUGA, S. T. et al. Codebook Design and Performance Analysis of Quantized Beamforming under Perfect and Imperfect Channel State Information. **Journal of Communication and Information Systems - JCIS**, v. 32, n. 1, p. 161–171, 2017. DOI: 10.14209/jcis.2017.16.

1.5.4 How to Read This Thesis

This thesis has three chapters that cover different aspects of massive MIMO systems. Every chapter is meant to be self-contained so that the reader can read them independently without loosing significant information.

2 MATRIX COMPLETION AS A SOLUTION FOR A FEEDBACK CHANNEL PROBLEM IN MASSIVE MIMO SYSTEMS

This chapter investigates the use of MC in order to reduce the FDD uplink feedback channel overhead, called here as the feedback channel problem. Our approach capitalizes on the low-rank structure of the MIMO channel.

The MC technique is capable of recovering an unknown low-rank matrix, exactly or approximately, from undersampled observations, with or without noise [38, 39]. Under mild conditions, from the knowledge of a fraction of its entries (the matrix elements [40]) the desired matrix can be recovered by minimizing the nuclear norm (sum of singular values) of the observed matrix. According to the MC theory, only a few randomly chosen entries of the matrix are enough for the recovery of the whole matrix with good accuracy. In this context, there is a vast body of literature on MC theory and algorithmic solvers, as well as on more general matrix approximation problems such as the *Netflix* problem [41] (see Figure 2.1), collaborative filtering, target estimation [42], sensor localization [43], machine learning [44], control [45], multi-linear algebra [46], and many others.

Figure 2.1 – Example of matrix completion problem in recommendation systems, e.g., given less than 1% of the movie ratings which the objective is to find missing ratings.

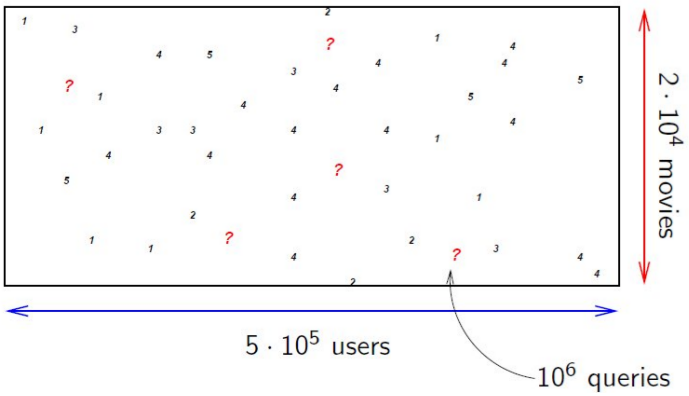

Source: [47]

2.1 Motivation

To fully utilize the spatial multiplexing and array gains expected with such a promising technology such MIMO, an accurate knowledge of the CSI at the BS is essential to apply linear precoders as a simple MRT or a ZFBF, for instance. Since Marzetta's paper [5] showed that TDD is preferable for massive MIMO systems, many researchers have focused on providing solutions for that. In TDD, the uplink pilots are exploited to estimate the channel directly at the BS. The FDD is generally considered to be more effective under symmetric traffic and delay-sensitive applications due to small latency, continuous channel estimation, and backward

compatibility. Moreover, in most wireless systems built today the FDD operation mode is generally employed. Consequently, it is important to identify and develop solutions for potential issues arising on FDD-based massive MIMO technique.

2.2 Objectives and Main Contributions

Knowing that the feedback rate is one critical aspect in real-world wireless systems, the aim is to provide a solution to the problem of CSI acquisition at the BS with reduced load in the feedback channel of FDD-based massive MIMO systems. To the best of our knowledge, this work is the first to propose the use of MC in a general CSI feedback and reconstruction framework for massive MIMO systems. In the present work, upon reception of downlink pilots from the Tx, for example a macro BS, the receiver side (Rx), i.e., a micro-BS or a UE undersamples either the received pilot data matrix or the estimated channel matrix (depending on the chosen scheme), and feeds only a fraction of their entries back to the Tx. By capitalizing on MC, the Tx recovers the downlink pilots for subsequent channel estimation, or to directly reconstructs the downlink channel. Thereby, the transmitter is able to design simple linear precoders [48, 49] and beamformers that consider a full-channel knowledge. Our results show that, when the channel matrix has a low-rank structure, the proposed feedback and reconstruction schemes yield accurate CSI estimation with minimal feedback overhead, which translates into a high energy efficiency and low complexity at the Rx, a desired feature for power-limited uplink transmissions.

2.2.1 Organization

We investigate the application of the MC technique as a solution to the CSI feedback and reconstruction problem. In this context, we explore the low-rank structure of the channel matrix for its accurate reconstruction from a few feedback information. We propose a general framework and show the usefulness of the proposed framework in two application scenarios: wireless backhauling communications and a MU uplink scenario. We discuss two feedback methods based on ECU and DDU, which are respectively based on undersampling of the estimated channel and/or the received data. Furthermore, we show that the decrease of the reconstruction error is related to the number of antennas in a massive MIMO system. We formulate the performance in terms of BER and goodput considering a minimum mean square error (MMSE) estimator. Summarizing, in Section 2.3.1, we introduce the feedback channel problem. Section 2.3.2 describes the system model. Section 2.3.3 addresses a formulation to solve the MC problem. Section 2.3.5 proposes a solution with a general framework based on two operation modes. Two application examples are presented in Section 2.4. In Section 2.5, the simulation results are shown. Finally, Section 2.6 brings some concluding remarks.

2.3 Proposed Framework to Channel Feedback and Reconstruction

2.3.1 Background

In massive MIMO, the spatial focusing of energy into ever-smaller regions of space potentially brings huge improvements in throughput and radiated energy efficiency. Other benefits could also include the extensive use of inexpensive low-power components, low latency communication, simplification of the media access control (MAC) layer, and robustness to intentional jamming [4]. To fully utilize the benefits of such a promising technology, an accurate knowledge of the CSI at the BS is essential to apply linear precoders such as a simple MRT or a ZFBF. Henceforth, we focus on FDD operation. In this context, one well-known problem is that the channel feedback overhead grows linearly with the number of antennas [8, 50, 51, 52]. Then, for practical feedback channels with limited transmission rate, the overhead to obtain full CSI becomes prohibitively large due to the massive number of antenna elements. Thus, relying on CSI to design the downlink transmission emerges as a bottleneck in FDD systems. Furthermore, for practical feedback channels, the rate is limited and it is acceptable not to assume the transmission of full CSI to the BS. In this context, the availability of CSI at the transmitter to design the downlink transmission is a bottleneck in FDD systems. It is worth mentioning that in this thesis, we consider that the uplink feedback channel is error-free. Although this assumption may not hold in practice, good channel coding is usually applied to add robustness on the feedback channel against channel induced errors.

Solutions for reducing the amount of data to be sent via a limited feedback channel usually resort to compressed sensing (CS) techniques. These solutions consider that the channel matrices admit a sparse representation, for instance, because of the shared and limited local scattering. Therefore, due to the sparse channel structure, CS techniques can reduce the training sequence and feedback overheads [20, 53, 54, 55, 56]. In [20], a scheme to exploit the hidden joint sparse structure of channel matrices via CS was proposed. In [53], an adaptive CS-based feedback scheme was proposed, where the feedback structure can be dynamically configured based on channel conditions, while [54] presents and discusses the use of sparsity-inspired CSI acquisition techniques for massive MIMO, as well as the underlying mathematical theory in FDD and TDD modes. In [55], based on the spatial correlation and channel conditions, the authors suggested two compression methods for channel feedback to reduce the feedback overhead. A hybrid limited feedback design is proposed for massive MIMO in [56]. They consider quantized and codebook based feedbacks.

Solutions based on CS, however, rely on an adequate choice of a basis that provides a sparse representation. If such a basis fails, it no longer represents the channel or its spatial characteristics properly [55]. Additionally, a proper basis may need to be sent to the receiver, which increases the signaling overhead in this case. Differently, the authors in [57] proposed a channel estimation algorithm based on MC technique, assuming a switch-based mmWave massive MIMO scenario. Here, MC is a technique that can be used to complete a matrix with

missing elements. Comparing to CS techniques, the authors showed that MC technique can achieve a near-optimal spectral efficiency with significantly lower complexity, since it does not require basis as in CS, and it is immune to array response mismatch, as well.

Another solution is to exploit spatial correlation information. For instance, [58] proposes to design grouping patterns, taking advantage of the spatial correlation mapping of multiple antenna elements to a single representative value, using pre-designed patterns therein referred to as antenna group beamforming (AGB). However, full CSI is not available at the transmitter. Instead, the proposed scheme uses the pattern index to select the antenna group and the codeword index for transmit beamforming, making such a scheme limited. Another solution is presented in [59], which consists of a feedback scheme based on channel vector quantization and beamforming. The authors propose codebooks and UE selection for scheduling based on reliability information, channel quality indicator, channel direction indicator and rate approximation. However, this solution does not provide CSI to the transmitter.

The idea of applying a completion technique to MIMO communication appeared in [60] to obtain direction of arrival (DoA) for colocated MIMO radars. The solution consists of either performing a matched filtering with a small number of randomly selected dictionary waveforms or undersampling the received signal at random sampling instants and forward the results to a fusion center. From the received samples and the sampling scheme, the fusion center applies a MC technique to estimate the full matrix. In [25], the authors proposed a solution to provide the CSI to the Tx for FDD massive MIMO systems. The proposal is to apply an algorithm based on MC concepts. They consider that all scheduled UEs directly feed the full received pilots back to which they apply a low-rank approximation for CSI recovery. Therein, the authors formulate an optimization problem to the estimation of the channel under a low-rank constraint without undersampling. However, full CSI is conveyed back to the Tx, which can be a bandwidth consuming process. The approach of [61] estimates the channel matrix by means of a MC technique. The method is numerically investigated by considering different scattering environments for the MIMO channel model in an indoor scenario. Therein, the authors do not assume a low-rank channel model.

This work advances further than [54, 61] by presenting the problem in detail, while linking it to the massive MIMO paradigm. We also discuss two relevant application scenarios where the proposed approach is appealing.

2.3.2 System Model

Consider a wireless communication system, where a BS represents the Tx and the Rx can be represented by others BSs or the UEs. The Tx and Rx are equipped with M_T and M_R antennas, respectively.

During the downlink training phase, the BS sends pilot sequences of length N_T to the Rx. The received signal at the Rx can be expressed as:

$$\mathbf{Y} = \mathbf{H}\mathbf{S}^T + \mathbf{N} \in M_R \times N_T, \tag{2.1}$$

where $\mathbf{H} \in C^{M_R \times M_T}$ is the channel matrix, $\mathbf{S} \in N_T \times M_T$ contains the pilot sequences, and $\mathbf{N} \in C^{M_R \times N_T}$ the additive white Gaussian noise term.

The channel model is expressed as a sum of a finite (small) number of specular paths, as follows:

$$\mathbf{H} = \frac{1}{\sqrt{P}} \sum_{p=1}^{P} \alpha_p \mathbf{a}_r(\theta_p) \mathbf{a}_t^T(\vartheta_p), \tag{2.2}$$

where P defines the number of paths, α_p is the fading amplitude associated with the p-th path, and the steering vector is defined as [62]:

$$\mathbf{a}_r(\theta_p) \triangleq \left[1,\ e^{-j2\pi \frac{ds}{\xi} \cos(\theta_p)}, \ldots, e^{-j2\pi \frac{(M_R-1)ds}{\xi} \cos(\theta_p)}\right]^T, \tag{2.3}$$

$$\mathbf{a}_t(\vartheta_p) \triangleq \left[1,\ e^{-j2\pi \frac{ds}{\xi} \cos(\vartheta_p)}, \ldots, e^{-j2\pi \frac{(M_T-1)ds}{\xi} \cos(\vartheta_p)}\right]^T, \tag{2.4}$$

where ds is the inter-element antenna spacing, ξ is the wavelength, and $\theta_p, \vartheta_p \in [0, \pi]$ are the angle of arrival (AoA) and angle of departure (AoD), respectively, associated with the p-th path. Furthermore, the channel model described in Equation (2.2) is a stochastic multipath channel [17].

2.3.3 Matrix Completion Technique

In this subsection, we discuss the low-rank matrix completion technique, following the nuclear norm minimization concept. The nuclear norm is alternatively known by several other names including the Schatten 1-norm, the Ky Fan r-norm, and the trace class norm. See [38, 63, 64] for a detailed discussion, full proofs and theoretical results of the exact and approximate recovery results to MC theory. The results developed in [63] extend the theory of CS to different structures, beyond the sparse structure. Furthermore, the MC theory benefits from the CS theory jointly with probability tools [65].

The problem can be defined as follows. There is a data matrix $\mathbf{Q} \in C^{n \times n}$ which we would like to know as precisely as possible. However, only some entries of this matrix are available and there is no way to find the unknown entries of it without imposing additional conditions. Thus, the problem is ill-posed. However, if the matrix has low-rank or has approximately low-rank, then accurate or even exact recovery is possible by nuclear norm minimization [45, 63, 66]. In this case, one may accurately recover a low-rank matrix from relatively few measurements. Some results have shown that this is indeed possible [38, 39, 43, 64, 67].

More specifically, let $\mathbf{Q}$ be the desired matrix to be reconstructed. We assume that only a few entries of $\mathbf{Q}$ are known. For instance, if a tuple $(i, j) \in \mathbf{\Omega}$, it means that the (i, j)-th entry of $\mathbf{Q}$ is known.

To undersample $\mathbf{Q}$, let $P_{\mathbf{\Omega}} : C^{n \times n} \rightarrow C^{n \times n}$ denote the sampling operator defined by

$$P_{\mathbf{\Omega}}(\mathbf{Q}) = \begin{cases} Q_{i,j}, & \text{if} \quad (i, j) \in \mathbf{\Omega} \\ 0, & \text{otherwise,} \end{cases} \tag{2.5}$$

where $Q_{i,j}$ is the (i, j)-th entry of $\mathbf{Q}$. The sampling operator simply undersamples its input matrix, setting the output matrix entries corresponding to the unknown elements of $\mathbf{Q}$ to zero.

For a great enough number of samples, sampling uniformly at random is expected to generate just a low-rank matrix with these samples. The classical problem of finding the best low-rank approximation to a given full matrix $\mathbf{Q}$ is equivalent to solving the optimization problem:

$$\begin{aligned} \hat{\mathbf{Q}} &= \arg\min_{\mathbf{X}} \ \operatorname{rank}(\mathbf{X}) \\ \text{s.t.: } & P_{\mathbf{\Omega}}(\mathbf{X}) = P_{\mathbf{\Omega}}(\mathbf{Q}), \end{aligned} \tag{2.6}$$

where $\mathbf{X}$ is the matrix of variables and $\hat{\mathbf{Q}}$ is a element-wise reconstruction of $\mathbf{Q}$ [45, 68]. Notice that the constraint in Equation (2.6) makes sure that the entries of $\mathbf{X}$ corresponding to the known entries of $\mathbf{Q}$ are equal. However, in general, problem in Equation (2.6) is know to be a nondeterministic polynomial-time (NP) hard problem [69]. An alternative method to solve the problem using convex relaxation is proposed [45] as follows:

$$\begin{aligned} \hat{\mathbf{Q}} &= \arg\min_{\mathbf{X}} \ \|\mathbf{X}\|_* \\ \text{s.t.: } & P_{\mathbf{\Omega}}(\mathbf{X}) = P_{\mathbf{\Omega}}(\mathbf{Q}). \end{aligned} \tag{2.7}$$

More specifically, despite the fact that nuclear norm minimization was observed to produce very low-rank solutions in practice [45, 64, 66], theoretical results showed that it produces the minimum rank solution [63].

The nuclear norm is a convex function, and can be formulated using semidefinite programming (SDP). Thereby, given a general matrix $\mathbf{Q}$, which may not be semidefinite or symmetric, the nuclear norm can be formulated in terms of SDP, by rewriting Equation (2.7) as follows:

$$\begin{aligned} \hat{\mathbf{Q}} &= \arg \min_{\mathbf{X}, \mathbf{Q}_1, \mathbf{Q}_2} \ \operatorname{tr}(\mathbf{Q}_1) + \operatorname{tr}(\mathbf{Q}_2) \\ \text{s.t.: } & P_{\mathbf{\Omega}}(\mathbf{X}) = P_{\mathbf{\Omega}}(\mathbf{Q}), \\ & \begin{bmatrix} \mathbf{Q}_1 & \mathbf{X} \\ \mathbf{X}^H & \mathbf{Q}_2 \end{bmatrix} \geq 0. \end{aligned} \tag{2.8}$$

where the optimization variables are $\mathbf{X}$, $\mathbf{Q}_1$ and $\mathbf{Q}_2$. The optimization problem in Equation (2.8) and Equation (2.7) are convex. Thereby, they can be solved using general solvers available in the literature, e.g., [70].

In [67], Candès and Plan proved that if the entries of the matrix are corrupted by noise, it is possible to recover the whole matrix with a few samples. Let us assume a noisy model as follows:

$$Q_{i,j} = M_{i,j} + Z_{i,j} \quad (i, j) \in \mathbf{\Omega}, \tag{2.9}$$

where $Z_{i,j}$ with $(i, j) \in \mathbf{\Omega}$ contains statistical or deterministic noise. Let us apply the sampling operator

$$P_{\mathbf{\Omega}}(\mathbf{Q}) = P_{\mathbf{\Omega}}(\mathbf{M}) + P_{\mathbf{\Omega}}(\mathbf{Z}) \tag{2.10}$$

where $\mathbf{Z} \in C^{n \times n}$. The matrix $\mathbf{M}$ can be recovered solving the following problem:

$$\begin{aligned} \hat{\mathbf{M}} &= \arg\min_{\mathbf{X}} \ \|\mathbf{X}\|_* \\ &\text{s.t.: } \|P_{\mathbf{\Omega}}(\mathbf{X} - \mathbf{Q})\|_F \leq \epsilon. \end{aligned} \tag{2.11}$$

Assume that $\|P_{\mathbf{\Omega}}(\mathbf{Z})\|_F \leq \epsilon$, where ϵ means a reconstruction error threshold. Furthermore, when the noise is white and Gaussian with variance σ_n^2, then $\epsilon^2 \leq (m + \sqrt{8m})\sigma_n^2$ with high probability [67], where m is the undersampling factor. The precision of estimation depends on the structure of the targeted matrix. The singular values need to be sufficiently spread, or incoherent (Candès [63] and Recht [64]) for reconstructing $\mathbf{Q}$ with only a few samples. In MC theory [38, 63, 64, 67] the sampling is done uniformly at random, and some simple hypotheses about the matrix $\mathbf{Q}$ were developed, which make it recoverable. Let us describe these hypotheses briefly.

Consider the singular value decomposition (SVD) of the rank-P matrix $\mathbf{Q}$:

$$\mathbf{Q} = \sum_{i=1}^{P} \sigma_i \mathbf{u}_i \mathbf{v}_i^H. \tag{2.12}$$

Consider the SVD of $\mathbf{Q}$ described on Equation (2.12), $\mathbf{P}_U$ and $\mathbf{P}_V$ as the orthogonal projections onto the column and row space of $\mathbf{Q}$ respectively (singular vectors):

$$\mathbf{P}_U = \sum_{i=1}^{P} \mathbf{u}_i \mathbf{u}_i^H, \quad \mathbf{P}_V = \sum_{i=1}^{P} \mathbf{v}_i \mathbf{v}_i^H.$$

We define the matrix $\mathbf{E}$ as

$$\mathbf{E} \triangleq \sum_{i} \mathbf{u}_i \mathbf{v}_i^H, \quad \mathbf{P}_U \mathbf{E} = \mathbf{E} = \mathbf{E}\mathbf{P}_V, \quad \mathbf{E}^H\mathbf{E} = \mathbf{P}_V, \quad \mathbf{E}\mathbf{E}^H = \mathbf{P}_U.$$

To recover the matrix from part of entries, the vectors $\mathbf{u}_i$ and $\mathbf{v}_i$ need to be "incoherent" (μ) in some sense.

More specifically, the assumptions are as follows:

Assumption 1. There exists $\mu_1 > 0$ such that for all pairs $(a, a') \in n \times n$ and $(b, b') \in n \times n$,

$$|\langle \mathbf{e}_a, \mathbf{P}_U \mathbf{e}_{a'} \rangle - \frac{P}{n_1} 1_{a=a'}| \leq \mu_1 \frac{\sqrt{P}}{n}, \tag{2.13}$$

$$|\langle \mathbf{e}_b, \mathbf{P}_V \mathbf{e}_{b'} \rangle - \frac{P}{n_2} 1_{b=b'}| \leq \mu_1 \frac{\sqrt{P}}{n}, \tag{2.14}$$

where id=sam]**e** is a canonical vector and 1_E the indicator function of an event E, e.g. $1_{a=a'}$ is equal 1 if $a = a'$ and 0 if $a \neq a'$. $|\langle \mathbf{A}, \mathbf{B} \rangle|$ is defined as $\mathrm{tr}\left(\mathbf{A}^H \mathbf{B}\right)$.

Assumption 2. There exists $\mu_2 > 0$ such that for all $(a, b) \in n \times n$

$$|E_{ab}| \leq \mu_2 \frac{\sqrt{P}}{n}. \tag{2.15}$$

If both assumptions hold, we say that the matrix $\mathbf{Q}$ obeys the strong incoherence property with parameter $\mu = \max(\mu_1, \mu_2)$.

Based on these hypotheses, [38] proposes the following theorem:

Theorem 1 *Let $\mathbf{Q} \in C^{n\times n}$ be a fixed matrix of rank-r obeying the strong incoherence property with parameter μ. Suppose we observe m entries of $\mathbf{Q}$ with locations sampled uniformly at random. Then, there is a positive numerical constant C such that if*

$$m \geq C\mu^2 nr \log_{10}^{\varrho} n, \tag{2.16}$$

where ϱ is an integer positive number, then $\mathbf{Q}$ is the unique solution to Equation (2.7) *with probability at least $1 - n^{-3}$, i.e., with high probability, nuclear norm minimization recovers all the entries of $\mathbf{Q}$ without error.*

2.3.4 Incoherence Property of Massive MIMO Channel

Following [38], the assumptions 1 and 2 of $\mathbf{H}$ when $r = P = 1$, can be measured by the singular vector. Comparing Equation (2.2) with the SVD of $\mathbf{H} = \sum_{i=1}^{P} \sigma_i \mathbf{u}_i \mathbf{v}_i^H$, the $\mathbf{u}_1 = \mathbf{a}_r(\theta)$ and $\mathbf{v}_1 = \mathbf{a}_t(\vartheta)$ are the singular vectors. Thus, all entries of $\mathbf{P}_U$ have the same modulus $1/M_R$ and those of $\mathbf{P}_V$ have the same modulus $1/M_T$. When $a = a'$ and $b = b'$,

$$\langle \mathbf{e}_a, \mathbf{P}_U \mathbf{e}_{a'} \rangle = [\mathbf{P}_U]_{a,a'} = \frac{1}{M_R}, \tag{2.17}$$

$$\left| \langle \mathbf{e}_a, \mathbf{P}_U \mathbf{e}_{a'} \rangle - \frac{1}{M_R} \right| = 0, \tag{2.18}$$

$$\langle \mathbf{e}_b, \mathbf{P}_V \mathbf{e}_{b'} \rangle = [\mathbf{P}_V]_{b,b'} = \frac{1}{M_T}, \tag{2.19}$$

$$\left| \langle \mathbf{e}_b, \mathbf{P}_V \mathbf{e}_{b'} \rangle - \frac{1}{M_T} \right| = 0. \tag{2.20}$$

When $a \neq a'$ and $b \neq b'$,

$$|\langle \mathbf{e}_a, \mathbf{P}_U \mathbf{e}_{a'} \rangle| = |[\mathbf{P}_U]_{a,a}| = \frac{1}{M_R}, \tag{2.21}$$

$$|\langle \mathbf{e}_b, \mathbf{P}_V \mathbf{e}_{b'} \rangle| = |[\mathbf{P}_V]_{b,b}| = \frac{1}{M_T}. \tag{2.22}$$

Thus, the incoherence property for assumption 1 and 2 with $\mu = 1$ is satisfied.

For $r = P \geq 2$, and a sufficiently large number of antennas, the singular vectors of the channel $\mathbf{H}$ converge to the steering vectors [57](see [71] for a detailed proof.). Thereby, all entries of the left and right singular vectors have the same modulus $1/\sqrt{M_R}$ and $1/\sqrt{M_T}$, respectively. Hence, $a = a'$ and $b = b'$

$$\langle \mathbf{e}_a, \mathbf{P}_U \mathbf{e}_{a'} \rangle = [\mathbf{P}_U]_{a,a} = \frac{P}{M_R}, \tag{2.23}$$

$$\langle \mathbf{e}_b, \mathbf{P}_V \mathbf{e}_{b'} \rangle = [\mathbf{P}_U]_{b,b} = \frac{P}{M_T}, \tag{2.24}$$

and, for $a \neq a'$ and $b \neq b'$,

$$|\langle \mathbf{e}_a, \mathbf{P}_U \mathbf{e}_{a'} \rangle| = [\mathbf{P}_U]_{a,a'} = \left| \sum_{i=1}^{P} u_{i,a} u_{i,a'}^* \right| \tag{2.25}$$

$$\leq \sum_{i=1}^{P} |u_{i,a}||u_{i,a'}^*| = \frac{P}{M_R}, \tag{2.26}$$

$$|\langle \mathbf{e}_b, \mathbf{P}_V \mathbf{e}_{b'} \rangle| = [\mathbf{P}_V]_{b,b'} = \left| \sum_{i=1}^{P} v_{i,b} v_{i,b'}^* \right| \tag{2.27}$$

$$\leq \sum_{i=1}^{P} |v_{i,b}||v_{i,b'}^*| = \frac{P}{M_T}. \tag{2.28}$$

Thus, equality $\mu = \sqrt{P}$ satisfies the incoherence property for assumptions 1 and 2 when M_T, M_R are very large. This means that when $\mathbf{H}$ is large, it obeys the strong incoherence property with $\mu \approx \sqrt{P}$, and can be recovered with a small number of samples.

2.3.5 General Problem

In this section, we are interested in solving a general feedback problem.

To illustrate this problem, consider a conventional feedback scheme in a MIMO system, where the full channel matrix is conveyed from the Rx back to the Tx. The number of bits to be fed back is given by $\nu = \kappa \log_2(M_R M_T)$, where κ depends on the accuracy of channel information at the Rx. Assuming $M_T = M_R = 100$ and $\kappa = 3$, the Rx needs $\nu = 39.8631$ bits to convey the full CSI to the Tx.

In this context, we resort to MC techniques to solve the feedback overhead problem, by exploiting the low-rank nature of the MIMO channel. The framework of the underlying idea is shown in Figure 2.2. The process is initialized with the Tx sending a forward data to Rx and,

Figure 2.2 – Framework structure.

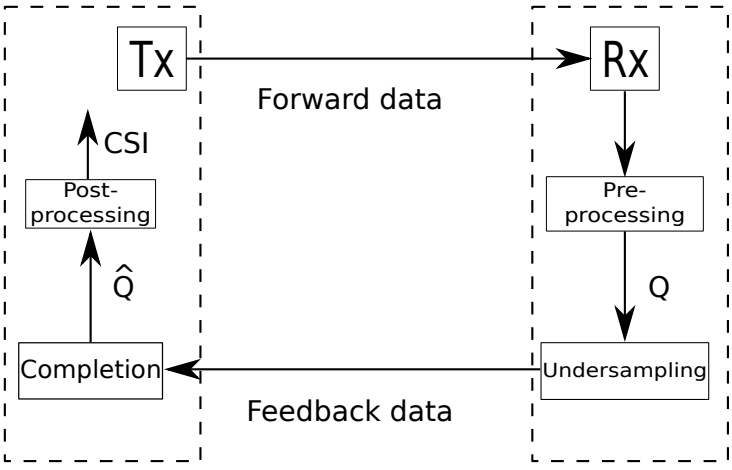

Source: Created by the author.

after a pre-processing, Rx sends a reduced feedback data to Tx. For example, if the technique

to obtain the CSI is based on pilot symbols, the forward data is a training sequence and the pre-processing block is the channel estimator. The parameter m is introduced to describe the undersampling factor related to the reduced feedback data. This factor is defined as a percentage of entries in the matrix $\mathbf{Q}$ (e.g., $m = 0.1$ means that 10% of total entries were sent).

After receiving forward data sent by Tx, Rx may first pre-process such forward data. The result is the matrix $\mathbf{Q}$. Then, Rx undersamples $\mathbf{Q}$ and the undersampled data are sent through the feedback channel. Tx receives the data and then applies MC to this matrix. At the end of this step, the matrix $\mathbf{Q}$ is in turn reconstructed as $\hat{\mathbf{Q}}$. Finally, after a post-processing (channel estimation), the CSI is made available at Tx.

Basically, there exist an information *a priori* at Tx needed to enable the application of MC. For instance, Tx must know the number of antennas at Rx and the rank of the channel matrix, which in general, are available at the BS [72]. Additionally, in particular applications some information may not be mandatory but beneficial, such as the undersampling factor, which is defined as the percentage of the entries of $\mathbf{Y}$ to be fed back, the data feedback mode, if multiple modes are pre-defined, and the data distribution, which can dictate the way the undersampling procedure is performed.

2.3.6 Rx Description

Although the framework is described for a single Rx, it can be extended to the case with multiple receivers, say K Rxs. For instance, in a wireless backhaul scenario, there might exist K micro-BSs as Rxs. As a second example, there might exist K UEs in a MU scenario, since each one may have different goals. Thus, the framework may be applied individually. On the other hand, the Tx along with multiple receivers may have the same goal. In this case, every Rx would perform equally as they were a single Rx, being the Tx responsible for aggregating the individual feedback data from the Rxs. As a third case, the Tx can make different subsets of Rxs to send back different types of feedback data. Note that, regarding the *a priori* information at Tx, it must apply for each link Tx-Rx and it is Rx-specific. That is, Tx has to know the number of antennas at each Rx, as well as the rank of each channel matrix.

2.3.7 Operation Modes

Herein, two types of feedback data are visualized: (a) the received signal matrix $\mathbf{Y}$, or (b) the estimated channel matrix $\hat{\mathbf{H}}$. Based on this, we define two operation modes:

- DDU: in this mode, a fraction of the received signal $\mathbf{Y}$ is the feedback data, which means that $\mathbf{Q} = \mathbf{Y}$. Therefore, there is no pre-processing step. Consequently, Rx operates as a simple sampling device. Tx applies the completion algorithm to reconstruct $\mathbf{Y}$. Due to the noise, the matrix $\mathbf{Y}$ is actually full-rank. Eventually, Tx obtains a filtered version of $\mathbf{Y}$, from which the channel matrix $\hat{\mathbf{H}}$ is estimated as a post-processing step.

- ECU: in this mode, a fraction of the estimated channel $\hat{\mathbf{H}}$ is the feedback data, which means that $\mathbf{Q} = \hat{\mathbf{H}}$. Therefore, the pre-processing is a channel estimation step performed by the Rx taking into account the received signal $\mathbf{Y}$. At Tx side, there is no post-processing step.

The main steps of the systematic message exchange between Tx and Rx are illustrated in Figure 2.3 for the DDU and ECU operating modes, respectively, and are summarized below:

- Tx sends the training sequence to Rx with a Tx preamble;
- Rx reads the Tx preamble. Then, Rx selects the mode and the undersampling factor. The extracted samples and index set are fed back to Tx along the with Rx preamble;
- Tx reads the Rx preamble. Then, Tx recovers the full data by using a MC algorithm.

Figure 2.3 – Message exchange and processing between Tx and Rx for the DDU and ECU modes.

(a) In the DDU mode, a fraction of the received signal is sent by the receiver via a limited feedback channel.

(b) In the ECU mode, a fraction of the estimated channel is sent by the receiver via a limited feedback channel.

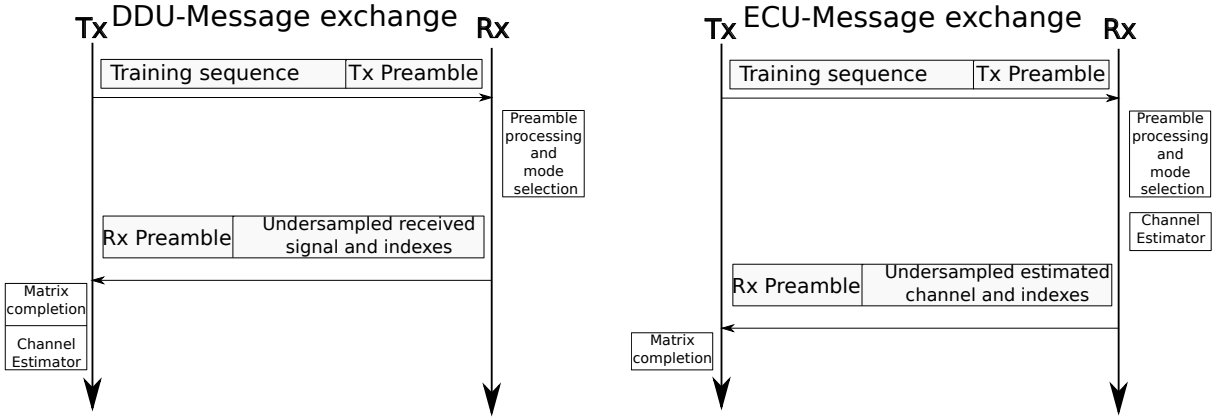

Source: Created by the author.

Basically, the preambles contain information about the pre-defined mode selection and undersampling factor, as described in Table 2.1. In Tx preamble a sequence of bits A = [A1, A2, A3] is used to choose between the DDU and ECU modes. A third mode, namely, full mode, is also covered, which coincides with the standard feedback scheme. The Rx preamble contains a sequence of bits B = [B1, B2, B3] to inform Tx what mode is in use. The bits A1 and B1 are reserved for extra modes and possible future implementations.

Note that the main difference between DDU and ECU modes is associated with the type of feedback data in Figure 2.4. Parameter T means the forward data time, T_f means the feedback data time, T_{us} is the time needed to begin the undersampling, τ is the total transmission interval, T_{DDU} and T_{ECU} stand for the data transmission time in DDU and ECU modes, respectively. In the DDU mode, the feedback data is the training sequence. Note that

in the DDU mode the Rx does not need to wait the reception of the entire incoming signal. On the other hand, in the ECU mode, the feedback data is the estimated channel. Thus, the Rx needs to wait the reception of the entire incoming signal to estimate the channel. Therefore, $T_{DDU} \geq T_{ECU}$.

Table 2.1 – Description of the Tx and Rx preamble.

Bits			**Downlink**	**Bits**			**Uplink**
A1	A2	A3	**Tx preamble**	B1	B2	B3	**Rx preamble**
	0	0	Full Mode - Defines that either DDU, ECU or full-CSI feedback (baseline) can be chosen, Rx selects the mode of operation.		0	0	Full Mode - Rx selects whether undersampling is used or not.
	0	1	DDU mode - Direct data undersampling, T_{us} is the time required for triggering the undersampling operation, i.e. the minimum value of T corresponds to the time required to read the preamble that defines the mode of operation.		0	1	DDU mode - Direct data undersampling.
	1	0	ECU mode - Estimated channel undersampling.		1	0	ECU mode - Estimated channel undersampling.

Source: Created by the author.

Figure 2.4 – Difference between DDU and ECU at the time.

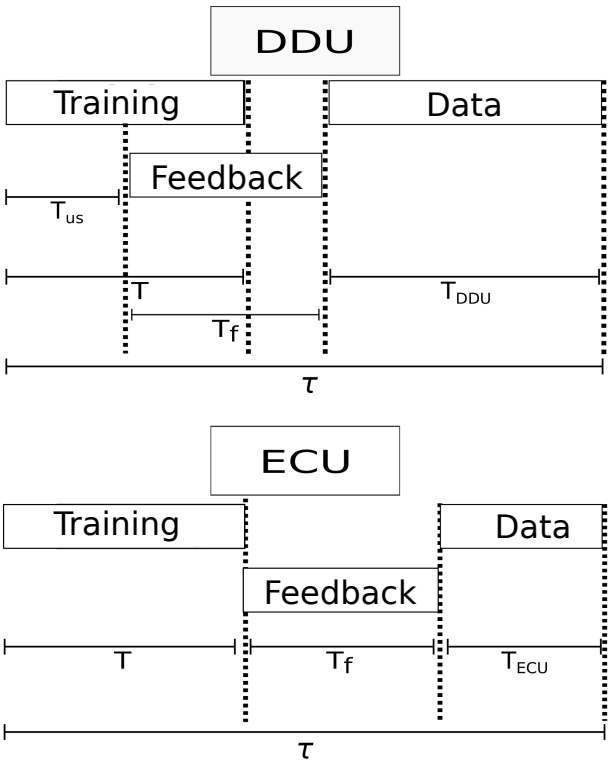

Source: Created by the author.

Remark 1 *The DDU mode has low computational complexity, low latency, and low energy consumption compared to the ECU mode, since it does not estimate the channel. If a full-duplex capability is available, that is more likely to be beneficial in the wireless backhaul scenario [2], Rx can feedback data to Tx while it is still receiving the signal* $\mathbf{Y}$*. Thus, Tx can obtain CSI more quickly and possibly use the time resources more efficiently by transmitting more data in the same data transmission interval, as illustrated in Figure 2.4. Besides, the computational burden associated with channel estimation is moved to the Tx side, which means that Rx saves energy as it does not need to estimate the channel* $\mathbf{H}$*. On the other hand, according to Equation* (2.1)*,* $\mathbf{Y}$ *contains an additive white noise term, which turns it a full-rank matrix. Even after a low-rank approximation within the matrix completion procedure, the reconstructed matrix* $\hat{\mathbf{Y}}$ *is still corrupted by the additive noise in the DDU mode, which is adverse for channel estimation. In other words, while the ECU estimates the channel directly from* $\mathbf{Y}$ *and reconstructs* $\hat{\mathbf{H}}$*, which is already a low-rank matrix, DDU makes use of low-rank approximations of* $\mathbf{Y}$ *to estimate the channel from a corrupted version of* $\mathbf{Y}$*.*

Remark 2 *The advantages and disadvantages of the two data feedback modes imply a tradeoff between DDU and ECU. It would be interesting to have a criterion to switch between modes whenever one is more advantageous than the other. For example, in a scenario of very high signal-to-noise ratio (SNR), DDU is no longer affected by noise and it would perform close to ECU (the simulation results confirm this claim). If the NMSE gap between both schemes is tolerable DDU might be preferable due to the considerable energy saving compared to ECU.*

In what follows, we illustrate the framework with two application examples: wireless backhauling and a clustered MU scenario.

2.4 Application Scenarios

In this section, we apply the proposed framework in two relevant scenarios. The first is a new problem imposed in massive MIMO systems with heterogeneous networks supporting a macro-cell layer with additional small cells, where wireless backhauling communications take place between the macro-BS and a micro-BS. The second one is related to MU channel estimation in a clustered MU massive MIMO system.

2.4.1 Application Scenario 1: Wireless backhauling

In dense cell deployments, wired backhaul becomes expensive or even infeasible due to the large number of network nodes to be connected. As an alternative to overcome this limitation, millimeter-wave wireless backhaul, e.g., in 60 GHz, can be adopted [73, 74, 75].

Here we assume a wireless backhaul system in which Tx and Rx are represented by a macro-BS and micro-BS, respectively. The Tx and Rx are equipped with massive MIMO arrays and operate in FDD. Figure 2.5 illustrates an application of the framework proposed in

Section 2.3.5 to the wireless backhauling scenario. In addition, we assume a small number of dominant scatterers and local scattering is limited. By the superposition of a few reflected signals, the channel matrix has low-rank and follows the model expressed in Equation (2.2). This is a typical assumption for channels in mmWave bands [76], i.e., there is a LOS path and only a few number of multipaths.

Figure 2.5 – Framework application in the wireless backhauling scenario. Two types of feedback data for the framework are presented. Tx is the macro-BS and Rx can be one or more micro-BSs equipped with massive MIMO arrays.

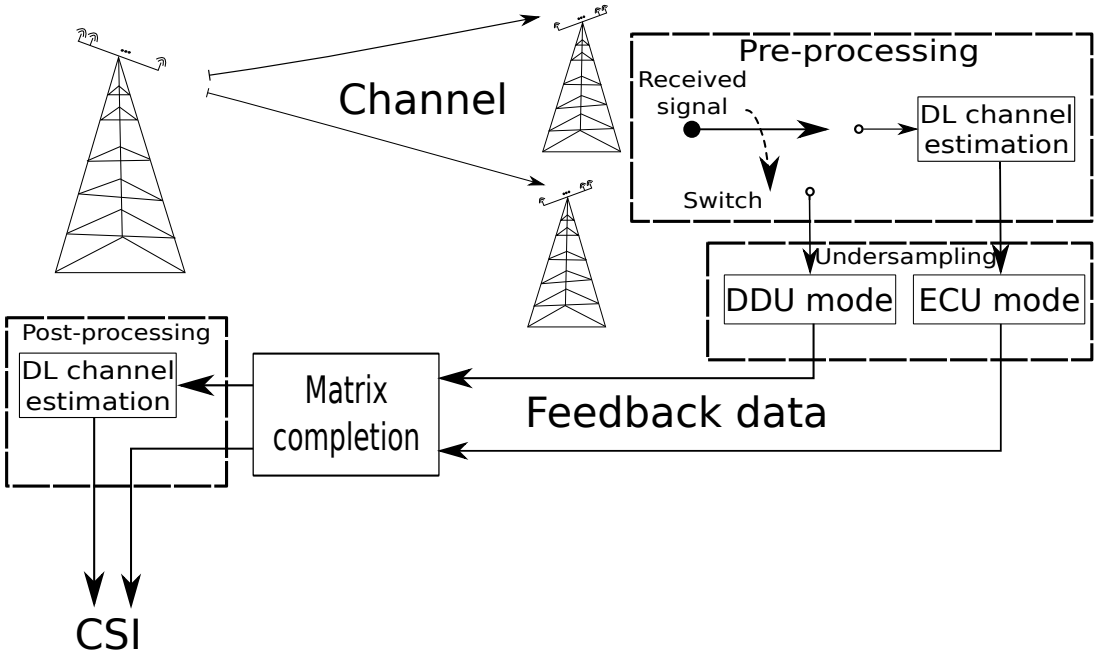

Source: Created by the author.

2.4.2 Application Scenario 2: MU

Consider a multi-UEs scenario where the UEs are spread across C_l spatial regions or clusters. We define a cluster as the association of the channel matrix with a spatial subspace. That is, UEs inside a cluster have approximately the same spatial channel. It worth mentioning that such clustered MU scenario can be exploited by scheduling and linear precoding schemes [16, 77, 78].

More specifically, let Tx be a massive BS equipped with M_T antennas, and let Rx denote K UEs equipped with M_R antennas each. Figure 2.6 shows the systemic view on how the proposed feedback and reconstruction framework can be applied in the MU scenario. We assume a poor scattering scenario with P specular multipaths, where $P \ll M_T$. Also, UEs are positioned close to one another in a way that UE clusters, which depend on the cluster spreading, can be formed. The UEs are spatially close to one another in a dense hot-spot area, and, thus, are grouped in a cluster.

Different from the wireless backhauling scenario, in the MU scenario the feedback data are spread over UE clusters. Note that each UE can operate in any mode. Thus, in order to

Figure 2.6 – This figure presents an application scenario in the MU scenario where each UE has a single (but not limited to) antenna. UEs are assumed to be close to one another (clustered UEs).

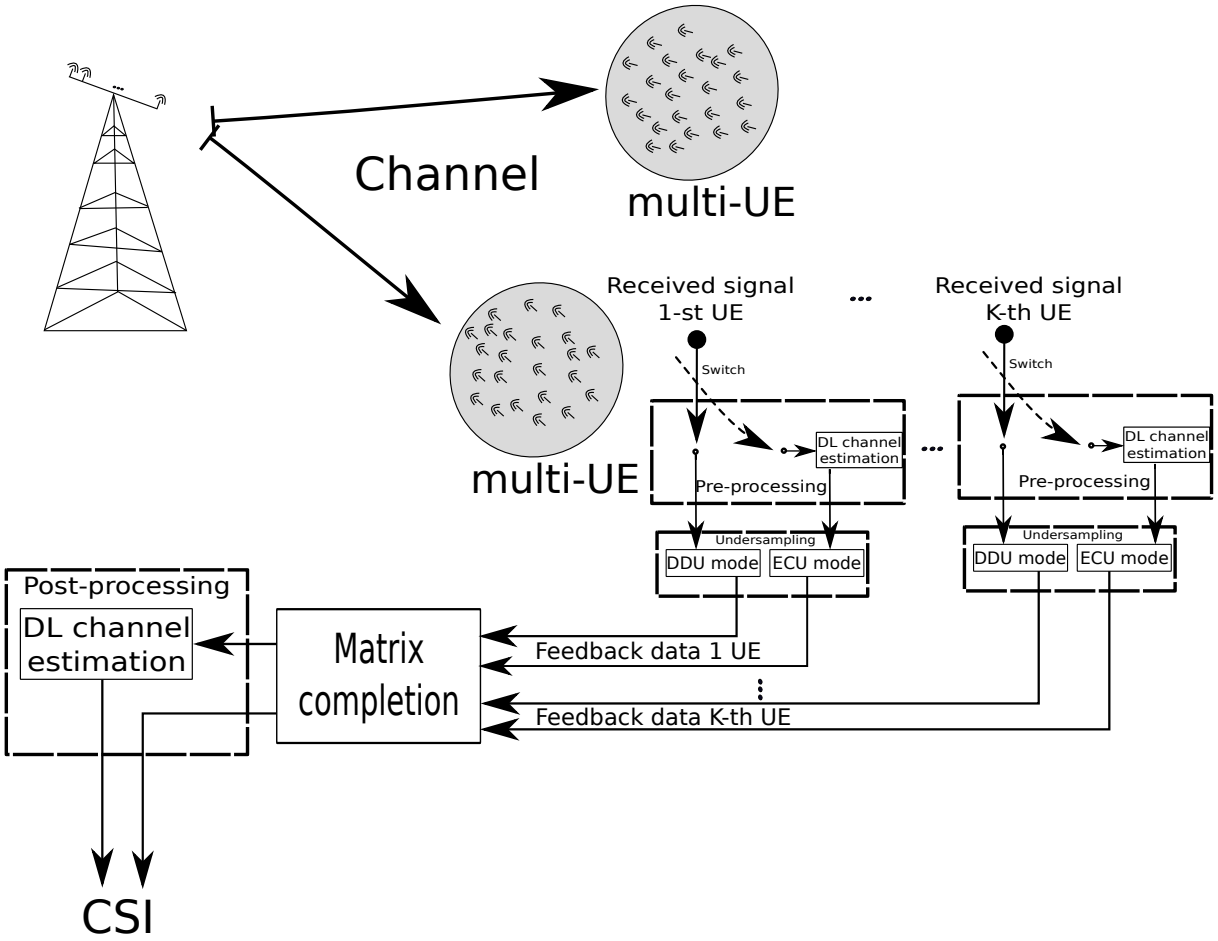

Source: Created by the author.

apply MC, BS folds all the received feedback data as a global matrix. We consider that the BS can separate each UE perfectly (i.e. no intra-cell interference). For building the global channel matrix, we follow the channel model described in Equation (2.2) so that

$$\mathbf{H}_T = [\mathbf{H}_1^T, \mathbf{H}_2^T, \ldots, \mathbf{H}_{C_lK}^T]^T \in C^{C_lKM_R \times M_T}.$$

The global received signal matrix is then given by

$$\mathbf{Y} = [\mathbf{Y}_1^T, \mathbf{Y}_2^T, \ldots, \mathbf{Y}_{C_lK}^T]^T \in C^{C_lKM_R \times N_T}$$

which concatenates the contributions from all UEs.

We consider that each cluster of UEs is far from the BS as showed in Figure 2.6, while the scattering cluster is near to the UEs. Thereby, the following model is adopted to describe the k-th UE channel matrix:

$$\mathbf{H}_k = \frac{1}{\sqrt{P}} \sum_{p=1}^{P} \alpha_p \mathbf{a}_r(\theta_p + \kappa_k)\mathbf{a}_t^T(\vartheta_p), \tag{2.29}$$

where κ_k represents the k-th UE angular deviation from the mean angle θ_p and is modeled as a zero-mean Gaussian random variable with variance σ_a^2 for each UE. The UEs resultant channels in each cluster are correlated, implying a low-rank global channel matrix [16, 19, 20].

Remark 3 *In MU massive MIMO, considering the physical finite scattering channel model of Equation* (2.29)*,* $\mathbf{H}$ *has a number of degrees of freedom* $r(M_T + M_R + K - r)$ *where* r *is the rank of* $\mathbf{H}_T$*,* $r = \min\{KM_R, C_lP, M_T\}$.

Since M_T and M_RK are larger than P, this model characterizes the small number of scattering propagation paths, where the scattering appear in groups (called clusters) with similar delays, AoAs and AoDs yielding an effective limited number of active directions, even if the number of physical objects is large [12]. Also, for other channel models, well known in the literature, such as the one ring model for uniform linear arrays (ULAs) [15], the limited number of scattering is observed, yielding a rank-deficient channel matrix [19].

For ECU, the matrix $\mathbf{Q}$ contains just a fraction of the matrix $\hat{\mathbf{H}}_T$. The BS can find $\mathbf{H}$ by solving the following problem:

$$\begin{aligned} \hat{\mathbf{H}}_T &= \arg\min_{\mathbf{X}} \ \|\mathbf{X}\|_* \\ &\text{s.t.: } P_{\mathbf{\Omega}}(\mathbf{X}) = P_{\mathbf{\Omega}}(\mathbf{Q}). \end{aligned} \tag{2.30}$$

In the DDU scheme, we exploit the low-rank structure of each compound channel matrix. In this mode, upon reception of the feedback information, the matrix $\mathbf{Q}$ contains just a fraction of the full matrix $\mathbf{Y}$. The reconstruction of received signal matrix $\hat{\mathbf{Y}}$ at the BS can be found by solving the relaxed problem:

$$\begin{aligned} \hat{\mathbf{Y}} &= \arg\min_{\mathbf{X}} \|\mathbf{X}\|_* \\ &\text{s.t.: } \|P_{\mathbf{\Omega}}(\mathbf{X} - \mathbf{Q})\|^2 \leq \epsilon, \end{aligned} \tag{2.31}$$

where the orthogonal projection $P_{\mathbf{\Omega}}(\mathbf{X} - \mathbf{Q})$ is defined in the same way as in Equation (2.11). After the reconstruction of $\mathbf{Y}$, the BS can apply the channel estimator to recover $\mathbf{H}$.

2.5 Simulation Results

In this section, we divide our simulations according to the two application examples discussed in the previous section. The reconstruction error of the full data matrix (DDU) is evaluated at a given Monte Carlo run, by computing the NMSE defined as $\|\mathbf{Y} - \hat{\mathbf{Y}}\|_F^2 / \|\mathbf{Y}\|_F^2$, where $\hat{\mathbf{Y}}$ is an estimate of the full data matrix. The NMSE results represent an average over 100 Monte Carlo runs, and are plotted as a function of the factor m. In this simulation, we assume the Tx is equipped with a ULA. A very accurate reconstruction is assumed when the NMSE is around 10^{-4} [39]. Performance evaluation are based on average NMSE versus SNR plots, NMSE versus undersampling factor m plots, BER versus SNR plots, and goodput (bit/s/Hz) versus SNR plots obtained by means of Monte Carlo runs.

Furthermore, the ECU scheme considers a MMSE channel estimator [79]. The transmitted symbols are mapped into the binary phase shift keying (BPSK) constellation and $N_T = M_T$. The estimated channel NMSE is calculated as: $\|\mathbf{H} - \hat{\mathbf{H}}\|_F^2 / \|\mathbf{H}\|_F^2$, in which $\hat{\mathbf{H}}$ is given by the MMSE estimator. The simulation results presented in this thesis are restricted to square dimensions in the target matrix. The reason for assuming square dimensions is because the MC technique always works well under square matrices in our simulations.

In this thesis, the motivation is to use the MC technique and the algorithms presented in the literature in the proposed framework (see Figure 2.2). Since the main differences in the algorithms are the formulation for the objective functions, we briefly describe them under the optimization variable $\mathbf{X}$ and the constrained undersampling to $P_{\mathbf{\Omega}}(\mathbf{X}) = P_{\mathbf{\Omega}}(\mathbf{Q})$. For the case which noise is present, the constraint follows $P_{\mathbf{\Omega}}(\mathbf{Q}) = P_{\mathbf{\Omega}}(\mathbf{H}) + P_{\mathbf{\Omega}}(\mathbf{N})$.

In singular value thresholding (SVT) algorithm, the idea is to use the singular value shrinkage operator [80] based on Uzawa's algorithm [81]. The objective function is written as:

$$\hat{\mathbf{Q}} = \arg\min_{\mathbf{X}} \ \tau_1 \|\mathbf{X}\|_* + \frac{1}{2}\|\mathbf{X}\|_F^2, \tag{2.32}$$

where τ_1 is the singular value thresholding. This algorithm is based on SVD with thresholding.

The fixed point continuation (FPC) algorithm described in [82] uses the connections with CS, under the vectorized version of matrix to solve the Lagrangian version of nuclear norm with the objective function written as follows:

$$\hat{\mathbf{Q}} = \arg\min_{\mathbf{X}} \ \lambda_1 \|\mathbf{X}\|_* + \frac{1}{2}\|\mathbf{A}(\mathbf{X}) - b\ \|_2^2, \tag{2.33}$$

for some $\lambda_1 > 0$, where $\mathbf{A} : \mathcal{R}^{n \times n} \mapsto \mathcal{R}^{1 \times n^2}$ is the matrix corresponding to the linear map $\mathcal{A}$ in a vector, $\mathcal{A}(vec\{\mathbf{X}\}) = \mathbf{b}$ is the projection of $\mathbf{X}$ onto the set of indices in $\mathbf{\Omega}$, where $\mathbf{b} \in \mathcal{R}^{1 \times 2n}$, and vec is vectorizing operator.

The grassman rank-one update subspace estimation (Grouse) is an algorithm based on subspace identification and tracking [83]. It can be seen as a similar algorithm for the spectral techniques presented in [39] with links for alternated minimization in [84]. Also, it can be understood as an adaptation of an incremental gradient procedure to update a QR or SVD decomposition, which the objective function is written as:

$$\hat{\mathbf{Q}} = \arg\min_{\mathbf{U}\Xi} \ \|\mathbf{U}\Xi - P_{\mathbf{\Omega}}(\mathbf{Q})\|^2, \tag{2.34}$$

where Ξ are the weights and $\mathbf{U}$ is any matrix whose columns spans $\mathbf{Q}$. Thus, given a $P_{\mathbf{\Omega}}(\mathbf{Q})$, we try to construct matrices $\mathbf{U}$ and $\boldsymbol{\Xi}$ so that $\mathbf{U}$ is unitary and $\mathbf{U}\boldsymbol{\Xi} \approx \mathbf{Q}$. The main difference to [39] is that the Grouse optimizes $P_{\mathbf{\Omega}}(\mathbf{Q})$ one column-by-column.

Furthermore, the objective function of the non-convex algorithm (NCon) is written as:

$$\hat{\mathbf{Q}} = \arg\min_{\mathbf{X}} \omega_1 \|\mathbf{X}\|_{p*}, \tag{2.35}$$

where $\|\cdot\|_{p*}$ is a nuclear norm minimization under a penalization p, meaning that p equals zero for rank and $p = 1$ for nuclear norm (convex). The ω_1 is a cooling parameter. The idea is use a

fractional value of p. The author shows an iterative solution to find this parameter by a cooling technique shown in [85]. The cooling algorithm consists of two iterative loops: the first solves the problem in the unconstrained form for a fixed ω_1, and the second reduces the value of ω_1.

The fast numerical hard threshold algorithm (FHT) and FST are fast algorithms based on iterative hard and soft thresholding. They are similar to the proximal algorithms in [86] targeting low-rank matrices and are characterized by fast converge. In the FHT algorithm, the objective function is written as:

$$\hat{\mathbf{Y}} = \arg\min_{\mathbf{X}} \ \omega_1 \,\mathrm{rank}(\mathbf{X}), \tag{2.36}$$

and for the FST algorithm, the objective function is written as:

$$\hat{\mathbf{Y}} = \arg\min_{\mathbf{X}} \ \omega_1 \|(\mathbf{X})\|_*. \tag{2.37}$$

For the unconstrained nuclear norm minimization problem using minimization split bregman (MSB) algorithm in [82], the objective function is written as:

$$\hat{\mathbf{Y}} = \arg\min_{\mathbf{X}} \ \omega_1 \|\mathbf{X}\|_* + \eta_1/2 \|\mathbf{X} - P_{\mathbf{\Omega}}(\mathbf{Q}) - \mathbf{B}_e\|_2^2, \tag{2.38}$$

where $\mathbf{B}_e$ are the Bregman relaxation variables and η_1 is a regularization parameter in MSB.

We set all these algorithms described above to have a tolerance regarding the singular values error is equal to 10^{-5}, and let the algorithms to run 500 iterations. Also, we assume that the rank is known and all algorithms have access to this information. For the SVT [80], parameter $\tau_1 = 5\sqrt{KM_RM_T}$, with stepsize equals $\frac{1.2}{\left(\frac{m}{M_T K M_R}\right)}$. In the Grouse [83], the stepsize is equal 0.1. In FPC [82], $\lambda_1 = 0.01$, and MSB [82] the regularization parameter $\omega_1 = \eta_1 = 0.001$. In FHT, FST and NCon [87] the parameter ω_1 is initialized with $= 0.7 \max(P_{\mathbf{\Omega}}(\mathbf{Q}))$ and updated by cooling algorithm iteratively. Furthermore, the NCon is chosen for the most simulations due to show a better performance under the NMSE measure. The main Matlab codes can be found in [88, 89].

Remark 4 *With relation to the use of these algorithms, we have adapted some of them to solve a general complex matrix set. The algorithms SVT, Grouse, FPC and spectral matrix completion (OptSpace) are originally proposed targeting real-valued matrices. Therefore, to use the aforementioned algorithms in complex-valued matrices, we split the MC reconstruction into two parts. At first, we apply MC on the real part, and after we treat the imaginary part as real one.*

2.5.1 Wireless Backhauling Scenario

Consider a system with $M_T = M_R$, where Rx is equipped with a ULA. Figure 2.7 describes a street scenario (e.g., wireless backhauling between a macro and a micro-BS). We consider a street with 10 meters width and 100 meters length. We assume P=5, which means that the channel matrix rank is equal to 5. The fading amplitude α_p in Equation (2.2) is calculated

using the path loss (PL) model adopted in [76, c.f. Table 1]. More specifically, it can be calculated as PL= $16\pi^2(\frac{R}{\xi})^{pe}$ for a given range distance R, wavelength ξ, and PL exponent n. The end-to-end distance is $R = 100$ meters, a carrier frequency of 60 GHz, and PL exponent $pe = 2.5$, representing a LOS scenario. The channel is composed by the sum of a LOS path and four non-LOS paths with one and two reflections according to Figure 2.7.

Figure 2.7 – Wireless backhaul scenario.

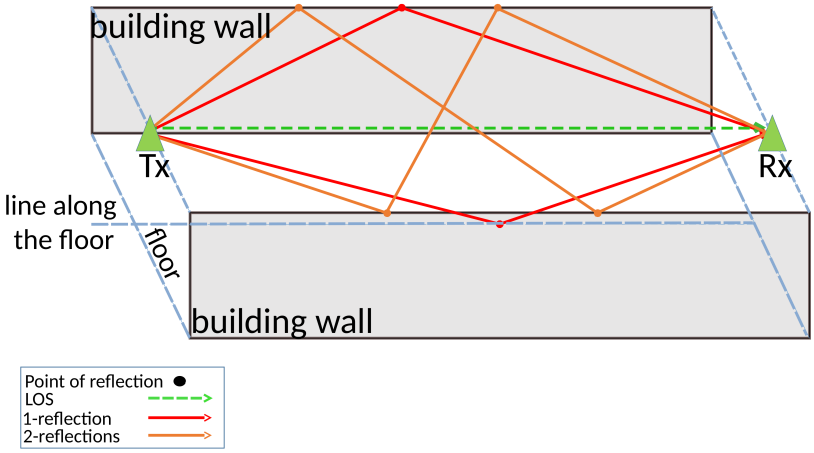

Source: Created by the author.

The simulation results are shown firstly considering that the channel matrix is perfectly known. In the next subsection, we present the simulation results considering the estimated channel. In Figures 2.8 to 2.11, we evaluate the cases when $M_T = M_R = 32$ and $M_T = M_R = 64$ antennas in ECU and DDU modes. Firstly, we evaluate the performance of all algorithms. In the end, we show the performance for the NCon algorithm. The relation between NMSE and number of antennas is presented in Figure 2.12. We evaluate the robustness of proposed MC approach considering the MMSE estimator in Figure 2.13 as a function of the antennas number. In the end, we provide in Figure 2.14 and Figure 2.15 the curves evaluating the BER and goodput with the MRT precoder for the case with $M_T = M_R = 32$.

2.5.2 ECU Recovery with Perfect Channel Knowledge

First, we consider the ECU under perfect channel knowledge at Rx and investigate the performance of the channel reconstruction. Figure 2.8 depicts the performance for $M_T = M_R = 32$ with ECU under a undersampling of factor $m \in [0.2; 0.6]$. Note that, in this scenario the FHT, SVT, FPC, OptSpace, and Grouse have low performance in terms of NMSE. The OptSpace for $m = 0.5$ yields an NMSE performance around 10^{-2}. As we have described in Remark 4, these algorithms are not developed to work with complex-valued matrices. The algorithms NCon, MSB and FST can achieve perfect recovery for $m = 0.35$, 0.4, and $m = 0.5$, respectively.

Figure 2.9 shows the ECU performance when $m \in [0.05; 0.3]$ and the number of antennas is increased to $M_T = M_R = 64$. As the preliminary simulation results presented in Figure 2.8, the algorithms FHT, SVT, OptSpace, FPC, and Grouse show poor performance

Figure 2.8 – Performance of NMSE results with ECU, $M_T = M_R = 32$ for all algorithms.

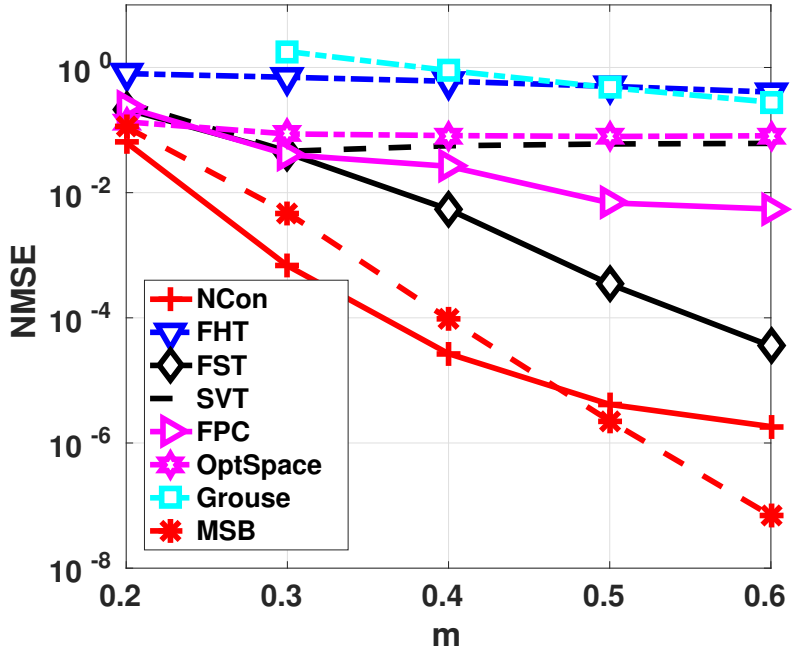

Source: Created by the author.

compared to the FST, NCon, and MSB in most of the results. Note that OptSpace and MSB begin at $m = 0.1$ since there was no output result with smaller values. In general, we can see that the matrix recovery accuracy improves as m increases. However, we can see that NCon algorithm has better performance than the others.

2.5.3 DDU Recovery with Perfect Channel Knowledge

Here, DDU is evaluated under perfect channel knowledge at the Tx. In the next section, both ECU and DDU modes will be compared under imperfect channel knowledge. We investigate the performance of the channel reconstruction with $M_T = M_R = 32$ and $M_T = M_R = 64$. In DDU, the simulation results are shown using only the NCon and FST algorithms, since our preliminarily results show that the other algorithms have poor performance. Figures 2.10 and 2.11 compare the performance for different undersampling factor m. Note that in both figures the algorithms have shown poor performance when SNR equals 10 dB. However, when the SNR is increased the NMSE is improved.

Finally, Figure 2.12 presents the NMSE performance while varying number of antennas using the NCon algorithm. We compare the ECU and DDU modes assuming SNR equals 30 dB. From Figure 2.12, we can see that the performance is improving while increasing the number of antennas, where the ECU always has better performance than DDU, since later mode's performance is limited by noise. Note that when $m = 0.3$, only 48 antennas are enough to achieve perfect reconstruction.

Figure 2.9 – NMSE results for ECU with $M_T = M_R = 64$ for all algorithms.

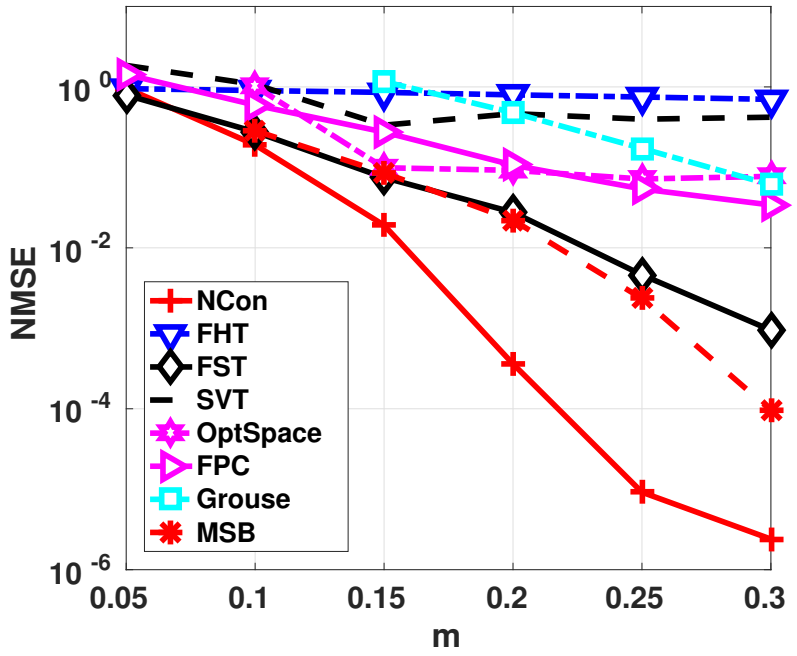

Source: Created by the author.

Figure 2.10 – Performance of NMSE results with DDU, $M_T = M_R = 32$ for $m \in [0.1; 0.7]$.
(a) NCon (b) FST

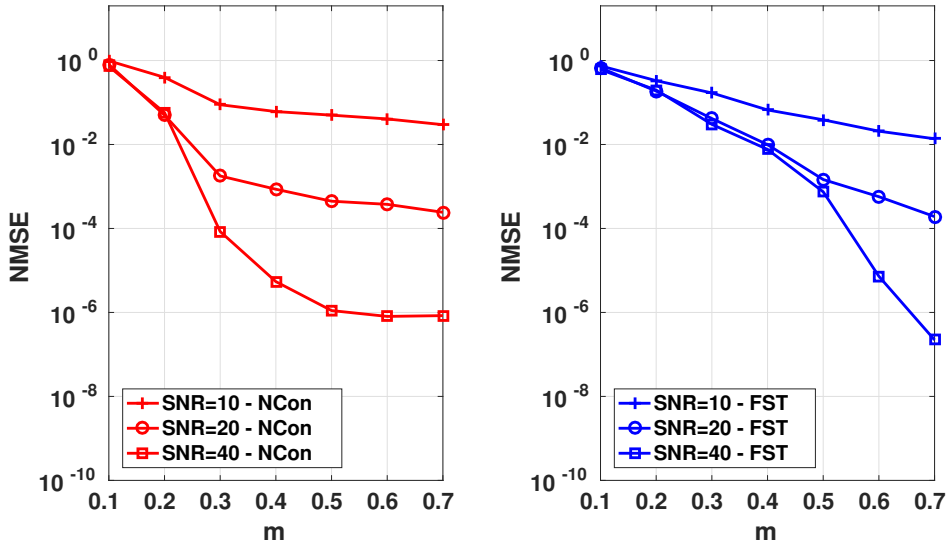

Source: Created by the author.

Figure 2.11 – Performance of NMSE results with DDU, $M_T = M_R = 64$ for $m \in [0.1; 0.7]$.
(a) NCon (b) FST

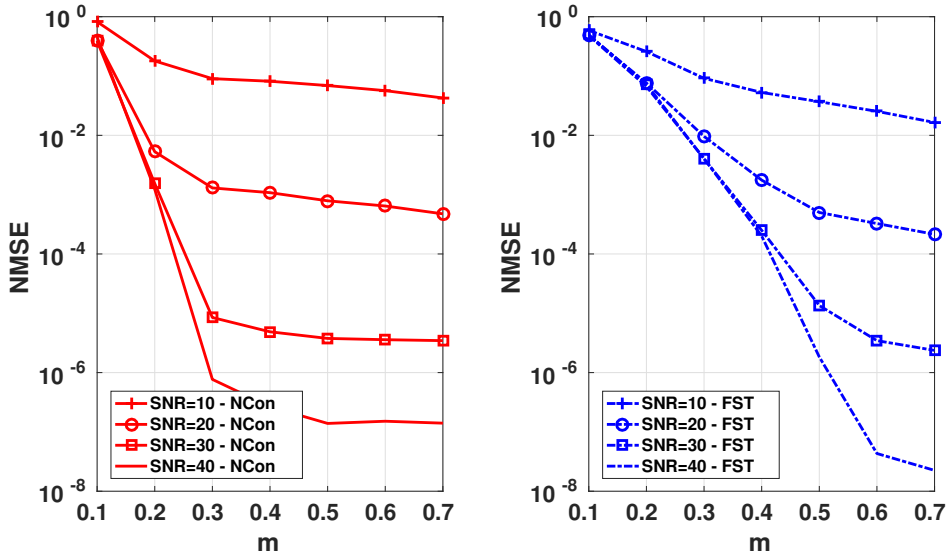

Source: Created by the author.

Figure 2.12 – NMSE performance for different antennas number for $m \in \{0.1,\ 0.2,\ 0.3\}$ for ECU and DDU with SNR equals 30 dB.

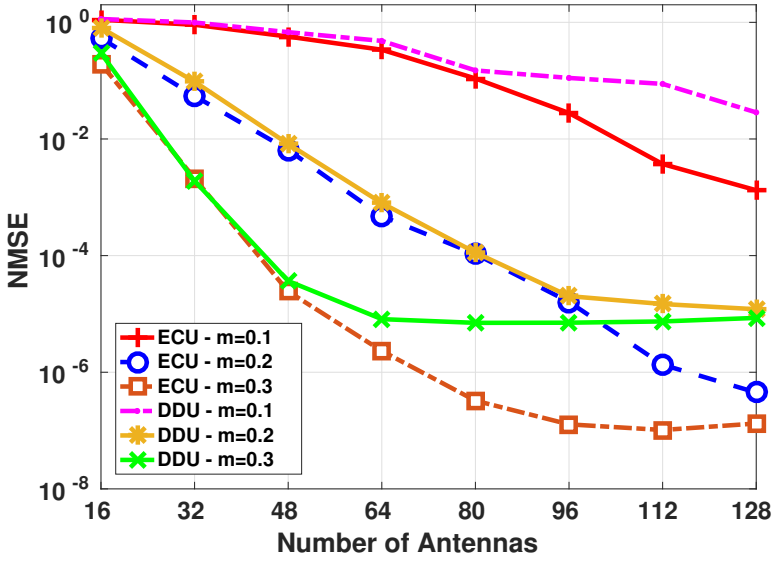

Source: Created by the author.

2.5.4 ECU and DDU Recovery with Imperfect Channel Knowledge

In the next simulation results, we consider the MMSE estimator and NCon algorithm. In Figure 2.13, the NMSE performance is evaluated. Compared to the Figure 2.12, these simulation results have showed a small performance loss for all m. For example, when $M_T = M_R = 48$, the NMSE in Figure 2.13 is equal to 10^{-4}, as compared to $10^{-4.5}$ in Figure 2.12, which indicates a performance loss of 11% for DDU mode. More simulation results are shown in Table 2.2 for $M_T = M_R \in \{32, 64\}$, $m \in \{0.1, \ldots, 0.7\}$, and SNR $\in \{10, 20, 30, 40\}$ dB. In this table, the data named MMSE means a lower bound since we are assuming conventional feedback i.e., $m = 1$.

Figure 2.13 – NMSE performance for different antennas number for $m \in \{0.1,\ 0.2,\ 0.3\}$ for ECU and DDU with imperfect channel knowledge.

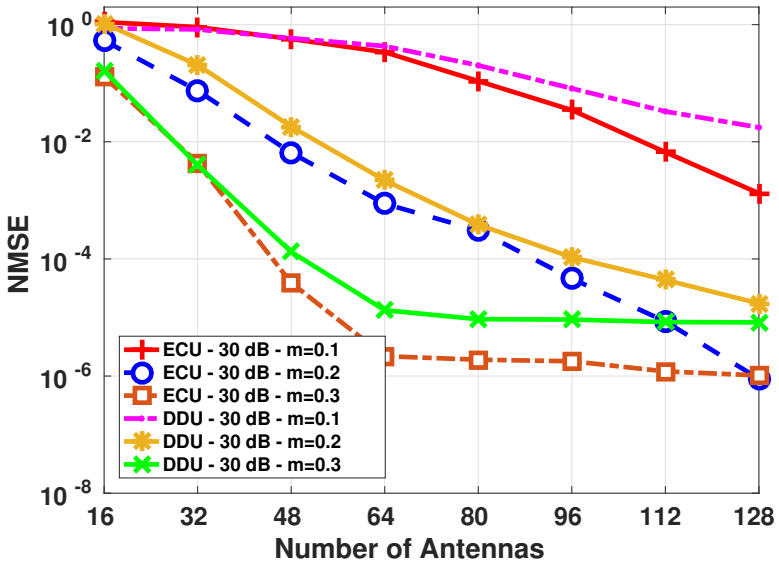

Source: Created by the author.

In Figure 2.14 and DDU in Figure 2.15, the BER evaluation considering the MRT is provided for $M_T = M_R = 32$ with ECU. Assuming that there is no channel coding at the transmitter, the channel is constant during a transmission block, and the noise is AWGN, the block error rate (BLER) can be expressed as a function of the BER of Figure 2.14 (a) following the formulation in [90, c.f. Chapter 3]:

$$\text{BLER} = 1 - (1 - \text{BER})^s, \tag{2.39}$$

where s is the number of transmitted symbols. In Figure 2.14 (b), we evaluate the goodput performance based on the BLER [91, 92] for a different fraction of estimated channel: where goodput$= s(1 - \text{BLER})$. The symbols are mapped in BPSK modulation, assuming $s = 100$ symbols per frame.

Figure 2.14 (a) shows the BER performance comparing different undersampling factors. Note that the full-performance ($m = 1$) is reached when $m = 0.3$. Hence, since in Figure 2.14 (b) the goodput is shown with respect to the BER, $m = 0.3$ and SNR equal to 14 dB

Table 2.2 – Performance of NMSE results with ECU and DDU , $M_T = M_R = 32$ and 64 for NCon algorithm.

$M_T = M_R = 32$									
SNR (dB)	m	0.1	0.2	0.3	0.4	0.5	0.6	0.7	MMSE
10	NMSE-ECU	$10^{-0.5}$	$10^{-1.5}$	10^{-2}	10^{-2}	10^{-2}	10^{-2}	10^{-2}	10^{-2}
	NMSE-DDU	$10^{-0.5}$	10^{-1}	10^{-1}	10^{-1}	10^{-1}	10^{-1}	10^{-1}	
20	NMSE-ECU	$10^{-0.5}$	10^{-2}	10^{-3}	$10^{-3.5}$	$10^{-3.5}$	$10^{-3.5}$	$10^{-3.5}$	$10^{-3.5}$
	NMSE-DDU	10^{-1}	$10^{-1.5}$	10^{-2}	$10^{-2.5}$	10^{-3}	10^{-3}	10^{-3}	
30	NMSE-ECU	$10^{-0.5}$	10^{-2}	10^{-3}	$10^{-4.5}$	$10^{-4.5}$	10^{-5}	10^{-5}	$10^{-5.5}$
	NMSE-DDU	10^{-1}	$10^{-1.5}$	10^{-3}	10^{-4}	$10^{-4.5}$	$10^{-4.5}$	10^{-5}	
40	NMSE-ECU	$10^{-0.5}$	10^{-2}	10^{-3}	$10^{-5.5}$	$10^{-5.5}$	10^{-6}	10^{-6}	$10^{-6.5}$
	NMSE-DDU	10^{-1}	$10^{-1.5}$	10^{-3}	10^{-5}	$10^{-5.5}$	10^{-6}	10^{-6}	
$M_T = M_R = 64$									
SNR (dB)	m	0.1	0.2	0.3	0.4	0.5	0.6	0.7	MMSE
10	NMSE-ECU	10^{-1}	10^{-2}	10^{-2}	10^{-2}	10^{-2}	10^{-2}	10^{-2}	10^{-2}
	NMSE-DDU	$10^{-0.5}$	10^{-1}	10^{-1}	10^{-1}	10^{-1}	10^{-1}	10^{-1}	
20	NMSE-ECU	10^{-1}	10^{-3}	10^{-3}	10^{-4}	10^{-4}	10^{-4}	10^{-4}	10^{-4}
	NMSE-DDU	$10^{-0.5}$	10^{-2}	$10^{-2.5}$	$10^{-2.5}$	10^{-3}	10^{-3}	$10^{-3.1}$	
30	NMSE-ECU	10^{-1}	$10^{-3.5}$	10^{-5}	10^{-5}	$10^{-5.5}$	$10^{-5.5}$	$10^{-5.5}$	10^{-6}
	NMSE-DDU	10^{-1}	$10^{-3.5}$	$10^{-4.5}$	$10^{-4.}$	10^{-5}	10^{-5}	$10^{-5.5}$	
40	NMSE-ECU	10^{-1}	10^{-4}	10^{-5}	10^{-6}	$10^{-6.5}$	$10^{-6.5}$	$10^{-6.5}$	$10^{-7.5}$
	NMSE-ECU	10^{-1}	$10^{-3.5}$	10^{-5}	10^{-6}	$10^{-6.5}$	$10^{-6.5}$	$10^{-6.5}$	

Source: Created by the author.

are enough for obtain full-performance for the MRT. This means that the MRT is robust against the reconstruction error. Notice that the low goodput performance for SNR values below 8 dB is due to the high BLER values. In Figure 2.15, we show the simulation results of DDU. In this mode, we can see that having $m = 0.3$ is enough to reach the full-performance, i.e., when $m = 1$.

Figure 2.14 – Performance $M_T = M_R = 32$ with ECU.
(a) BER versus SNR results. (b) Goodput versus SNR.

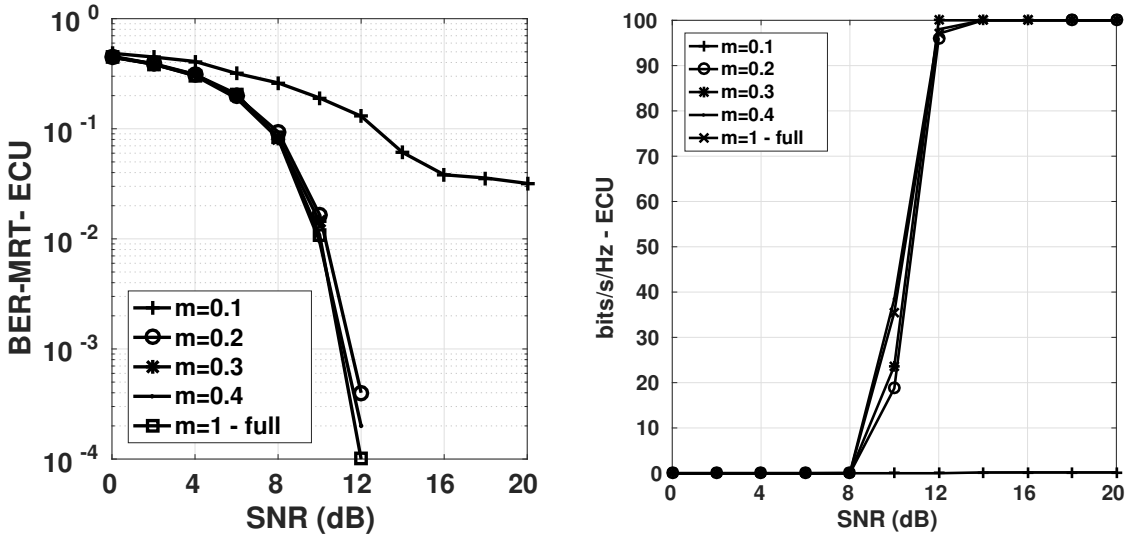

Source: Created by the author.

Figure 2.15 – Performance $M_T = M_R = 32$ with DDU.

(a) BER versus SNR results. (b) Goodput versus SNR.

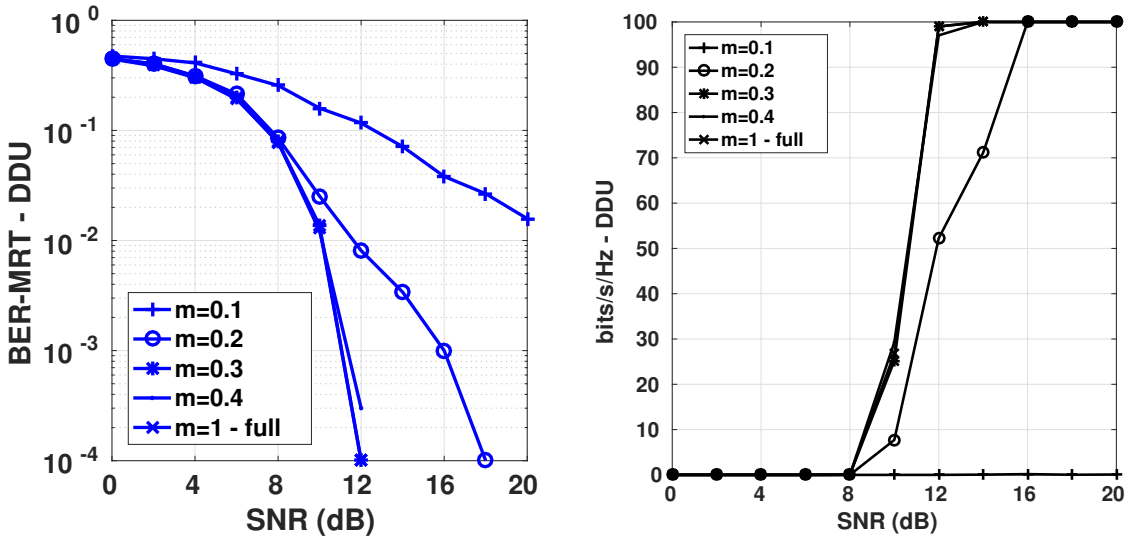

Source: Created by the author.

2.5.5 MU Scenario

In this section, we evaluate the performance of the proposed schemes, considering the Tx as BS equipped with $M_R = 100$ and the Rx as K UEs with the same number M_R of antennas. For instance, assuming $C_l = 2$, Fig. 2.6 means that we are considering two independent clusters of multi-UEs. We assume $P = 1$, and the angular deviation κ_k of each UE has a variance $\sigma_a^2 = 5$.

Figure 2.16 – Performance for the channel recovery with ECU for UE with $M_R = 100$.

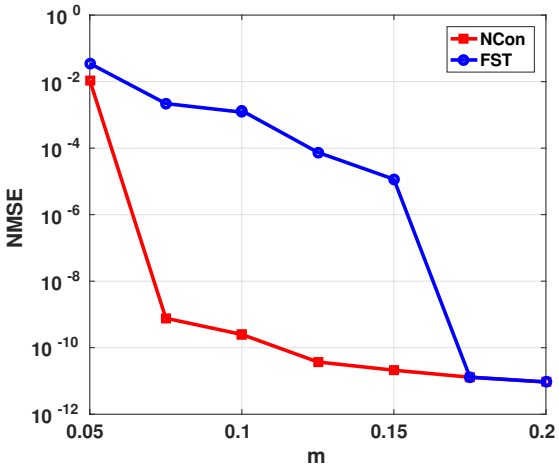

Source: Created by the author.

In the first simulation, we consider an example in a scenario to future implementations (for instance, a mmWave communication), in which, the UE and BS have the same number of antennas. In this case, we generate the correlated channel with $K = C_l = 1$, yields rank one.

Figure 2.16 shows the performance of the ECU to $M_T = M_R = 100$. Note that ECU converges with $m \leq 0.1$ to perfect recovery, saving more than 90% of feedback information. In this case, the NCon algorithm has better performance results to $m = 0.1$.

Figure 2.17 – Performance for the channel recovery with the ECU, $K = 5$, $M_R = 10$, and $C_l = 2$ (rank=2).

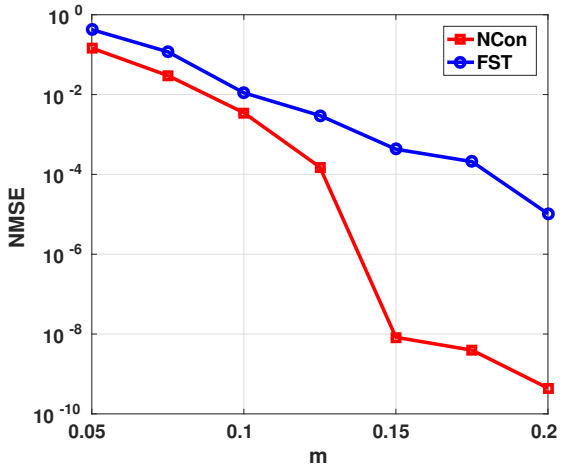

Source: Created by the author.

Figure 2.17, we consider a scenario with $K = 5$, $M_R = 10$ and $C_l = 2$ (rank=2). The performance results showed that ECU can recover the channel matrix with perfect reconstruction in $m = 0.1$, i.e., less of 10% of the feedback when NCon is used. Note that compared to Figure 2.16, the performance is worse for $m = 1$ for both algorithms due to rank is equal to 2. However, the NCon achieves perfect reconstruction. FST can achieve the perfect reconstruction with $m = 0.25$.

Figure 2.18, we compare the performances of ECU and DDU. In this case, we limit the results to FST. Observe that DDU has a reasonable recovery (NMSE=10^{-3}) requiring at least SNR $\geq$ 20 dB and $m = 0.3$. Specifically, it achieves the perfect reconstruction with SNR = 40 dB and $m = 0.35$.

In order to evaluate the performance and robustness of the proposed framework under a practical scenario, we consider a controlled error in the CSI and the MRT precoder [48]. The imperfect CSI is modeled as $\hat{\mathbf{H}} = \mathbf{H} + \mathbf{E}$, where $\mathbf{E} \approx \mathcal{N}(0, \sigma_e^2)$ and $\sigma_e^2 \in \{0.1, 0.05, 0.01\}$. Firstly, let us show the results for the imperfect CSI in Figure 2.19. Under a lower level of channel estimation error ($\sigma_e^2 = 0.01$), the performance is the same of the perfect channel. Under $\sigma_e^2 \in \{0.05, 0.1\}$, the performance losses when BER is equal to 10^{-2} become 2 dB and 5 dB, respectively.

In Figure 2.20, we show the BER performance of MRT applying ECU with $K = 10$, $M_R = 1$ and $C_l = 10$ (rank=10). We provide simulation results to $m \in \{0.1,\ 0.2,\ 0.3,\ 1\}$. The performance of the algorithm to very accurate reconstruction is achieved with $m = 0.3$ which is when the performance of the proposed framework with MRT is the same as that of an accurate

Figure 2.18 – Performance for the recovery with DDU and ECU using FST, $K = 20$, $M_R = 1$, and $C_l = 5$ (rank=5).

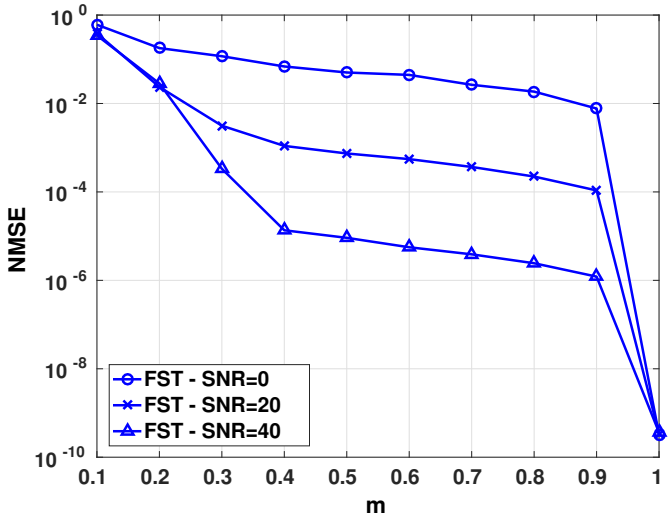

Source: Created by the author.

Figure 2.19 – Performance for the MRT precoding with estimated channel error, 10 UE, $M_R = 1$, and $C_l = 10$ (rank=10).

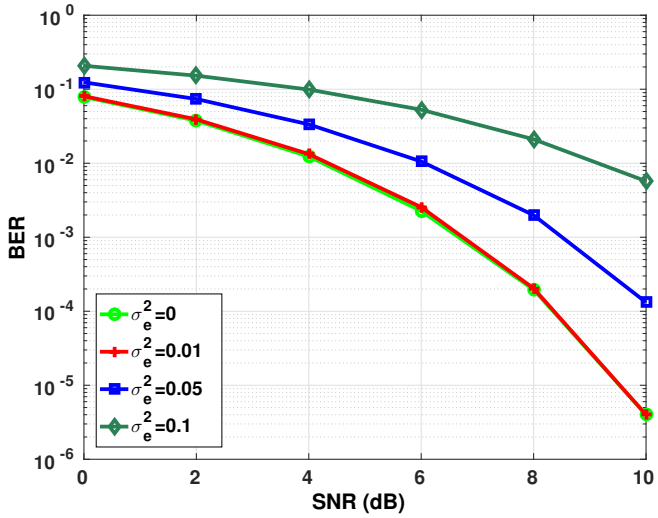

Source: Created by the author.

CSI. When $m \in \{0.1,\ 0.2\}$ the performance loss compared to the full channel feedback is equal to 2.5 dB and 17.5 dB for a BER of 10^{-3}, respectively.

Figure 2.20 – Average BER performance for the channel recovery with ECU, $K = 10$, $M_R = 1$, and $C_l = 10$ (rank=10).

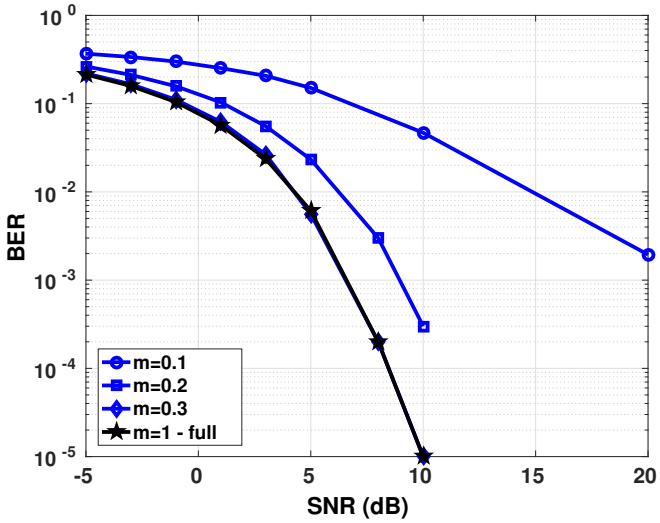

Source: Created by the author.

Following the same evaluation of the last scenario, the BLER in Equation (2.39), in Figure 2.21, we show the goodput based on the BLER for different undersampling factors. The

Figure 2.21 – Comparison for the goodput, 10 UE, $M_R = 1$, and $C_l = 10$ (rank=10).

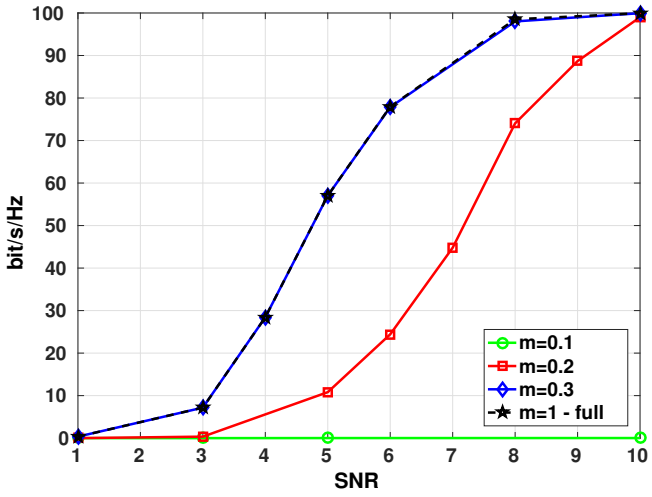

Source: Created by the author.

symbols are mapped onto a BPSK constellation, and $s = 100$ symbols per frame is assumed. At $m = 0.1$, the goodput is almost zero due to high BLER. At $m = 0.2$, we can achieve full goodput only with SNR=10 dB. Furthermore, when $m = 0.3$, the performance results are as that of full feedback channel $m = 1$.

As we can see in Figure 2.20, $m = 0.3$ is enough to achieve full performance. Thus, since Figure 2.20 is related to the goodput of Figure 2.21, we conclude that in this scenario, the proposed CSI reconstruction method achieves the ideal goodput performance with only $m = 0.3$, which is a remarkable result.

Considering the Figure 2.19 and 2.20, we evaluate the proposed framework with ECU, under imperfect CSI, applying MRT with $m \in \{0.1,\ 0.2,\ 0.3,\ 0.4\}$. The results are shown in Figure 2.22 and compared to the perfect CSI ($\sigma_e^2 = 0$). With $m = 0.3$, the BER performance is the same as the estimated channel error $\sigma_e^2 = 0.01$. Thereby, even under imperfect CSI, 70% of feedback data is saved. When $\sigma_e^2 = 0.05$, the estimation error is increased, and thereby, the performance loss is about 2 dB. For $m = 0.4$, the loss of performance is around 1 dB. For $m = 0.2$, the average BER performance has the same loss as in Figure 2.19 until $\sigma_e^2 = 0.01$. When the error of estimation is increased to $\sigma_e^2 = 0.05$, the loss of performance is around 3 dB. Thereby, $m = 0.2$ is enough to the average BER performance be close to the case on full-feedback as showed the Figure 2.19.

Figure 2.22 – Average performance for the BER with estimated channel error, $K = 10$, $M_R = 1$, and $C_l = 10$ (rank=10).

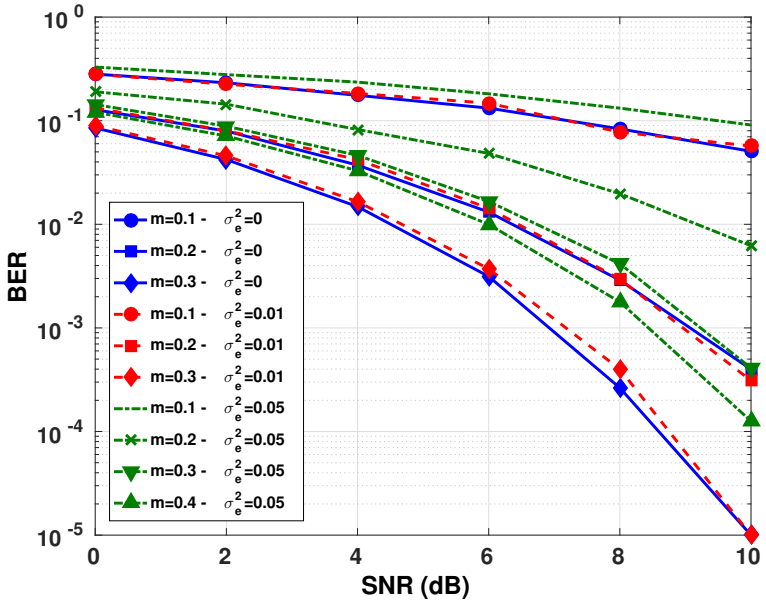

Source: Created by the author.

2.6 Summary

This chapter pointed out some fundamentals of MC and an application on massive MIMO. We proposed the framework to channel feedback and reconstruction in the massive MIMO systems that are important to the context of this thesis. The chapter contains original contributions which are the development of two application cases. Then, we have provided results suggesting that matrix completion can be used in FDD-based massive MIMO systems

to reduce the amount of feedback information to be sent to the BS into a low rank channel. Our numerical results have shown that matrix completion algorithms can achieve an accurate recovery of the downlink channel with a small feedback overhead. Consequently, the proposed scheme cope with limited-capacity uplink feedback channels. Due to undersampling at the UEs, energy consumption can be reduced to lower levels compared with the conventional full-rate sampling case. These benefits are possible thanks to the low-rank structure of the channel matrix, which happens in a massive MIMO scenario characterized by finite scattering propagation.

In the next chapter, we propose a novel precoding scheme based on knowledge of the CSI at the BS.

3 LOW-COMPLEXITY HEURISTICS TO BEAM SELECTION AND RATE ADAPTATION

In this chapter, we propose a novel formulation for a precoder design considering a practical rate assignment based on the MCS of the LTE table, beam selection, and power optimization, that exploits the geometric sparsity of the MU massive MIMO channel.

3.1 Motivation

In massive MIMO, the systems have potential to achieve high data rates and its robustness against interference, fading, hardware imperfections and failure [4]. When the number of antennas grows towards infinity, the effect of additive noise decreases, as well as the required transmitted energy per bit [5]. However, when the number of BS antennas is moderate, interference among MUs appears and has to be effectively handled. Under the MU perspective, these systems have a huge potential to decrease power consumption and to improve the communication system performance [9]. Transmit beamforming is one of the techniques that achieves enhanced performance in MU massive MIMO systems, determining the complex antenna gains that optimize some performance criterion, e.g., sum rate.

Recent studies have demonstrated that, as the spatial dimension increases, physical MIMO channels exhibit poor scattering [11, 18, 22, 23]. This particularly is the case in macrocell urban environments, where the propagation links between the UE and BS are often blocked by large buildings or when clusters of multipaths are shared by the same UEs [93, 94, 95].

In this context, it is important to develop transmit beamforming (or precoder) in the sparse scenarios when the number of BS antennas is large and the interference among MU is one bottleneck of the system.

3.2 Main Contributions

Assuming knowledge of the beamspace channel, the beamspace precoder consists of selecting and optimizing the power of the beams steered to the MU in order to maximize the SINR at the UE. In the analysis, we consider two different channel models. Furthermore, we propose low-complexity heuristics to beam selection and rate adaptation in sparse massive MIMO system and the contributions are summarized as follows:

- We propose a precoder design considering a practical rate assignment (based on the MCS of the LTE table), beam selection, and power optimization that exploits the geometric sparsity of the MU massive MIMO channel using its beamspace representation. We show an optimal solution to capacity following the MRT principle combined with beam selection, called MRT with selection.

- We design a new heuristic to simplify the beam selection and power optimization procedure based on Lagrangean relaxation [96].
- We show that, for a sparse channel, performance improvements can be achieved by selecting the proper beams followed by MRT beamforming on these beams. In the end, we propose three additional simple heuristics with low-complexity to beam selection in the beamspace domain. For these heuristics, we solve the problem in two steps: i) selection of beams based on the MRT, ii) power allocation per UE. The first heuristic uses MRT as an initial point and removes beams whose removal increases the SINR. The second heuristic sequentially assigns single beams to UEs using a sub-optimal solution provided by the Munkres algorithm [97]. The third heuristic takes the previous heuristic as an initial point, then allocates more beams, provided that this allocation improves the SINR. We show that adding and/or removing some beams improves the system performance. Simulation results show that our optimal solution can achieve a better performance than the ZFBF scheme. Besides, compared to the linear MRT precoder, the proposed low-complexity heuristics improve the performance under a scenario with channel sparsity.

3.2.1 Organization

This chapter is organized as follows: In Section 3.3, some preliminaries on transmit beamforming are presented. Section 3.4 presents the system model and the main assumptions. Section 3.5 presents the problem formulation and the proposed heuristics. In Section 3.7, simulations results are shown. Finally, Section 3.8 brings some concluding remarks and perspectives.

3.3 Background

Transmit beamforming structures have been analyzed by the authors of [9]. In particular, they show that optimal beamforming can be seen as a tradeoff between MRT, which is optimal in the absence of interference, and ZFBF, that cancels the multi-user interference (MUI). In this latter case, the ZFBF implies a significant computational complexity compared to the MRT [9].

In [98], classical beamforming is defined as a single steering vector of interest where the aim is to ensure that of the inner product between beamforming weight vector and the steering vectors of interest be large, whereas the inner product of the beamforming weight vector and all other steering vectors is small, i.e., to mitigate interference. It is applied to both receive beamforming and unicast transmit beamforming for a single receiver. For MU transmit beamforming in the downlink case, when the transmitter has multiple antennas, multiple transmit beamforming weight vectors are designed to carry different cochannel unicast transmissions, each meant to reach the receiver of different UE. These vectors are created to balance the interference between different transmissions. This concept was introduced in [99], where some

downlink beamforming techniques have been developed. In [100], convex optimization methods are introduced to solve the problem.

Along the last years, several works have investigated precoding schemes, as in [95, 101, 102, 103, 104]. In [95], the sparsity property of the MU channel matrix is exploited to obtain a sparse approximate inverse. However, this scheme still requires many operations to compute a matrix inverse. A way to lower complexity is proposed in [101], where the authors propose a beam domain multiple access (BDMA) transmission scheme in which MU are served by different beams. These beams are the eigenvectors of the channel matrix. The BDMA algorithm exploits the channel coupling matrices of a stochastic MIMO channel model [105]. When considering the so-called virtual channel [106], the matrices collecting the eigenvectors are discrete fourier transform (DFT) matrices. In this case, the beams are fixed and do not depend on the channel. Although BDMA is near optimal, it does not consider the sparsity of the beam domain channel and does not allow to schedule more than one UE per transmitting beam. In [102], a low-complexity transceiver design was proposed, namely semi-random beam pairing (SRBP), for sparse multipath massive MIMO channels [106]. The idea is to transmit simultaneous data streams, and in the end, to decouple them using successive interference cancellation (SIC). However, it is well known that SIC can propagate errors, mainly if the number of streams is large.

In the search for low complexity solutions, the authors in [103] proposed a precoder design, based on the maximization of the minimum SINRs perceived by MUs, under an equal quality of service (QoS) constraint. This max-min formulation leads to a quasi-convex optimization problem that can be solved by a low complexity algorithm based on relaxation techniques. One way to achieve maximum sum rate in a practical scenario is considering to joint optimize MCSs and transmit beamforming [104, 107]. In these approaches, the rate adaptation consists in assigning MCSs for MUs (for example, according to the 3rd Generation Partnership Project (3GPP) LTE table provided in [72], c.f., Chap. 5). In general, this formulation leads to a MILP problem. In most cases, it is impractical to real systems due to its high computational complexity.

3.4 System Model and Assumptions

In this section, we introduce the system model and some general assumptions for two different channel models based on beam domain channel representation. Furthermore, we address the beam selection problem.

3.4.1 General Definitions

Consider a downlink scenario composed of a single massive MIMO BS with M_T transmit antennas and K UEs, each one being equipped with a single antenna. We assume that all UEs share the same time-frequency resource and that the BS has the knowledge of the channel.

We model the received signal y_k, with $k \in \{1, \ldots, K\}$, at the k^{th} UE as:

$$y_k = \mathbf{h}_k^H \left(\mathbf{w}_k x_k + \sum_{i \neq k}^{K} \mathbf{w}_i x_i \right) + n_k, \tag{3.1a}$$

$$= \mathbf{h}_k^H \mathbf{W}\mathbf{x} + n_k, \quad k \in \{1, \ldots, K\}, \tag{3.1b}$$

where n_k represents the additive noise at the receive antenna, which is complex Gaussian with zero mean and variance σ_n^2; $\mathbf{h}_k \in C^{M_T \times 1}$ is the multiple-input-single-output (MISO) channel, and $\mathbf{w}_k \in C^{M_T \times 1}$ is the k^{th} UE precoder.

Writing the emitted symbol vector as $\mathbf{x} = \begin{bmatrix} x_1 & \ldots & x_K \end{bmatrix}^{\mathrm{T}}$, the precoder matrix $\mathbf{W}$ is given by $\mathbf{W} = \begin{bmatrix} \mathbf{w}_1 & \ldots & \mathbf{w}_K \end{bmatrix} \in C^{M_T \times K}$ as in Equation (3.1b). The global received signal taking into account all UEs is given by:

$$\mathbf{y} = \begin{bmatrix} y_1 & \ldots & y_K \end{bmatrix}^{\mathrm{T}} = \mathbf{H}^H \mathbf{W}\mathbf{x} + \mathbf{n}, \tag{3.2}$$

where $\mathbf{n} = \begin{bmatrix} n_1 & \ldots & n_K \end{bmatrix}^{\mathrm{T}} \in C^{K \times 1}$ is the global noise vector, and $\mathbf{H} = \begin{bmatrix} \mathbf{h}_1 & \ldots & \mathbf{h}_K \end{bmatrix} \in C^{M_T \times K}$ is the channel matrix.

Following [21, 106, 108], the so-called virtual channel representation is written as:

$$\mathbf{h}_k = \mathbf{A}_T \mathbf{g}_k \in C^{M_T \times 1}, \tag{3.3}$$

where $\mathbf{g}_k \in C^{M_T \times 1}$ is the beam domain channel vector of the virtual channel, $\mathbf{A}_T \in C^{M_T \times M_T}$, is the array steering matrix given by

$$\mathbf{A}_T = \begin{bmatrix} \mathbf{a}_T(\theta_0) & \ldots & \mathbf{a}_T(\theta_{M_T - 1}) \end{bmatrix} \in C^{M_T \times M_T}, \tag{3.4}$$

which can be set up as a DFT matrix, is given by:

$$\mathbf{a}_T(\theta) = \frac{1}{\sqrt{M_T}} \begin{bmatrix} 1 & e^{-j2\pi\theta} & \ldots & e^{-j2\pi\theta(M_T - 1)} \end{bmatrix}^{\mathrm{T}},$$

where $\theta = d\frac{\sin(\phi)}{\chi}$ is the azimuth spatial frequency, ds is the antenna spacing and ξ is the wavelength. The angle ϕ measures the angle between the impinging ray and the normal to the array. Note that we assume the same array steering matrix $\mathbf{A}_T$ for all UEs. This assumption reduces the complexity of the model and it is known that the channel for each UE can be represented using the same basis when M_T is sufficiently large [15, 17, 18, 101].

Following [23, 109] the extension for a rectangular uniform planar array (UPA) using the same DFT matrix for all UEs can be done. However, a Kronecker product is used to represent the azimuth and elevation spatial frequencies in two dimensional arrays [23]. Furthermore, the array structure does not affect the precoder design (based on beam selection). Consequently, other bases and array structures can be used to represent the channel.

Rewriting Equation (3.1) with Equation (3.3), we obtain:

$$y_k = \mathbf{g}_k^H \mathbf{A}_T^H \mathbf{w}_k x_k + \mathbf{g}_k^H \mathbf{A}_T^H \sum_{i \neq k}^{K} (\mathbf{w}_i x_i) + n_k, \tag{3.5}$$

so that the received signal for all UEs can be written as follows:

$$\mathbf{y} = \mathbf{G}^H \mathbf{A}_T^H \mathbf{W}\mathbf{x} + \mathbf{n}, \tag{3.6}$$

where $\mathbf{G} = \begin{bmatrix} \mathbf{g}_1 & \dots & \mathbf{g}_K \end{bmatrix} \in C^{M_T \times K}$. Considering unit-power uncorrelated symbols ($\mathcal{E}\left\{\mathbf{x}\mathbf{x}^H\right\} = \mathbf{I}_K$) the SINR_k at the k-th UE can be expressed as:

$$\text{SINR}_k = \frac{|\mathbf{h}_k^H \mathbf{w}_k|^2}{\sum\limits_{i \neq k}^{K} |\mathbf{h}_k^H \mathbf{w}_i|^2 + \sigma_n^2}. \tag{3.7}$$

3.4.2 Independent and Identically Distributed Beam Domain Channel Model

Considered $\mathbf{G}$ generated as:

$$\mathbf{G} = \Sigma \odot \tilde{\mathbf{G}}, \quad \text{with} \quad \tilde{\mathbf{G}} \approx \mathcal{CN}(0, 1), \tag{3.8}$$

where $\odot$ is a Hadamard product. The sparsity of the channel model is described by the matrix $\Sigma \in M_T \times K$ whose elements are i.i.d. Bernoulli random distributed of parameter sp. The sparsity level is the average number of zero elements of Σ and is equals $\chi = 1 - sp$. The non-zero entries of $\mathbf{g}_k$ can be modeled as Bernoulli random variables as in [21]. Since the distances between the UE and the BS are larger than the distance between the antennas, the assumption of equal probability of a non-vanishing path for each UE is reasonable. When the number of antennas increases to a massive number, the channel composed by a low number of scatterers tends to be sparse in the beam domain due to the fact that resolvable paths contribute less [22]. Thereby, the sparse massive channel is well represented using the virtual channel model.

The parameter χ is introduced to describe the sparsity of the channel, and this is defined as the non-zero probability of entries in the distinct virtual channel matrix. Following [21], the entries of $\mathbf{G}$ are defined as random variables taking values from a complex normal distribution $\mathcal{CN}(0, 1)$, i.e., the entries in the sparse virtual channel matrix under the above i.i.d. assumption follows the Gaussian-Bernoulli distribution.

3.4.3 Geometric-Stochastic Beam Domain Channel Representation

Following [11, 23], in some scenarios (e.g., in mmWave) the multipath channel consists of a sparse set of single-bounce components. In this context, the poor scattering effects can result in the virtual angular domain with a sparse channel matrix representation [12, 18]. The non-zero coefficients are related to the approximately disjoint subsets of paths and are modeled as independent complex Gaussian random variables. The number of non-zero entries on $\mathbf{g}_k$ defines a fixed number of beams simultaneously used at the BS, and this quantity depends on the sparsity level. Thereby, $\mathbf{G}$ is sparse with level equals χ and most of the power is concentrated in a few dominants entries.

Then, $\mathbf{g}_k$ can be modeled as:

$$\mathbf{h}_k = \sum_{p=1}^{P} \alpha_{k,p} \mathbf{a}_T(\theta_{k,p}), \tag{3.9}$$

$$\mathbf{g}_k = \mathbf{A}_T^H \mathbf{h}_k, \tag{3.10}$$

where P is the number of scatterers (c.f. Fig. 3.1); $\mathbf{a}_T(\theta_{k,p})$ represents the steering vector with $\theta \in [-\pi, \pi]$ and $\alpha_{k,p}$ represents the complex gain of path p, which follows a $\mathcal{CN}(0, 1)$ distribution. Furthermore, following [11], we assume that the smallest elements in $\mathbf{g}_k$ can be neglected.

3.4.4 Beam Selection

Considering the previous beam channel discussion in the last subsections, let us define the selection vector as:

$$\mathbf{s}_k = \begin{bmatrix} s_{1,k} & \dots & s_{M_T,k} \end{bmatrix}^{\mathrm{T}}, \tag{3.11}$$

where $s_{t,k} \in \{0, 1\}$ defines the selection of transmit beam t for user k. However, in a more general case, $s_{t,k}$ may actually be considered as a "gain" and be a complex scalar. Then, the beamformer can be written as:

$$\begin{aligned} \mathbf{w}_k &= s_{t,k} \cdot \mathbf{a}_T(\theta) \\ &= s_{t,k} \cdot \frac{1}{\sqrt{M_T}} \begin{bmatrix} 1 & e^{-j2\pi \cdot \theta_{M_T}} & \dots & e^{-j2\pi(M_T-1)\theta_{M_T}} \end{bmatrix}^{\mathrm{T}} \\ &= \sum_{t=0}^{M_T-1} s_{t,k} \mathbf{a}_T \left(\frac{t}{M_T - 1} \right) = \mathbf{A}_T^T \mathbf{s}_k = \mathbf{A}_T \mathbf{s}_k. \end{aligned} \tag{3.12}$$

Hence, the received signal in Equation (3.1) can be rewritten as:

$$\begin{aligned} y_k &= \mathbf{h}_k^H \left(\mathbf{w}_k x_k + \sum_{i \neq k}^{K} \mathbf{w}_i x_i \right) + n_k, \\ &= \mathbf{g}_k^H \mathbf{A}_T^H \left(\mathbf{A}_T \mathbf{s}_k x_k + \sum_{i \neq k}^{K} \mathbf{A}_T \mathbf{s}_i x_i \right) + n_k, \\ &= \mathbf{g}_k^H \left(\mathbf{s}_k x_k + \sum_{i \neq k}^{K} \mathbf{s}_i x_i \right) + n_k, \\ &= \mathbf{g}_k^H \mathbf{S}\mathbf{x} + n_k \quad \forall k, \end{aligned} \tag{3.13}$$

where $\mathbf{S} = \begin{bmatrix} \mathbf{s}_1 & \dots & \mathbf{s}_K \end{bmatrix}$. The complete signal (3.2), can then be rewritten as:

$$\mathbf{y} = \mathbf{G}^H \mathbf{S}\mathbf{x} + \mathbf{n}, \tag{3.14}$$

where the beam domain channel matrix can be expressed as $\mathbf{G} = \begin{bmatrix} \mathbf{g}_1 & \dots & \mathbf{g}_K \end{bmatrix}$.

To exemplify an application scenario, we could assume a low-number of scatterers, where $P \ll M_T$, some overlapped AoDs, and shared scatterers among UEs depending on the

Figure 3.1 – Illustration of a scenario with a low-number of the scatterers. Note that some scatterers are shared by different UEs.

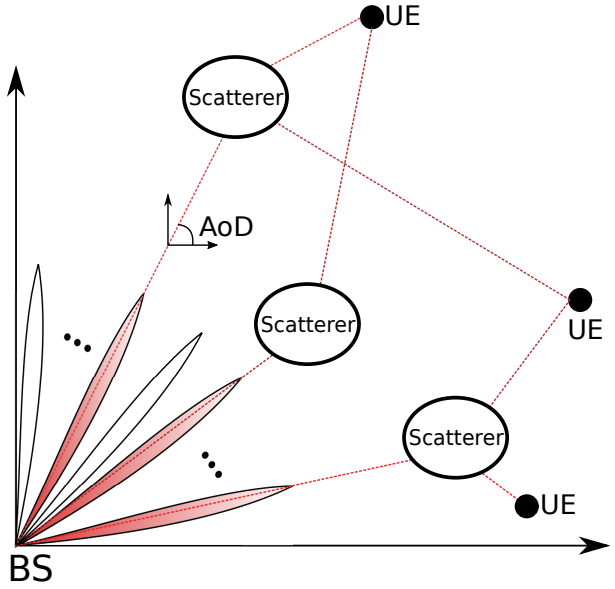

Source: Created by the author.

cluster distribution [21, 110] (see Figure 3.1). Then paths between BS and the UE are highly correlated. It is a result of a small angular spread of the incoming/outgoing rays at the BS. For instance, consider two simple cases following the virtual channel model with six uniformly spaced virtual angles (six transmit antennas), three UEs and three multipath clusters. Remember that in this model, the path gain of each UE is linked to the DFT matrix, describing the AoDs. For simplicity, consider one to represent the complex path gains, and zero otherwise. Regarding the virtual channel model, this scenario has the following structure:

$$\mathbf{G}^H = \begin{bmatrix} 1\,0\,0\,0\,0\,1 \\ 0\,0\,0\,1\,0\,0 \\ 0\,0\,1\,0\,0\,0 \end{bmatrix}.$$

In this interference-free case, there not exist any interference since $\mathbf{G}^H$ has not nonzero elements in the same columns. Furthermore, the sparsity level is measured by the ratio of zero elements of $\mathbf{G}^H$ over the total number of elements KM_T, $\chi = 1-(4/(3\cdot 6) = 1-0.222) \approx 78\%$. Consider a second example with:

$$\mathbf{G}^H = \begin{bmatrix} 1\,0\,0\,0\,0\,1 \\ 0\,0\,1\,1\,0\,0 \\ 1\,0\,1\,0\,0\,0 \end{bmatrix}.$$

Notice that interference exist since $\mathbf{G}^H$ has more than one nonzero element in a columns 1 and 3. In this example, the sparsity level is $\chi = 1-6/(3\cdot 6) = 1-0.333 \approx 67\%$.

3.5 Problem Formulation

In the classical MIMO formulation, transmit beamforming (or precoding) can be optimized to maximize some performance utility metric, which is generally a function of the SINR of the active UEs. [9, 111]. In general, two approaches can be taken: i) to optimize a performance criterion for given transmit power constraints or ii) to minimize the total transmit power under given SINR constraints. The first approach assumes the following transmit power constraint:

$$\mathrm{tr}\left(\mathbf{W}^H\mathbf{W}\right) = \sum_{k=1}^{K} \|\mathbf{w}_k\|_2^2 = Po = \sum_{k=1}^{K} Po_k.$$

Considering a per UE power constraint the optimization problem can be expressed as

$$\begin{aligned} &\max_{\mathbf{w}_1,\ldots,\mathbf{w}_K} f(\mathrm{SINR}_1, \ldots, \mathrm{SINR}_K) \\ &\text{s.t.: } \|\mathbf{w}_k\|_2^2 = Po_k, \qquad \forall k \in \{1, \ldots, K\}, \end{aligned} \tag{3.15}$$

where $f(\mathrm{SINR}_1, \ldots, \mathrm{SINR}_K)$ is some suitable function of the SINRs and Po_k is the power allocated to the k^{th} UE. A possible performance criterion is the sum rate:

$$\text{sum rate} = \sum_{k=1}^{K} \log_2(1 + \mathrm{SINR}_k). \tag{3.16}$$

The second optimization problem consists of minimizing the total transmit power which can be formulated as:

$$\begin{aligned} &\min_{\mathbf{w}_1,\ldots,\mathbf{w}_K} \sum_{k=1}^{K} \|\mathbf{w}_k\|_2^2 \\ &\text{s.t.: } \mathrm{SINR}_k = \gamma_k. \end{aligned} \tag{3.17}$$

The parameters γ_k are the SINRs that each UE shall be granted at the optimum of Equation (3.17), using as little transmit power as possible. The γ-parameters can, for example, describe the SINR required to achieve certain data rates. However, the optimization of UE transmit beamforming is generally a nondeterministic polynomial-time (NP) hard problem [9, 98, 112].

Classical precoders can be easily expressed in the beam domain such as the MRT, where the performance (sum rate) is limited due to MUI [113]. This MUI can be avoided thanks to ZFBF [95, 111, 114], at the cost of some computational complexity (due to the number of operations required to compute the pseudo-inverse $O(K^2M_T^2)$).

Moreover, these beamformers use full (instantaneous) channel knowledge, which asks for large CSI feedback to the BS [115]. To alleviate this feedback load, it is possible to transmit only on one beam. Hence, only second order statistics are needed, which are long-term parameters that vary slowly compared to the complex gain [101, 105]. Using only the beam gain knowledge from the channel covariance matrix, the authors of [101] propose to select a single beam using the maximum beam gain. However, this limits the performance (rate) per UE.

3.6 Proposed Solution

In this section, we propose a precoder design considering a practical rate assignment (based on MCS, c.f. Table 3.1), beam selection, and power optimization per beam that assumes the beam domain channel model for massive MIMO (c.f., Equations (3.8) and (3.10)). We design a new heuristic to simplify the beam selection and power optimization procedure based on Lagrangean relaxation [96]. Furthermore, we propose three other low-complexity heuristics.

3.6.1 General Definitions

Firstly, because $\mathbf{g}_k$ is named beam domain channel, we call $\mathbf{s}_k$ the virtual beamformer or virtual precoder, since Equation (3.14) and Equation (3.2) have the same form. Based on this, we rewrite the classical beamforming problem as a "virtual beamforming" problem.

The SINR in Equation (3.7) can be expressed in terms of $\mathbf{g}_k$ and $\mathbf{s}_k$ as:

$$\mathrm{SINR}_k = \frac{|\mathbf{g}_k^H \mathbf{s}_k|^2}{\sum\limits_{i \neq k}^{K} |\mathbf{g}_k^H \mathbf{s}_i|^2 + \sigma_k^2}. \tag{3.18}$$

Note that if SINR_k is maximum, $\sum\limits_{i \neq k}^{K} |\mathbf{g}_k^H \mathbf{s}_i|^2$ is minimum. The useful signal power is $\mathbf{g}_k^H \mathbf{s}_k \mathbf{s}_k^H \mathbf{g}_k = \left|\mathbf{g}_k^H \mathbf{s}_k\right|^2$, whereas the interference power is $\sum_{i \neq k} \left|\mathbf{g}_k^H \mathbf{s}_i\right|^2$. Thus, minimizing the MUI boils down to:

$$\begin{aligned} &\min \sum_i \sum_{i \neq k} |\mathbf{g}_k^H \mathbf{s}_i|^2 \\ &\text{s.t.: } \|\mathbf{s}_k\|_2^2 = Po_k. \end{aligned} \tag{3.19}$$

Starting from Equation (3.19), we can minimize the overall interference (over all UEs k). Noting that $|\mathbf{g}_k \mathbf{s}_k|^2$ is a constant, minimizing $\sum\limits_k \sum\limits_{i \neq k} |\mathbf{g}_k^H \mathbf{s}_i|^2$ is equivalent to minimizing $\sum\limits_k^K \sum\limits_i^K |\mathbf{g}_k^H \mathbf{s}_i|^2$ and the MUI minimization problem can be rewritten as:

$$\begin{aligned} &\min \sum_i \sum_k |\mathbf{g}_k^H \mathbf{s}_i|^2 \\ &\text{s.t.: } \|\mathbf{s}_k\|_2^2 = Po_k, \quad \forall k, \end{aligned} \tag{3.20}$$

where $\min \sum\limits_i \sum\limits_k |\mathbf{g}_k^H \mathbf{s}_i|^2 = \min \left\|\mathbf{G}^H \mathbf{S}\right\|_{\mathrm{F}}^2$.

3.6.2 Optimal Solution via Beam Selection, Power Beam Optimization and Rate Assignment: A MILP Formulation

In this subsection, the aim is to find an optimal solution to the performance achieved by beam selection using integer linear programming (ILP) and MRT with selection. The problem is mainly to find a feasible set of beams such that MRT on these beams delivers optimal

performance. Moreover, we write the problem to maximize the sum rate using a set of discrete rates, similarly to [104, 116], supported by a set of beam gains. For instance, in the practical cellular communication systems such as LTE, the rate of each UE takes discrete rate values determined by specific MCSs assigned to each UE. Corresponding to each MCS and rate, a minimum received γ level is required. See Table 3.1 for more details.

Table 3.1 – Data rates and minimum received γ requirements of LTE systems [72, 104].

Index	υ	0	1	2	3	4	5	6	7	8	9	10	11	12	13	14	15
Data Rate	δ	0	0.1523	0.2344	0.3770	0.6010	0.8770	1.1758	1.4766	1.9141	2.4063	2.7305	3.3223	3.9023	4.5234	5.1152	5.5574
SINR Level (dB)	γ	0	-9.478	-6.658	-4.0898	-1.798	0.3999	2.424	4.489	6.367	8.456	10.266	12.218	14.122	15.849	17.786	19.809

The rate of the k^{th} UE from the associated γ could be obtained by applying the Shannon capacity formula: $\log_2(1+\gamma_k)$. However, these values are continuous and should be discretized according to some criterion. In the simulations section, we will discuss the discretization[1]. Due to this limitation, we assume that the Table 3.1 is a good point to start. Let us express the rates δ as a set Δ, and γ_k as the γ achieved by index υ. We assume that the *binary* variables s represent the selected beam and q the rate assignment, as follows:

$$s_{t,k} = \begin{cases} 1, & \text{if the } t^{th} \text{ beam is assigned to the } k^{th} \text{ UE,} \\ 0, & \text{otherwise.} \end{cases}$$

$$q_{k,\upsilon} = \begin{cases} 1, & \text{if the UE}_k \text{ is using only the rate } \delta_\upsilon, \\ 0, & \text{otherwise.} \end{cases}$$

The υ index corresponds to the rate in the set $\Delta = \{\delta_1, \ldots, \delta_\upsilon\}$ as defined in Table 3.1 (c.f., $\log_2(1+\gamma_k) = \delta_\upsilon$ for all $\gamma_{\upsilon-1} \leq \gamma_k < \gamma_\upsilon$, and $\upsilon \geq 1$).

We consider a constraint on the maximum tolerable level of MUI, termed hereafter limited multi-user interference (LMUI)[2]. Thereby, the SINR in Equation (3.7) can be expressed in terms of the LMUI as:

$$\text{SINR}_k = \frac{|\mathbf{g}_k^H \mathbf{w}_k|^2}{\text{LMUI} + \sigma_{nk}^2}. \tag{3.21}$$

The SINR considering a minimal γ requirement for each UE can be formulated as follows:

$$\text{SINR}_k \geq \sum_{\upsilon \in \Delta} \gamma_k q_{k,\upsilon}, \tag{3.22}$$

where γ_k represents the minimum SINR. Note that the constraint in Equation (3.22) is non-convex, even if the binary variables are relaxed to be continuous variables taking values in [0, 1]. Using Equation (3.21), we get an equivalent inequality as an alternative to Equation (3.22), as follows:

$$|\mathbf{g}_k^H \mathbf{w}_k|^2 \geq \sum_{\upsilon \in \Delta} \gamma_k q_{k,\upsilon} A, \tag{3.23}$$

[1] There is optimal values for that, but find them is out of scope in this work.

[2] This limit is required for supporting a MCS and it is based on control the temperature-interference between primary and secondary UEs into cognitive radio system in [117].

where $A = \text{LMUI} + \sigma_{nk}^2$ and $\mathbf{w}_k$ is the precoder for each k.

Our goal is to maximize the sum rate. Thus, the objective function can be written as:

$$\max_{q,s} \sum_{k} \sum_{\upsilon} \delta_\upsilon q_{k,\upsilon}, \tag{3.24}$$

where $\sum_k \sum_\upsilon \delta_\upsilon q_{k,\upsilon}$ represents the downlink sum rate with discretized rate values.

We must ensure that each UE chooses only one rate [104, 107] as follows:

$$\sum_{\upsilon \in \Delta} q_{k,\upsilon} \leq 1, \forall k. \tag{3.25}$$

Then, Equation (3.25) is a constraint on the binary variables for the k^{th} UE be served with only one-rate, $\sum_{\upsilon\in\Delta} q_{k,\upsilon} = 1$, or the k^{th} UE be not served, $\sum_{\upsilon\in\Delta} q_{k,\upsilon} = 0$. Therefore, considering Equations (3.23) to (3.25), the problem for selecting beams and discrete rates for MUs can be expressed as a binary integer linear programming (BILP) problem, as follows:

$$\max_{q,s} \sum_{k} \sum_{\upsilon} \delta_\upsilon q_{k,\upsilon} \tag{3.26a}$$

$$\text{s.t.: } |\mathbf{g}_k^H(\mathbf{w}_k \odot \mathbf{s}_k)|^2 \geq \sum_{\upsilon\in\Delta} \gamma_{k,\upsilon} q_{k,\upsilon} A_k, \quad \forall k \tag{3.26b}$$

$$\sum_{\upsilon\in\Delta} q_{k,\upsilon} \leq 1, \forall k \tag{3.26c}$$

$$\sum_{i\neq k}^{K} |\mathbf{g}_k^H(\mathbf{w}_i \odot \mathbf{s}_i)|^2 \leq \text{LMUI}, \quad \forall k \tag{3.26d}$$

$$s_{t,k} \in \{0, 1\} \quad \forall k \tag{3.26e}$$

$$q_{k,\upsilon} \in \{0, 1\} \quad \forall k. \tag{3.26f}$$

The formulation consists in selecting discrete rates and beam gains such that the sum rate is maximized for a given LMUI level. Notice that, in this proposal, the problem is to maximize the sum rate of all UEs, assuming each achievable rate δ_υ is chosen from a predefined discrete rate set Δ.

Furthermore, we assume that the precoder $\mathbf{w} = \mathbf{g}$ where we aim to maximize the MRT with selection. Then, Equation (3.26) can be written as:

$$\max_{q,s} \sum_{k} \sum_{\upsilon} \delta_\upsilon q_{k,\upsilon} \tag{3.27a}$$

$$\text{s.t.: } \sum_{\upsilon\in\Delta} \gamma_{k,\upsilon} q_{k,\upsilon} A_k - |\mathbf{g}_k^H(\mathbf{g}_k \odot \mathbf{s}_k)|^2 \leq 0, \quad \forall k \tag{3.27b}$$

$$\sum_{\upsilon\in\Delta} q_{k,\upsilon} \leq 1, \forall k \tag{3.27c}$$

$$\sum_{i\neq k}^{K} |\mathbf{g}_k^H(\mathbf{g}_i \odot \mathbf{s}_i)|^2 \leq \text{LMUI}, \quad \forall k \tag{3.27d}$$

$$s_{t,k} \in \{0, 1\}, \quad \forall k \tag{3.27e}$$

$$q_{k,\upsilon} \in \{0, 1\}, \quad \forall k. \tag{3.27f}$$

Note that the problem in Equation (3.27) is not assuming power constraints. As long as, the beams ($\mathbf{g}_k$) do not change with the power, the variables $s, q \in \{0, 1\}$ select the rates and beams, respectively. Thereby, the problem should be solved in two steps. First, it selects beam gains and rates and afterwards it optimizes the power. However, the optimal solution on performance is not achieved because the power optimization is made in a second step and per UEs. Moreover, optimally solving a BILP problem can incur into high computational complexity [118]. We discuss the complexity analysis in Section 3.7.3.

Since the difficulty of solving the ILP is restricting a solution to binary values, this problem could be relaxed in parts. It means that the binary selection in the beams s can be relaxed to positive continue values s'. Therefore, this problem is expressed as a MILP formulation:

$$\max_{q,s'} \sum_{k} \sum_{\upsilon} \delta_{\upsilon} q_{k,\upsilon} \tag{3.28a}$$

$$\text{s.t.:} \sum_{\upsilon \in \Delta} \gamma_{k,\upsilon} q_{k,\upsilon} A_k - |\mathbf{g}_k^H (\mathbf{g}_k \odot \mathbf{s}'_k)|^2 \leq 0, \quad \forall k \tag{3.28b}$$

$$\sum_{\upsilon \in \Delta} q_{k,\upsilon} \leq 1, \forall k \tag{3.28c}$$

$$\sum_{i \neq k}^{K} |\mathbf{g}_k^H (\mathbf{g}_i \odot \mathbf{s}'_i)|^2 \leq \text{LMUI}, \quad \forall k \tag{3.28d}$$

$$s'_t \leq Po_k^{1/2}, \quad \forall k \tag{3.28e}$$

$$q_{kt} \in \{0, 1\}, \quad \forall k. \tag{3.28f}$$

Note that this formulation consists in a power optimization of beam selection $\mathbf{s}'$ since it can assume any continue positive value limited to available total transmit power, i.e., $\sum_{kt} {s'_{t,k}}^2 \leq Po$.

In general, even with relaxation, the problem is complex to solve because it involves a joint optimization of discrete and continuous variables. In the next subsection, we present a heuristic based on Lagrangean relaxation for reducing the complexity of this MILP formulation.

3.6.3 Lagrangean Relaxation via Dual Subgradient Optimization Algorithm

The idea follows the approach of [9] to optimize the MU precoder. The method aims to solve the MILP formulation (3.28) in the dual variable space [96, 119], where the optimization problem becomes the unconstrained maximization of a non-differentiable concave function. Consequently, since the function is non-differentiable, the problem can be solved by using a standard iterative subgradient algorithm. The MILP maximization in Equation (3.28) is converted to a dual minimization problem (or the maximization of the negative objective function) by "relaxing" (or "dualizing") a specially determined subset of MILP constraints. The relaxation involves adding these constraints to the MILP objective function Equation (3.28a) weighted by dual variables (i.e., the Lagrangean multipliers). Then, the so-obtained Lagrangean relaxed problem is still a maximization problem in the MILP variable space but parameterized by the dual multipliers. The optimization of this problem generates a value of the dual objective. Since

Lagrangean relaxed problem is parameterized by the dual multipliers, the value of the dual function will depend on the appropriate values of the multipliers. Consequently, to solve the dual problem, we must obtain those dual variables (or multipliers).

Since the dual function is convex, we explore the dual variable space through a heuristic subgradient optimization method. In this process, from a dual solution, we follow the direction of the subgradient vector of the dual function. The obtained values for the dual multipliers are applied to define a new instance of the Lagrangean relaxed problem, that is solved in the next iteration to obtain a new dual function value.

Thereby, the method is solved by successive iterations, each consisting of a minimization step of the Lagrangean relaxed problem and of a maximization step of the dual problem via a subgradient optimization. During these steps, the best MILP and dual solutions are stored. From duality theory, the maximal value of the best dual solution constitutes an upper bound on the optimal MILP objective function value. Note that the method produces a sub-optimality gap along the iterations. Finally, the algorithm ends when the sub-optimality gap diminishes under a threshold, or a maximal number of iterations is reached.

Let us explain the relationship between the Lagrangean relaxed problem and our problem. The first step to find the dual version of the problem is to build the partial Lagrangean function $L(\mathbf{q}, \mathbf{s}', \boldsymbol{\lambda})$ by "relaxing" (or "dualizing") the constraints Equation (3.28b), that is, by adding these constraints to the MILP objective function Equation (3.28a) weighted by the dual variables λ_k (i.e., the Lagrangean multipliers):

$$L(\mathbf{q}, \mathbf{s}', \boldsymbol{\lambda}) = -\sum_{k}\sum_{\upsilon}\delta_{\upsilon}q_{k\upsilon} + \sum_{k}\lambda_k\left(\sum_{\upsilon\in\Delta}\gamma_{k\upsilon}q_{k\upsilon}A_k - |\mathbf{g}_k^H(\mathbf{g}_k \odot \mathbf{s}_k')|^2\right). \tag{3.29}$$

The minimization of the partial Lagrangean function $L(\mathbf{q}, \mathbf{s}', \boldsymbol{\lambda})$ constitutes the so-called Lagrangean relaxed version of the primal Equation (3.30):

$$W(\boldsymbol{\lambda}) = \min\ L(\mathbf{q}, \mathbf{s}', \boldsymbol{\lambda}) \tag{3.30a}$$

$$\text{s.t.:}\ \sum_{\upsilon\in\Delta} q_{k\upsilon} \le 1, \quad \forall k \tag{3.30b}$$

$$\sum_{i\neq k}^{K} |\mathbf{g}_k^H(\mathbf{g}_i \odot \mathbf{s}_i')|^2 \le \text{LMUI}, \quad \forall k \tag{3.30c}$$

$$s_t^{'} \le Po_k^{1/2}, \quad \forall k \tag{3.30d}$$

where $W(\boldsymbol{\lambda})$ is the dual function, whose maximization comes up to the dual problem Equation (3.31) to solve via the subgradient descent method:

$$\max_{\boldsymbol{\lambda}} W(\boldsymbol{\lambda}) \tag{3.31a}$$

$$\text{s.t.:}\ \boldsymbol{\lambda} \ge 0. \tag{3.31b}$$

The Lagrangean relaxed primal problem Equation (3.30) can be separated into two independent subproblems, defined on a different groups of decision variables $\mathbf{q}$ and $\mathbf{s}'$,

respectively, since the linking constraint Equation (3.28b) between $\mathbf{q}$ and $\mathbf{s}'$ has been relaxed. The first subproblem Equation (3.32) selects the UE-data rate assignment $\mathbf{q}$, while the second one Equation (3.33) finds the optimized power beam associated to the UEs, represented by $\mathbf{s}'$.

$$\min_{\mathbf{q}} -\sum_{k}\sum_{\upsilon}\delta_{\upsilon}q_{k\upsilon} + \sum_{k}\lambda_{k}\left(\sum_{\upsilon\in\Delta}\gamma_{k\upsilon}q_{k\upsilon}A_{k}\right) \tag{3.32}$$

s.t.: (3.30b).

$$\min_{\mathbf{s}'} -\sum_{k}\lambda_{k}|\mathbf{g}_{k}^{H}(\mathbf{g}_{k}\odot\mathbf{s}'_{k})|^{2} \tag{3.33}$$

s.t.: (3.30c), (3.30d).

This decouple results in two less complex subproblems than the original MILP problem. The power beam allocation subproblem Equation (3.33) can be solved by well-known linear programming (LP) algorithms in polynomial time. On the other hand, the UE-data rate assignment subproblem Equation (3.32) can be solved separately for each UE k, yielding to the next trivial solution Equation (3.35):

$$w_{k\upsilon} = \delta_{\upsilon} - \lambda_{k}\gamma_{k\upsilon}A_{k}, \tag{3.34}$$

$$q^{\star}_{k\upsilon} = \begin{cases} 1, & \text{if } \upsilon = \arg\max_{\{\upsilon\in\Delta|w_{k\upsilon}\geq 0\}} w_{k\upsilon} \\ 0, & \text{otherwise.} \end{cases} \tag{3.35}$$

Since, for each UE k, the set of values $w_{k\upsilon}$ are sorted by construction, this solution can be found by a standard binary search algorithm performing $O(log_2(|\Delta|))$ comparisons.

The optimization of both LP subproblems parameterized by the current multipliers $\boldsymbol{\lambda}$ delivers a value for the dual function $W(\boldsymbol{\lambda})$ and a solution $\{\mathbf{q}^{\star}, \mathbf{s}'^{\star}\}$ to the Lagrangean relaxed primal problem. We must note that the UE-data rate assignment $\mathbf{q}$ could not be feasible since we have relaxed the constraints (3.28b). Then, we build a feasible primal solution by keeping $\mathbf{s}'^{\star}$ and taking as feasible UE-data rate assignment $\mathbf{q}^{feas}$ the largest UE data rate supported by $\mathbf{s}'^{\star}$, i.e. meeting the constraints Equation (3.28b), for each UE k. Afterwards, the method explores the dual solution space by using a subgradient update step to move from the current $\boldsymbol{\lambda}$ to a new set of values.

Since we know from Equation (3.30) that the dual function is a convex function subject to the non-negativity constraints, represented by the vector $\boldsymbol{\lambda}$, a descent step method used in unconstrained optimization is suitable for the dual exploration. In particular, a subgradient vector is used as search direction because the dual function is piecewise linear, and then non differentiable. This subgradient vector, $\boldsymbol{\varrho}$, is calculated as:

$$\boldsymbol{\varrho} = \nabla W(\boldsymbol{\lambda}) = \sum_{\upsilon\in\Delta}\gamma_{k\upsilon}q_{k\upsilon}A_{k} - |\mathbf{g}_{k}^{H}(\mathbf{g}_{k}\odot\mathbf{s}'_{k})|^{2}. \tag{3.36}$$

Then, the new $\boldsymbol{\lambda}$ in the dual space in the next iteration $l+1$ is updated by the subgradient step as:

$$\boldsymbol{\lambda}^{l+1} = \max\{\boldsymbol{\lambda}^{l} + \tau\boldsymbol{\varrho}, \mathbf{0}\}, \tag{3.37}$$

where τ is the fixed step size.

The new dual multipliers $\boldsymbol{\lambda}^{l+1}$ are replaced in the Lagrangean function Equation (3.29), yielding to new instances of the Lagrangean relaxed subproblems Equations (3.32) and (3.33) for the $(l+1)^{\text{th}}$ iteration. Then, after solving them, a new subgradient optimization step follows. The method continues by solving in an alternate way Lagrangean relaxed primal subproblems and dual problems at each iteration until a stopping criterion is met.

In this work, the algorithm is stopped when any of the following conditions is satisfied first: (1) the *optimality* gap between the objective function (3.28a) evaluated for $\mathbf{q}^{feas}$ and the *upper bound* $\overline{W}$ diminishes under a threshold *thr*; (2), at least one Lagrange multiplier becomes null; or (3), a maximal number of iterations $l_{\max}$ is reached. The upper bound $\overline{W}$ is calculated as follows:

$$\overline{W} = \sum_{k=1}^{K} \log_2(1 + \text{SINR}_k^{UB}), \tag{3.38}$$

$$\text{SINR}_k^{UB} = \min\left(|\mathbf{g}_k^H(\mathbf{g}_k \odot \mathbf{s}'_k)|^2, \gamma_{MAX}\right). \tag{3.39}$$

where $s'_t = Po_k^{1/2}$ and γ_{MAX} is the largest SINR level allowed in the system (e.g, the value associated to the last index $\upsilon \in \Delta$ in Table 3.1). Finally, the rationale behind the second stopping criterion is related to the impact of the $\boldsymbol{\lambda}$ multipliers in the Lagrangean relaxed primal subproblems. If λ_k becomes null, the subproblem (3.32) will assign the largest data rate available allowed in the the system to the UE k, whereas the subproblem (3.33) will allocate a null amount of power to UE k. That results is an abrupt transition in the λ_k evolution: from a smooth decreasing till reaching zero, we pass suddenly to a huge increment. In other words, the UE with the smallest impact on the objective function (the closest λ_k to zero) becomes presumably the UE with the highest impact. This change modifies drastically the solution $\mathbf{s}'^{\star}$ delivered by the subproblem (3.33), and, hence the feasible UE-data rate assignment $\mathbf{q}^{feas}$ built from $\mathbf{s}'^{\star}$ as aforementioned. The second stopping criterion prevents such situation.

3.6.4 Low Complexity Heuristics

In some practical systems, it could be impossible to apply the last heuristic because its computational complexity becomes too high. Motivated by this fact, we propose three low-complexity heuristics to select the transmit beams. These heuristics are simple and less complex compared to the previous solutions in Section 3.6. In the following, the heuristics are presented.

3.6.5 Heuristic 1 – Minimum-Interference Greedy Assignment

This heuristic tries to minimize interference (equivalently maximize SINR). Consider two UEs as an example. For each pair i, k of UEs, we maximize $\dfrac{\mathbf{g}_i^H\mathbf{s}_i + \mathbf{g}_k^H\mathbf{s}_k}{\mathbf{g}_i^H\mathbf{s}_k + \mathbf{g}_k^H\mathbf{s}_i}$. More specifically, this heuristic follows the steps:

1. Initialize with $\mathbf{s}_k = \mathbf{g}_k$;

2. For all pairs i, k of UEs, test all beams t. If removing $s_{t,k}$ leads to a higher SINR, turn this to 0.

The idea is to minimize the interference and, under this perspective, this heuristic marginally improves the SINR, compared to the simple MRT approach. This heuristic is more formally described by the pseudo-code presented in Algorithm 1.

Algorithm 1: Minimum-Interference Greedy Assignment

Input : A $\mathbf{G}^H$ matrix of size $K \times M_T$
Output : An $\mathbf{S}$ matrix of size $K \times M_T$

Initialize $\mathbf{S} = \mathbf{G}$;
Define the interference limit $\mathbf{g}_i^H \mathbf{s}_k + \mathbf{g}_k^H \mathbf{s}_i$;
while *Exist an UE that violates the interference limit* **do**
    Remove the beam of the UE;
    Re-evaluate the limit;
end

3.6.6 Heuristic 2 – Munkres-based Assignment

Inspired again by the MRT scheme, we consider in this proposed heuristic that each UE will get assigned only one beam, which will concentrate the whole power allocated to that UE, and that each beam will be assigned to at most one UE. Since we are concerned with the overall performance of the K UEs, we can consider the following alternative optimization problem

$$\mathbf{S}^\star = \arg\max_{\mathbf{S}} \left\{ \mathbf{1}_{M_T}^{\mathrm{T}} (\mathbf{G} \odot \mathbf{S}) \mathbf{1}_K \right\}, \tag{3.40a}$$

$$\text{s.t.: } \mathbf{S}\mathbf{1}_K = \mathbf{1}_K, \quad \mathbf{1}_{M_T}^{\mathrm{T}} \mathbf{S} \leq \mathbf{1}_{M_T}^{\mathrm{T}}, \quad \mathbf{S} \in \mathcal{B}^{M_T \times K}, \tag{3.40b}$$

which implies that each UE will be assigned a single beam and each beam will be assigned to a single UE. The above assignment problem corresponds to a maximum matching in a bipartite graph and can be solved optimally using Munkres algorithm [97]. This heuristic is more formally described by the pseudo-code presented in Algorithm 2.

In spite of involving the solution of an optimization problem, the Munkres algorithm solves the assignment problem with $O\left(\min\left(K^3, M_T^3\right)\right)$ complexity [97]. Notice that, whenever there are more beams than UEs, the output of this heuristic could be augmented by assigning additional beams to the UE.

3.6.7 Heuristic 3 – Minimum Interference Greedy Assignment with Munkres Initialization

Based on the previous heuristic, one can consider augmenting the obtained solution by assigning new beams to the UE whenever it does not compromise the overall performance. In this case, a slightly modified heuristic could be applied which combines aspects of the two

Algorithm 2: Munkres-based Assignment

Input : A $\mathbf{G}^H$ matrix of size $K \times M_T$
Output : An $\mathbf{S}$ matrix of size $K \times M_T$

Define $\mathbf{G}'$ *so that* $g'_{i,j} = 1/g_{i,j}$;
$\mathbf{S} \leftarrow$ *munkres*$(\mathbf{G}')$;

previous heuristics. Denoting by $\mathcal{B}_i$ the set of beams assigned to UE i and by $\mathcal{K}_t$ the set of UEs using the beam t, the heuristic is described as follows. We assume in Algorithm 3 that the unsatisfied UE are those whose minimum SINR requirement is not satisfied. The basic idea

Algorithm 3: Minimum Interference with Munkres Initialization

Input : A $\mathbf{G}^H$ matrix of size $K \times M_T$
Output : An $\mathbf{S}$ matrix of size $K \times M_T$

Define $\mathbf{G}1$ *so that* $g'_{i,j} = 1/g_{i,j}$;
$\mathbf{S} \leftarrow$ *munkres*$(\mathbf{G}')$;
while *there is no unsatisfied UE* **do**
  Select the scheduled UE i *and the beam* $t \notin \mathcal{B}_i$ *with highest ratio*
  $$\frac{\mathbf{g}_i^{\mathrm{H}} \sum\limits_{t' \in \mathcal{B}_i} s_{t',i} + \mathbf{g}_i^{\mathrm{H}} s_{t,i}}{\max\limits_{i' \in \mathcal{K}_t} \left\{0,\ \mathbf{g}_{i'}^{\mathrm{H}} s_{t,i'}\right\}};$$
  if *all UEs are satisfied when assigning beam* t *to UE* i **then**
    Allocate beam t *to UE* i;
  else
    Break;
  end
end

behind the above heuristic is to allocate a new beam to the UE such that the gain is maximized and that the interference (from the worst interferer) is minimized.

After the beam selection/assignment step, a power allocation among UEs is performed along the lines of [9].

3.7 Simulations Results

In this section, we compare the performance of linear precoders as well as the schemes based on heuristics and the corresponding optimal solution provided by the MILP formulation described in Section 3.5. The power allocation per UE applied in Heuristics 1, 2, 3, ZFBF and MRT can be reproduced following the supplementary material in [9].

We assume a system with $M_T = 64$ antennas and scenarios with different sparsity levels. For all simulations, we ensure that the sparsity level is less than or equal to χ. The curves are plotted as a function of the SNR= $|\mathbf{H}_k^H \mathbf{w}_k|^2/\sigma_k^2$ and the average sum rate is described by (3.16). Following (3.21), the SINR of the k^{th} UE achieves the best performance when the

LMUI is equal zero. Therefore, we present the best solutions with the best beam selection in the interference-free case.

In all simulations, we use 1000 channel realizations. In the simulation results we assume the two channel models presented in Section 3.4: One is called i.i.d. and other is a geometric-stochastic channel, both with the same specified sparsity level χ. In the i.i.d. channel model the elements of $\mathbf{g}$ follow a zero-mean circularly symmetric complex Gaussian distribution, $\mathbf{g}_k \in \mathcal{CN}(0, \mathbf{I}_{M_T})$ following (3.8). In the geometric-stochastic channel, each element in $\mathbf{G}$ was generated according to Equation (3.10). In this model, we generate the channel removing the smallest elements in $\mathbf{g}_k$ until reaching a required sparsity level χ. We consider $L = 20$ scatterers following [120], which are enough to capture the channel characteristics. As for the optimal solutions, we solve (3.28) (i.e., the MILP problem) and the Lagrangean relaxation (LA) described in Section 3.6.3 using the CPLEX solver of [121]. For the Lagrangean, we assume $\tau = 10^{-6}$ and $l_{max} = 1000$. Furthermore, we illustrate the performance results letting the proposal selects rates in reference a extended range of SNRs, more specifically $\Delta \in [0,\ 12]$ bits/symbol per UE. Also, the heuristics are evaluated under a scenario with imperfect channel knowledge.

Figure 3.2 (a) shows the performance results under the parameters of Table 3.1. Note that the performances of all schemes are upper limited at 22 bits per symbol, since the data in table 3.1 restricts the problem to assign at most the rate of 5.5 bits/symbol per UE, ($\Delta \in [0;\ 5.5]$). Then, in the solutions, the maximum sum rate is $K \times 5.5 = 22$ bits per symbol.

The improved results of our proposal compared to ZFBF comes from a better management of beam power in the beam domain, whereas in the second step (i.e., the UE power optimization), the heuristic for ZFBF distributes equally the power among all non-zero beams of each UE. Besides that, ZFBF "wastes" power in the process of eliminating interference (ill-conditioning) (see fig. 3.4). However, when the sparsity level is decreased (more non-zero elements), the ZFBF can increase the performance (better conditioning), as we can see in Figure 3.5. Different from MILP and Lagrangean relaxation (LA) simulation results, in the low-complexity heuristics we consider a beam selection followed by UE power optimization according to [9]. The ZFBF and MRT follow with the same power optimization.

Considering the low-complexity heuristics, MRT and ZFBF, in the low SINR, MRT and heuristic 2 are good options since MUI is not dominant and the heuristics have low complexity with similar performance. In the medium and high SINR ranges, the performance of MRT is limited by MUI. In this case, the knowledge about the beams exploited by the proposed heuristic leads to improvements in the sum rate. The heuristic 1 is based on MRT and hence, using knowledge about the beams improves the rate. In heuristic 2, the allocation of just one beam per UE has low performance in the low SINR. However, under high SINRs the performance is increased since the K beams are interference-free. The result of heuristic 3 is similar to that of MRT and heuristic 1 for low SINR. However, for medium and high SINR values the performance has improved compared to the MRT because of the potential addition of extra beams to each UE.

In fig. 3.2 (b) we evaluate the proposal considering the stochastic-geometric channel

Figure 3.2 – Performance of optimal solution (MILP), Lagrangean relaxation, ZFBF, MRT and three proposed heuristics with $K = 4$, $M_T = 64$ and $\chi = 90\%$.

(a) Performance using an i.i.d. channel model.

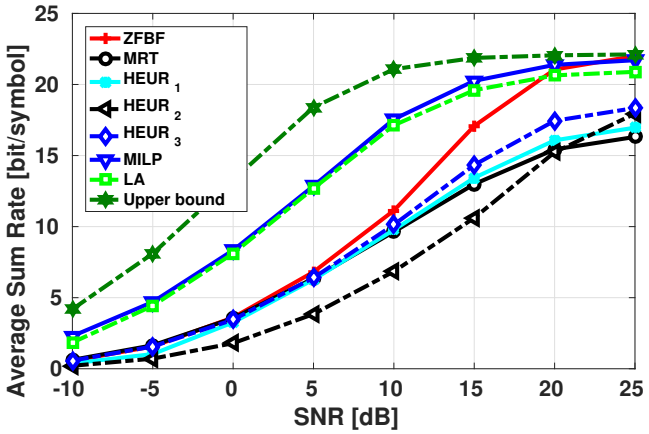

(b) Performance using geometric-stochastic channel model.

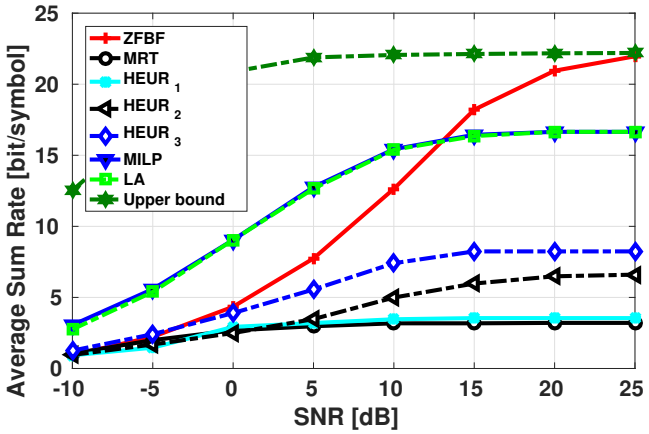

Source: Created by the author.

model in Section 3.4.3.

Note that the ZFBF has similar performance since it is able to eliminate the MUI in any scenario. However, MRT losses performance. Hence, the heuristics performance is affected, since we have more interference beams, reducing the overall performance. One reasonable explanation for this behavior is that in the stochastic-geometric channel the accuracy of the model is better than that of the i.i.d. channel model, thus capturing the interference among beams more effectively. While in the i.i.d. channel model the geometry of interference follows a Bernoulli distribution.

Note that the Lagrangean relaxation can achieve the maximum performance of the MILP for almost all SNRs values. The upper bound curve is achieved by (3.38), and the thr (gap) is adapted for each SNR. For low SNR values, we use higher values for thr. Otherwise, for high SNR values, we use lower values for thr since the gap between the MILP and upper bound solution is smaller. Thus, we adapt the threshold values to ensure a small number of iterations for achieving the MILP solution. Note that the value thr for each channel model can

be set differently. The average number of iterations is equal to ten and is sufficient to reach a good convergence. For the i.i.d. channel model, $thr = 0.4$ is enough to reach a MILP solution for low SNR values. For the geometric-stochastic channel model, $thr = 0.6$ for low SNR values, and for high SNR values, $thr = 0.25$, are enough to achieve MILP solutions.

In the optimal solution for beam selection, some beams are not used. Therefore, the "less is more" principle [90, c.f. Figure 3.8 - Chapter 3] that usually plays an important role in ZFBF takes effect, i.e., fewer beams with more power lead to a better allocation. In Figure 3.3, we present the optimal average number of selected beams according to the MILP solution and the average number of total beams with $\chi = 90\%$. In general, in this interference-free solution, when more power can be allocated, the MILP solution reduces the number of beams to be equal to the number of UE.

Figure 3.3 – Average number of selected beams for $K = 4$.

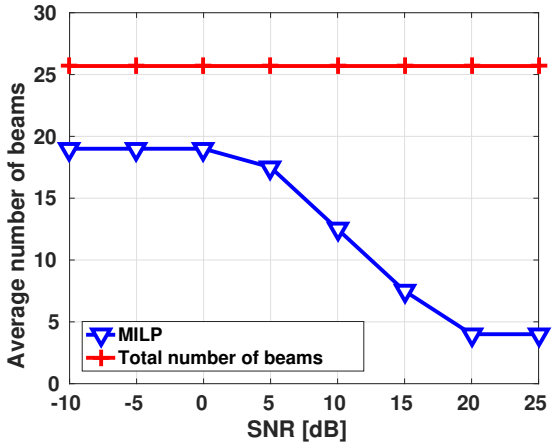

Source: Created by the author.

Figure 3.4 illustrates an example of beam selection and power optimization for a SNR $= -10$ dB and shows 2 UEs. The reduction of beam number is recognized where some of them are not used, compared to the MRT, which uses all beams, and to the solution MILP. Note that in some cases power is allocated where there are no beams for the ZFBF. It happens because ZFBF needs eliminate all interference beams. Thereby, some part of power is wasted out in the process.

Figure 3.5 (a) illustrates MILP and the performance of ZFBF with the i.i.d. channel for χ equal to 90%, 70% and 50% and for $K = 4$. When the sparsity level has decreased, the ZFBF performance is increased. The best solution for our proposal is found with $\chi = 70\%$. Figure 3.5 (b) considers the geometric-stochastic channel. The best solution is found with $\chi = 90\%$. When the sparsity level is decreased, the performance of the MILP solution is decreased. When the level of the sparsity of $\mathbf{G}$ is decreased, there is more interference, and the performance degrades. The ZFBF performance is increased with the decreasing of sparsity levels for both channel models.

Figure 3.4 – Illustrative example for beams selection and power optimization using MILP, ZFBF and MRT.

(a) UE - 1.

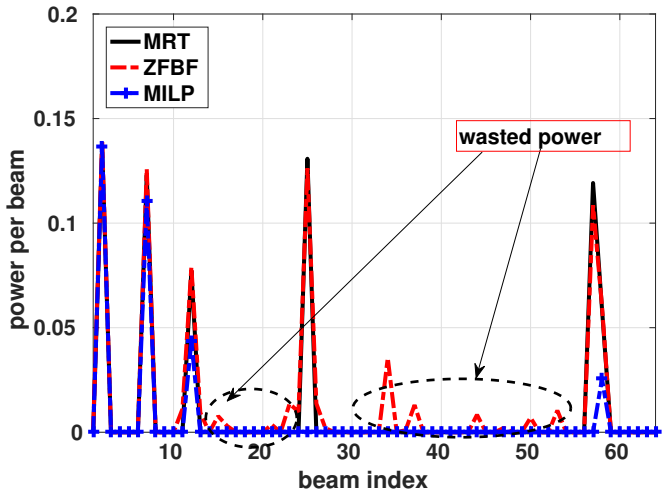

(b) UE - 2.

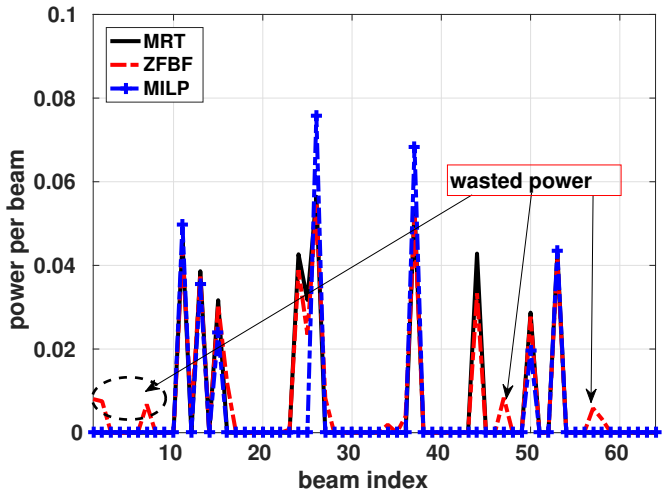

Source: Created by the author.

3.7.1 MCS with Extended Range

In the next simulations, the constraint of Table 3.1 is relaxed. In Figure 3.6 (a), we evaluate the proposed scheme by relaxing the rates and assuming more discrete values in the range $\Delta \in [0,\ 12]$ bits/symbols for each UE instead of imposing the small number of discrete rate values of Table 3.1. The analogous results considering the geometric-stochastic channel model are shown in Figure 3.6 (b).

Note that the simulation results for the MILP and LA have shown a good performance and are not limited to 22 bits per symbol. In worth mentioning that we performed the previous simulation results based on the MCS of the LTE table. In upcoming wireless communication standards with massive MIMO, higher rates are expected. Thereby, these results show a good performance of MRT with selection for LTE MCS with extended range.

Figure 3.5 – Comparative performance of MILP and ZFBF with different sparsity levels for $K = 4$ and channel models.

(a) With Table 3.1 values using i.i.d. channel model.

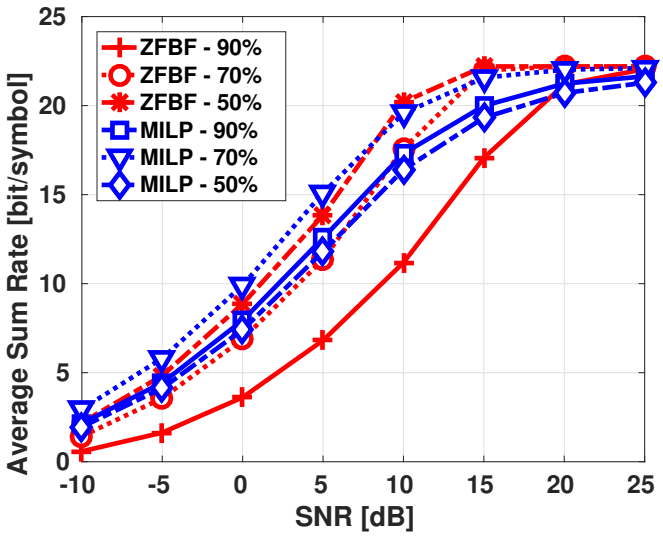

(b) With Table 3.1 values using geometric-stochastic channel model.

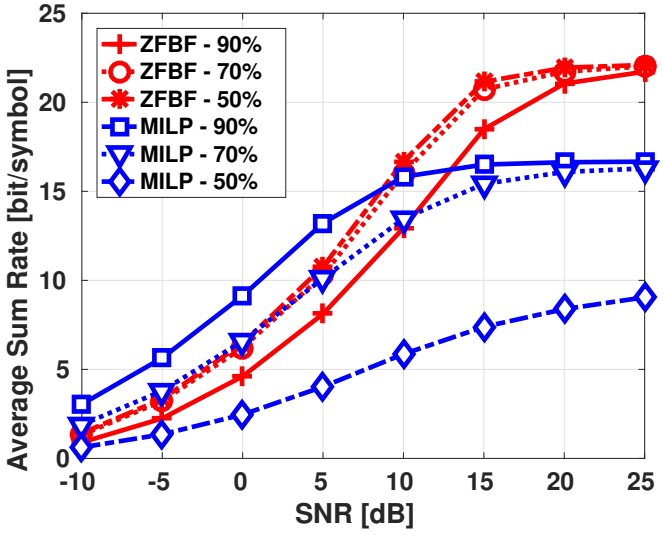

Source: Created by the author.

Figure 3.6 – Performance of optimal solution (MILP), Lagrangean relaxation, ZFBF and MRT to $K = 4$, $M_T = 64$ and $\chi = 90\%$.

(a) For an extended range of rate values using i.i.d. channel model.

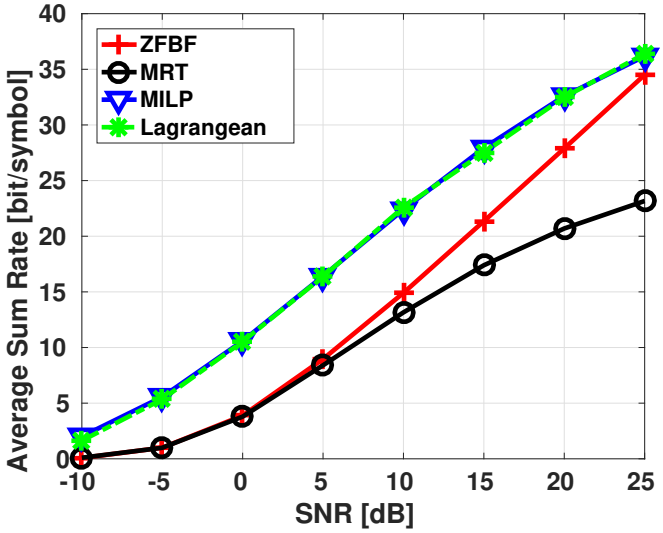

(b) For an extended range of rate values with geometric-stochastic channel model.

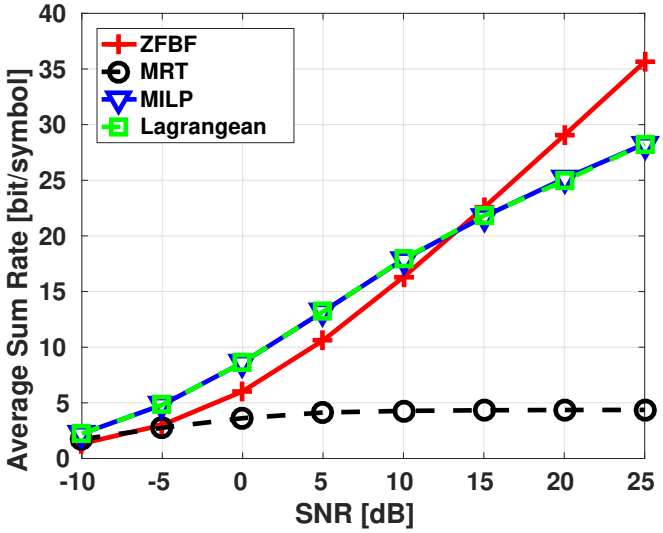

Source: Created by the author.

3.7.2 Heuristics Robustness

In order to evaluate the performance and robustness of the proposed heuristics under a practical scenario, we consider a controlled error in the CSI. The imperfect CSI is modeled as $\hat{\mathbf{G}} = \mathbf{G} + \mathbf{E}$, where $\mathbf{E} \approx \mathcal{CN}(0, \sigma_e^2)$ and $\sigma_e^2 \in \{0.1, 0.5\}$. In Figure 3.7, we present the results for the average sum rate with the channel $\chi = 90\%$ and $K = 4$. As for the MRT, the heuristics are robust to the error. All heuristics have small performance losses in both channel models.

Figure 3.7 – Performance of three proposed heuristics to $K = 4$, $M_T = 64$ with $\chi = 90\%$.
(a) Imperfect CSI using i.i.d. channel model.

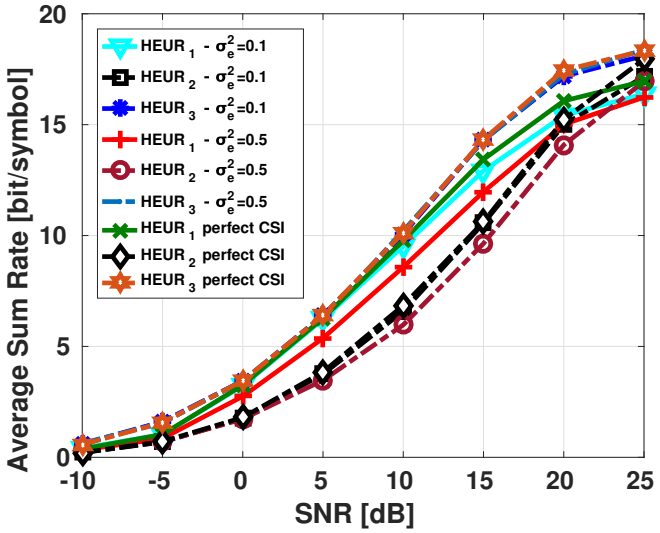

(b) Imperfect CSI with geometric-stochastic channel model.

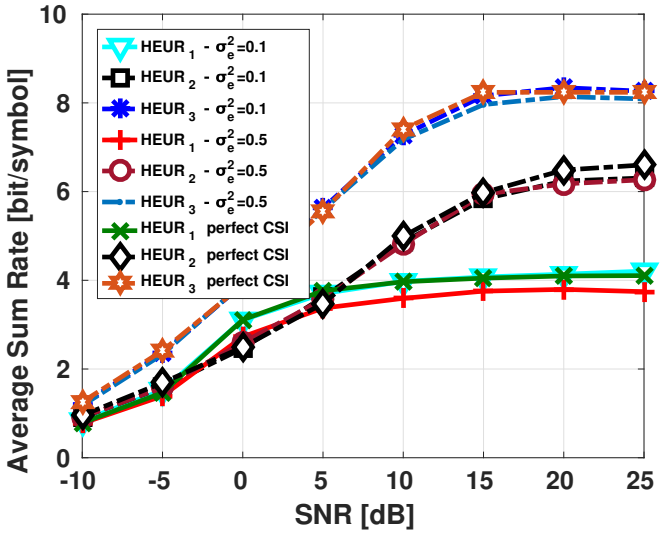

Source: Created by the author.

In general, the channel estimator can reach an estimate with precision more than 0.1. Thus, the proposed heuristics have shown a good robustness to imperfect channel knowledge.

3.7.3 Complexity Analysis

The computational complexity gives an upper bound on the computational resources required by an algorithm and is represented by the asymptotic notation $O(\cdot)$. LP problems are usually solved by *Active Set Methods*, where the Simplex Method is the standard approach, or by *Interior Point Methods* [122]. In our case, CPLEX [121] reports the use of dual version of the Simplex algorithm to solve all the LP problems presented in this work. Simplex complexity can be computed as the product of the number of Simplex iterations by the number of elementary operations at each iteration (that is exactly of $O(n_r n_c)$, where n_c is the number of variables and n_r is the number of constraints in the *Standard Form* of a LP problem). On the other hand, the number of Simplex iterations has an exponential crude bound of $O\left(n_c^{n_r}\right)$ [123], [124], but in the most of the practical cases this bound is of $O(n_r + n_c)$ [122]. When $n_r \ll n_c$ in the primal version of a LP, the number of variables and constraints in the *Standard Form* of the dual version becomes close to n_c, allowing estimating a practical upper bound on the Simplex Complexity of $O\left(n_c^3\right)$. That is the case of our LP problems since $K \ll M_T$, and then, $n_r \ll n_c$. For the case of a MILP problem, like the problem (3.28), the CPLEX solver uses the branch-and-bound (BnB) algorithm. For an arbitrary number of discrete variables n_d, the number of LP subproblems of $O\left(n_c^3\right)$ to be solved is at least $(\sqrt{2})^{n_d}$ [118], yielding to a total complexity estimation of id=ram]$O\left((\sqrt{2})^{K|\Delta|} \cdot (K|\Delta| + KM_T)^3\right)$ where $|\Delta|$ is the cardinality of a set Δ, for the problem (3.28) . In the Lagrangean approach, the solution is reached solving l iterations for the two LP Lagrangean relaxed subproblems (3.32) and (3.33). The first one can be solved by K binary searches of complexity $O(log_2(|\Delta|))$, meanwhile the second one is solved by a the Dual Simplex with a complexity of $O\left(n_c^3\right) = O\left(K^3 M_T^3\right)$ as indicate before. Assuming that $K \ll M_T$ in the massive MIMO case, the complexity of MILP, Lagrangean, precoders and heuristics can be expressed as in Table 3.2.

Table 3.2 – Complexity evaluation.

Solution	**Complexity**
ψ_{MILP}	$O\left((\sqrt{2})^{K\|\Delta\|} \cdot (K\|\Delta\| + KM_T)^3\right)$
ψ_{LA}	$O\left(l \cdot (K \log_2(\|\Delta\|) + K^3 M_T^3)\right)$
ψ_{MRT}	$O(KM_T)$
ψ_{ZFBF}	$O\left(K^2 M_T^2\right)$
ψ_{HEUR_1}	$O(KM_T) + O\left(K^2 M_T\right)$
ψ_{HEUR_2}	$O\left(\min\left(K^3, M_T^3\right)\right)$
ψ_{HEUR_3}	$O\left(\min\left(K^3, M_T^3\right)\right) + O(KM_T)$

Source: Created by the author.

In the MILP formulation, $(\sqrt{2})^{K|\Delta|}$ LP subproblems are solved with polynomial complexity on $|\Delta|$, K and M_T, while in the Lagrangean approach, l less complex LP subproblems are solved with sub-linear complexity on $|\Delta|$ and polynomial on K and M_T. Moreover, this number of l problems does not depend on the size problem (K and $|\Delta|$) as the MILP case, but the method accuracy ϵ, that is, the absolute optimality gap, since the Lagrangean approach is a

subgradient method whose worst-case complexity is $O\left(1/\epsilon^2\right)$ iterations [125]. Then, fixing an arbitrary ϵ, we can bound the Lagrangean complexity, in contrast to the MILP formulation.

The complexity of heuristic 1 (ψ_{HEUR_1}) is basically the MRT with the addition of the beam selection complexity $O\left(K^2 M_T\right)$. The complexity of heuristic 2 (ψ_{HEUR_2}) is low because the algorithm finds one beam per UE. Heuristic 3 combines the complexity of heuristic 2 (ψ_{HEUR_2}) and the complexity of beams searching for additional beams. Therefore, heuristics 1 and 3 are more complex than MRT due to the additional complexity in selecting extra beams. However, they are less complex than ψ_{ZFBF}. The heuristic 2 is less complex compared to MRT, however it is only suitable for high SNR and sparsity levels.

Comparing the optimal solution given by MILP or Lagrangean relaxation, the performance of proposed heuristics have low performance. However, this loss in performance is explained by significant reduction of complexity.

3.8 Summary

In this chapter, we have formulated a precoder design using two different sparse beam channel models. We have shown the best solution for MRT with selection and proposed three simple heuristics to select the beams in a massive-BS MU scenario. The proposed heuristics have a good performance under high sparsity levels compared to the MRT precoder, and we show that beam selection improves the system performance with low-complexity.

Furthermore, we have given the optimal solution to select the beams, assign the data rates and the transmit powers to MUs for a practical system using the LTE table. We have proposed a less complex heuristic using Lagrangean relaxation and have shown that the proposed approach achieves the optimal solution.

4 MINIMIZATION OF PILOT CONTAMINATION EFFECT WITH SPACE-TIME PILOT TRANSMISSION SCHEME

In this chapter, we propose a novel pilot decontamination technique based on space-time pattern pilot transmission to mitigate the destructive effect of pilot contamination.

4.1 Motivation

The rapid increase in number of UEs demands higher cell densification and higher data rates. However, densification of the cells can produce severe interference among BSs. A promising technology to deal with this tendency is the massive MIMO technology.

A well known problem of massive MIMO is the interference created by the pilot contamination. The pilot contamination appears when all transmissions are synchronous and neighboring cells share both frequency and pilot signals (also known as a reference signal). The pilot contamination effect emerges with the dearth of orthogonality between the desired and interfering pilot sequences that affect the accuracy of channel estimation, which decreases the system spectral efficiency [49]. When the same pilot sequence is reused in different BSs, the interfering signals affect the channel estimation. Thereby, the performance of channel estimation is limited by the interfering signals from other BSs. Also, the pilot contamination occurs when two UEs are transmitting the same pilot sequence in the uplink to the BS.

Conventional MIMO systems, where the number of UEs is low, can afford to have much more pilot sequences than active terminals, which makes the risk of pilot "collision" rather small. Meanwhile, massive MIMO is supposed to have 10 times more active UEs at the same time/frequency resource than conventional systems. Thus, if it has 10× more UEs, the pilot contamination might be 10× more severe [10].

4.2 Main Contributions

In this chapter, we propose a pilot transmission method to reduce the negative impact of pilot contamination in high density massive MIMO systems. In particular, we propose a space-time pilot transmission technique based on ST-RPS that uses Bernoulli distribution, where the channel estimation is done using MMSE estimator. Despite the conceptual simplicity of the proposed scheme, simulation results show that it improves the channel estimation accuracy.

4.2.1 Organization

This chapter is organized as follows. In Section 4.3, some techniques to mitigate the pilot contamination are presented. Section 4.4 presents the system model. Section 4.5 formulates the proposed ST-RPS scheme. In Section 4.6, simulation results are shown. Finally, Section 4.7 brings some conclusions, remarks, and future works.

4.3 Background

Recent works have proposed different schemes to minimize the interference generated by the pilot contamination. The authors in [126] proposed a precoding scheme assuming that each BS linearly combines messages aimed to terminals of different cells that reuse the same pilot sequence. In [127], the authors proposed a pilot reuse scheme based on pilot sequence hopping, where each UE chooses a new pilot sequence in each transmission slot. By contrast, the proposed method in [114] relies on multi-cell joint-processing. Also, the authors of [19] proposed a method based on coordinated pilot allocation between cells during the channel estimation procedure by exploiting second order channel statistics. In [10], the authors made an interesting analysis under different pilot reuse, where it is shown that the pilot sequences should be allocated to a finite number of transmit antennas. In [128], the authors proposed a channel estimation algorithm that exploits the path diversity in both angle and power domains. However, the proposed schemes above require cells coordination and are impractical in high density networks. Nevertheless, there are works based on blind channel estimation, see [129], which avoid the use of pilot sequences and cells coordination. However, long estimation periods are necessary to achieve good estimation.

4.4 System Model

We consider a system with L cells, where each cell has a centralized BS. This BS is composed of a single massive MIMO BS with M_T transmit antennas and one UE with a single antenna in the edge of cell. The number of multiple RF chains is assumed to be less than M_T. Furthermore, we assume that the communication channel is unknown at the UE, and the BSs are not using any coordination. The received signal at the UE can be written as follows (see Figure 4.1):

$$\mathbf{y} = \sqrt{\frac{\rho_d}{M_T}}\mathbf{S}_1\mathbf{h}_1 + \sum_{\ell=2}^{L}\sqrt{\frac{\rho_i}{M_T}}\mathbf{S}_\ell\mathbf{h}_\ell + \mathbf{n} \tag{4.1}$$

where $\mathbf{y} \in C^{\tau\times 1}$ vector, τ is the length of pilot sequence, $\mathbf{h}_1 \in C^{M_T\times 1}$ is the channel between the BS_1 and UE, and $\mathbf{h}_\ell$, $\ell = 2, \cdots, L$, are the channels of interfering cells. $\mathbf{n}$ represents the noise vector, which is complex Gaussian with zero mean and variance σ_n^2, $\mathbf{S} \in C^{\tau\times M_T}$ is an orthogonal training sequence ($\mathbf{S}^H\mathbf{S} = \mathbf{I}$), ρ_d and ρ_i are the transmit powers for desired and interference cells, respectively. All channels are assumed to be quasi-static, subject to frequency-flat fading, and the BSs are equipped with a ULA. The channel model is described as:

$$\mathbf{h}_\ell = \frac{1}{\sqrt{P}}\sum_{i=1}^{P}\mathbf{a}(\vartheta_{\ell i})\alpha_{\ell i}, \tag{4.2}$$

Figure 4.1 – System with L cells and a single UE.

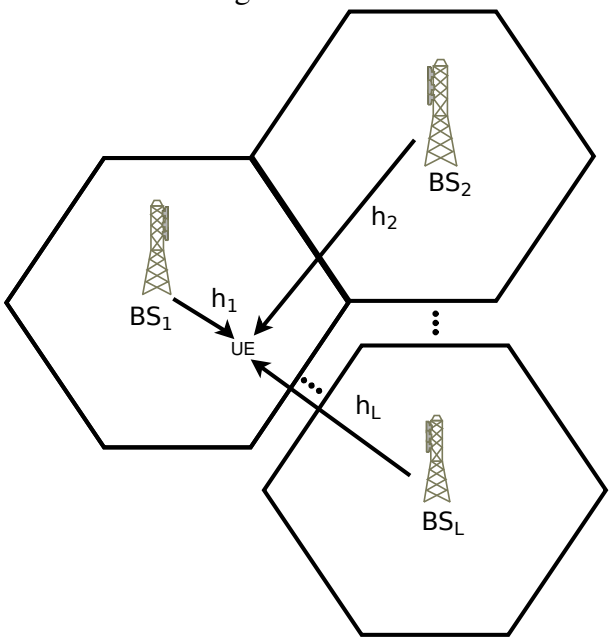

Source: Created by the author.

where P represents the number of i.i.d. multipaths, $\alpha_{\ell i} \sim \mathcal{CN}(0, \sigma_\ell^2)$ is independent over channel index ℓ and path index i. The steering vector $\mathbf{a}(\vartheta_{\ell i})$ is given by:

$$\mathbf{a}(\vartheta_{\ell i}) \triangleq \left[1 \; e^{-j2\pi \frac{ds}{\xi} cos(\vartheta_{\ell i})} \ldots e^{-j2\pi \frac{(M_T-1)ds}{\xi} cos(\vartheta_{\ell i})}\right]^T, \tag{4.3}$$

where ds is the antenna spacing at the BS, ξ is the signal wavelength and $\vartheta_{\ell i} \in [-\pi/2, \pi/2]$ is a random AoD.

4.5 Proposed Solution: ST-RPS

The channel estimation performance is limited by the interfering signals from other BSs due to the dearth of orthogonality between the desired and interfering pilot sequences. When the same pilot sequence is reused in all BSs, the interfering signals affect the desired channel estimation (c.f., $\sum_{\ell=2}^{L} \mathbf{S}_\ell \mathbf{h}_\ell$ in Equation (4.1)).

In this context, we propose to minimize the effect of interference on channel estimation by the ST-RPS scheme. For that, the transmission of pilot sequences has to be slightly modified. We define a factor, i.e., a percentage $1 - p_r$, $p_r \in [0;\ 1]$, that represents the number of symbols that are transmitted during the training period τ. For instance, $p_r = 0$ means that all sequences are transmitted, and $p_r = 1$ means that no sequence is transmitted. To further clarify the idea, the proposal is illustrated in the block diagram in Figure 4.2 (a). Furthermore, we assume that the statistical covariance of the channel, pattern selection, and pilot sequence are known at the UE and we assume equal power allocation per transmitted symbol. The transmitted signals (symbols) during the training period are represented in Figure 4.2 (b) and written as

follows:

$$\mathbf{S} = [\mathbf{s}_1^T \dots \mathbf{s}_\tau^T]^T, \tag{4.4}$$

$$\mathbf{X}_\ell = \mathbf{\Phi}_\ell \odot \mathbf{S}, \tag{4.5}$$

where $\mathbf{s}_i$ is the $\in 1 \times M_T$ is the pilot sequence vector associated with the i-th symbol period, $i = 1, \cdots, \tau$ and $\mathbf{\Phi}_\ell \in A^{\tau \times M_T}$ belongs to the Bernoulli distribution, being $A = \{0, 1\}$, and $\mathbf{\Phi}(A)$ has the probability density function (p.d.f.) $\mathcal{P}(0) = p_r$ and $\mathcal{P}(1) = 1 - p_r$.

Figure 4.2 – Example of transmission frame structure of a communication system.
(a) Block diagram of the system model.

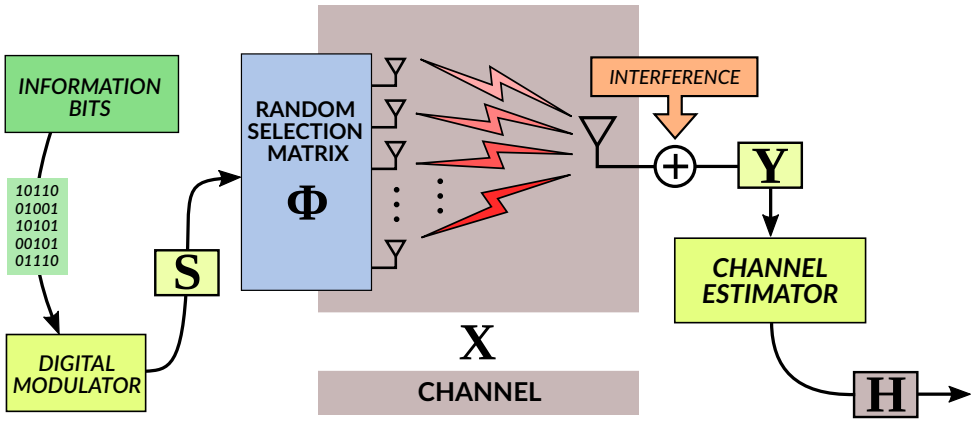

(b) Example of transmission.

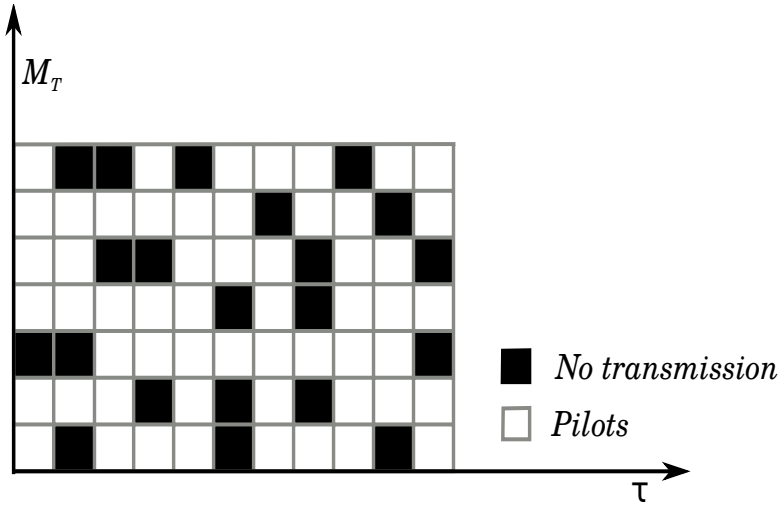

Source: Created by the author.

Note that the matrix $\mathbf{\Phi}_\ell$ models the random space-time pattern to transmit the pilot symbols at the BS. The scheme ensures that a fixed percentage of symbols are selected for each BS. Note that, for a given time slot, there is a probability that no pilot symbol is transmitted on any antenna (this would mean a "black column" in Figure 4.2 (b)). However, this probability depends on the fixed percentage of antennas and training period, i.e., ${p_r}^\tau$. For massive MIMO, where the M_T is usually large, this probability is small and asymptotically equal to zero.

The received signal can be expressed as:

$$\mathbf{y} = \sqrt{\frac{\rho_d}{M_T(1-p_r)}}\mathbf{X}_1\mathbf{h}_1 + \sum_{\ell=2}^{L}\sqrt{\frac{\rho_i}{M_T(1-p_r)}}\mathbf{X}_\ell\mathbf{h}_\ell + \mathbf{n}] \tag{4.6}$$

where $\mathbf{y} \in C^{\tau\times 1}$, $\mathbf{X}_1 = \mathbf{\Phi}_1 \odot \mathbf{S}$ and $\mathbf{X}_\ell = \mathbf{\Phi}_\ell \odot \mathbf{S}$ are the modified training sequences. The factor $\frac{1}{(1-p_r)}$ in Equation (4.6) is the weighting to ensure proper normalization of the emitted power.

We evaluated this proposal based on the MMSE channel estimator as in [79]. The estimator is based on the following cost function:

$$\mathbb{J}(\mathbf{W}_e) = \min_{\mathbf{W}_e} \mathbb{E}\{\|\mathbf{h}_1 - \mathbf{W}_e\mathbf{y}\|_2^2\}, \tag{4.7}$$

where the $\mathbf{W}_e$ matrix contains the weights of the MMSE estimator, and the expectation ($\mathbb{E}$) is taken over the channel realizations. Rewriting the cost function given in Equation (4.7):

$$\begin{aligned}\mathbb{J} &= \mathbb{E}\{(\mathbf{h}_1 - \mathbf{W}_e\mathbf{y})(\mathbf{h}_1 - \mathbf{W}_e\mathbf{y})^H\}\\ \mathbb{J} &= \mathbb{E}\left\{\mathbf{h}_1\mathbf{h}_1^H\right\} - \mathbb{E}\left\{\mathbf{h}_1\mathbf{y}^H\mathbf{W}_e^H\right\} - \mathbb{E}\left\{\mathbf{W}_e\mathbf{y}\mathbf{h}_1^H\right\} + \mathbb{E}\left\{\mathbf{W}_e\mathbf{y}\mathbf{y}^H\mathbf{W}_e^H\right\}.\end{aligned} \tag{4.8}$$

Deriving with respect to $\mathbf{W}_e$ and equaling to zero [130]:

$$\begin{aligned}\frac{\partial\mathbb{J}}{\partial\mathbf{W}_e} &= -\mathbb{E}\{\mathbf{h}_1\mathbf{y}^H\} + \mathbf{W}_e\mathbb{E}\{\mathbf{y}\mathbf{y}^H\},\\ \mathbf{W}_e &= \mathbb{E}\{\mathbf{h}_1\mathbf{y}^H\}\mathbf{R}_{yy}^{-1},\end{aligned} \tag{4.9}$$

where $\mathbf{R}_{yy} = \sum_{\ell=1}^{L}\mathbf{X}_\ell\mathbf{R}_\ell\mathbf{X}_\ell^H + \sigma_n\mathbf{I}$, and $\mathbb{E}\{\mathbf{y}\mathbf{h}_1^H\} = \mathbf{R}_1\mathbf{X}_1^H$, the estimated channel is $\hat{\mathbf{h}}_1 = \mathbf{W}_e\mathbf{y}$.

Considering a full transmission (p_r=0, where $\mathbf{X}_\ell = \mathbf{X}_1 = \mathbf{S}$, $\mathbf{X}_\ell^H\mathbf{X}_\ell = \mathbf{S}^H\mathbf{S} = \mathbf{I}$, $\forall\ell$), the MMSE estimator is written as follows:

$$\mathbf{W}_e = \mathbf{R}_1\mathbf{S}^H\left(\sum_{\ell=1}^{L}\mathbf{S}\mathbf{R}_\ell\mathbf{S}^H + \sigma_n\mathbf{I}\right)^{-1} \tag{4.10a}$$

$$= \mathbf{R}_1\left(\sigma_n\mathbf{I} + \mathbf{S}^H\mathbf{S}\textstyle\sum_{\ell=1}^{L}\mathbf{R}_\ell\right)^{-1}\mathbf{S}^H \tag{4.10b}$$

$$= \mathbf{R}_1\left(\sigma_n\mathbf{I} + \textstyle\sum_{\ell=1}^{L}\mathbf{R}_\ell\right)^{-1}\mathbf{S}^H \tag{4.10c}$$

where $\mathbf{R}_\ell = \frac{\sigma_\ell^2}{\sqrt{P}}\sum_i^P\mathbb{E}\{\mathbf{a}(\theta_{\ell i})\mathbf{a}(\theta_{\ell i})^H\} = \sigma_\ell^2\mathbb{E}\{\mathbf{a}(\theta_\ell)\mathbf{a}(\theta_\ell)^H\}$ is the covariance matrix. Equation (4.10a) and Equation (4.10c) are equivalent, thanks to the matrix inversion identity:

$$(\mathbf{I} + \mathbf{A}\mathbf{B})^{-1}\mathbf{A} = \mathbf{A}(\mathbf{B}\mathbf{A} + \mathbf{I})^{-1}. \tag{4.11}$$

The covariance can be decomposed into the following expression:

$$\mathbf{R}_\ell = \mathbf{U}_\ell\mathbf{\Lambda}_\ell\mathbf{U}_\ell^H \tag{4.12}$$

where $\mathbf{U}_\ell \in C^{M_T\times P}$ is the signal eigenvector matrix and $\mathbf{\Lambda}_\ell \in \mathcal{R}^{P\times P}$ is an eigenvalue matrix with $P < M_T$. Then, the ST-RPS decreases the pilot contamination effect by considering valid the assumption as follows:

Lemma 1 (Orthogonality condition based on covariance matrices by [19])

$$\mathbf{U}_{\ell}^{H}\mathbf{U}_1 \approx \mathbf{0}, \forall i \neq 1, M_T \rightarrow \infty. \tag{4.13}$$

It indicates that the interference will fall in the null space of covariance matrix when the number of antennas goes to infinity.

Rewriting the MMSE solution of Equation (4.10c) and using Equation (4.12), the estimated channel can be written as:

$$\begin{aligned} \hat{\mathbf{h}}_1 &= \mathbf{W}_e\mathbf{y} \\ \hat{\mathbf{h}}_1 &= \mathbf{R}_1 \left(\textstyle\sum_{\ell=1}^{L} \mathbf{R}_\ell + \sigma_n\mathbf{I}\right)^{-1} \mathbf{S}^H\mathbf{y}. \end{aligned} \tag{4.14}$$

In the asymptotic regime the covariance can be eigen-decomposed as:

$$\textstyle\sum_{\ell=2}^{L} \mathbf{R}_\ell = \mathbf{V}\mathbf{\Lambda}\mathbf{V}^H \tag{4.15}$$

where $\mathbf{V}$ is the eigenvector matrix such as $\mathbf{V}^H\mathbf{V} = \mathbf{I}$ and span $\{\mathbf{V}\}$ is included in the orthogonal complement of span $\{\mathbf{U}_1\}$. Then,

$$\hat{\mathbf{h}}_1 \approx \left(\mathbf{U}_1\mathbf{\Lambda}_1\mathbf{U}_1^H(\mathbf{V}\mathbf{\Lambda}\mathbf{V}^H + \mathbf{U}_1\mathbf{\Lambda}_1\mathbf{U}_1^H + \sigma_n\mathbf{I})^{-1}\mathbf{S}^H\right)\mathbf{y}. \tag{4.16}$$

Following [19], the asymptotic orthogonality between $\mathbf{U}_1$ and $\mathbf{V}$, the *Lemma* 1, and considering $\frac{|\mathbf{U}_1^H\mathbf{h}_\ell|}{|\mathbf{U}_1^H\mathbf{h}_1|} \rightarrow 0,\ \forall \ell \neq 1$, when $M_T \rightarrow \infty$, the estimated channel is:

$$\begin{aligned} \hat{\mathbf{h}}_1 &\approx \mathbf{U}_1\mathbf{\Lambda}_1 (\sigma_n\mathbf{I} + \mathbf{\Lambda}_1)^{-1} \mathbf{U}_1^H \left(\sum_{\ell=1}^{L} \mathbf{S}^H\mathbf{S}\mathbf{h}_\ell + \mathbf{S}^H\mathbf{n}\right) \\ \hat{\mathbf{h}}_1 &\approx \mathbf{U}_1\mathbf{\Lambda}_1 (\sigma_n\mathbf{I} + \mathbf{\Lambda}_1)^{-1} \left(\mathbf{U}_1^H\mathbf{S}^H\mathbf{S}\mathbf{h}_1 + \mathbf{U}_1^H \textstyle\sum_{\ell=2}^{L} \mathbf{h}_\ell + \mathbf{S}^H\mathbf{n}\right) \\ \hat{\mathbf{h}}_1 &\approx \mathbf{U}_1\mathbf{\Lambda}_1 (\sigma_n\mathbf{I} + \mathbf{\Lambda}_1)^{-1} \left(\mathbf{U}_1^H\mathbf{h}_1 + \mathbf{U}_1^H \textstyle\sum_{\ell=2}^{L} \mathbf{h}_\ell + \mathbf{S}^H\mathbf{n}\right) \\ \hat{\mathbf{h}}_1 &\approx \mathbf{U}_1\mathbf{\Lambda}_1 (\sigma_n\mathbf{I} + \mathbf{\Lambda}_1)^{-1} \left(\mathbf{U}_1^H\mathbf{h}_1 + \mathbf{S}^H\mathbf{n}\right). \end{aligned} \tag{4.17}$$

This result is identical to channel estimation with interference-free [19].

4.5.1 Interference Reduction with ST-RPS

Consider a scenario without coordination among the BSs. Then, $\mathbf{U}_1$ is orthogonal to $\mathbf{h}_\ell$ for $M_T \rightarrow \infty$, i.e. non-overlapping between desired and interference[1].

Consider that the ST-RPSs scheme is applied at the BSs, i.e., $\mathbf{X}_\ell \neq \mathbf{X}_1, \forall \ell > 1$, where each $\mathbf{\Phi}_\ell$ belongs to independent Bernoulli distributions, $\mathcal{P}(\mathbf{\Phi}_1, \mathbf{\Phi}_\ell) = \mathcal{P}(\mathbf{\Phi}_1)\mathcal{P}(\mathbf{\Phi}_\ell)$, we have the following definition:

[1] The authors in [19] proposed a protocol for coordination of BSs in an effort to try to satisfy the non-overlapping AoA constraint.

Definition 1 (No collision) *Assuming that there exists a random space-time pattern such as*

$$\mathbf{\Phi}_\ell \mathbf{\Phi}_i^H = \begin{cases} \mathbf{0}, & \ell \neq i, \\ \mathbf{J}, & \ell = i, \end{cases}$$

the pilot contamination vanishes.

Notice that in this case without pilot sequence collision, first, the pattern requires coordination among BSs, where one BS needs to inform the used seed for generating the pattern. Second, since the factor reduces the number of pilot sequences, the performance of the channel estimation is decreased. For example, when the BSs have the same antennas number and training period, the number of pilot sequences will be halved to avoid the collision.

Consider that $P < M_T$ and BSs without coordination. Following the same procedure to find Equation (4.17), the pilot contamination (measurement of the interference) can be written as:

$$\begin{aligned} \text{Mpc} &= \left\| \mathbf{W}_e \sum_{\ell=2}^{L} \mathbf{X}_\ell \mathbf{h}_\ell \right\|_2^2, \\ &= \left\| \mathbf{R}_1 \mathbf{X}_1^H \left(\sum_{\ell=2}^{L} \mathbf{X}_\ell \mathbf{R}_\ell \mathbf{X}_\ell^H + \mathbf{X}_1 \mathbf{R}_1 \mathbf{X}_1^H + \sigma_n \mathbf{I} \right)^{-1} \sum_{l=2}^{L} \mathbf{X}_\ell \mathbf{h}_\ell \right\|_2^2, \\ &= \left\| \mathbf{R}_1 \left(\sigma_n \mathbf{I} + \mathbf{D}\mathbf{R}_1 \right)^{-1} \mathbf{X}_1^H \sum_{l=2}^{L} \mathbf{X}_\ell \mathbf{h}_\ell \right\|_2^2, \\ &= \left\| \mathbf{U}_1 \mathbf{\Lambda}_1 \mathbf{U}_1^H \left(\sigma_n \mathbf{I} + \mathbf{D}\mathbf{U}_1 \mathbf{\Lambda}_1 \mathbf{U}_1^H \right)^{-1} \mathbf{X}_1^H \sum_{l=2}^{L} \mathbf{X}_\ell \mathbf{h}_\ell \right\|_2^2, \\ &= \left\| \mathbf{U}_1 \mathbf{\Lambda}_1 \left(\mathbf{U}_1^H \mathbf{D} \mathbf{U}_1 \mathbf{\Lambda}_1 + \sigma_n \mathbf{I} \right)^{-1} \mathbf{U}_1^H \mathbf{D}_1 \sum_{\ell=2}^{L} \mathbf{h}_\ell \right\|_2^2, \end{aligned} \tag{4.18}$$

where $\mathbf{D} = \mathbf{X}_1^H (\sum_{\ell=2}^{L} \mathbf{X}_\ell \mathbf{R}_\ell \mathbf{X}_\ell^H + \mathbf{X}_1), \ \forall \ell$, and $\mathbf{D}_1 = \mathbf{X}_1^H \sum_{\ell=2}^{L} \mathbf{X}_\ell$.

Thus, we establish the following conjecture:

Conjecture 1 *Let* $\mathbf{X}_1 = \mathbf{\Phi}_1 \odot \mathbf{S}$ *and* $\mathbf{X}_\ell = \mathbf{\Phi}_\ell \odot \mathbf{S}$ *the matrices that replace* $\mathbf{S}$ *with probability* $p_r \neq 0$ *at the BSs, and a degenerated* $\mathbf{R}_l \in l = 1, \ldots, L$*, which* $\mathbf{D}_{1\ell}$ *has the function to orthogonalise such as the large number of antennas in Lemma 1, hence the pilot contamination is mitigated with a limited number of antennas, i.e., Mpc* $\rightarrow 0$ *due to:*

$$\frac{|\mathbf{U}_1^H \mathbf{D}_1 \mathbf{h}_\ell|}{|\mathbf{U}_1^H \mathbf{h}_1|} \rightarrow 0, \ \forall l > 1. \tag{4.19}$$

Knowing that the nullity is complement of the rank, when the matrix is degenerate the null space will be large [40]. Thereby, the interference signal spans the null space of $\mathbf{R}_1$ with much less antennas using the ST-RPS scheme, as we can see in Figure 4.4.

The interference elimination effect was shown before in [19, 128] for the BS equipped with ULA. Thereby, $\mathbf{U}_1$ becomes orthogonal for $\mathbf{U}_\ell$ as was proven in [19] for *Lemma 1*. The MMSE estimator can fully eliminate the pilot contamination when $M_T \to \infty$ under specific "non-overlap" conditions on the distributions of multipaths AoAs. However, using ST-RPS the interference will vanish with much less antennas. Thus, the "orthogonalization" effect with $M_T \to \infty$ appears in the same way when ST-RPS is applied for a finite number of antennas.

The knowledge of the pattern selection is an additional information for the MMSE estimator at the UE, more specifically the seed for each BS to generate of sequences. Without this information, the proposed scheme can not achieve good performance. Notice that the MMSE estimator knows all covariance matrices since the UE is on the border of the cell, it can harvest and store these matrices along time. The achieved improvements depend on the covariance matrix. This rank has to be small to enable ST-RPS to work well. Thus, this proposed scheme is appropriate for scenarios which have only a few multipaths, i.e., $P \ll M_T$ as in the massive MIMO case [12].

4.6 Simulation Results

In this section, we provide some preliminary simulation results to confirm the ST-RPS has good performance in terms of minimizing the pilot contamination effect. The performance is shown considering the MMSE estimators with the pilot sequence length $\tau = M_T$. We consider the number of multipaths equals $P = 20$ following [120]. We consider two ULAs (L=2) with the distance between the antennas spacing equal to $\xi/2$ and $\rho_i = 1$. In all simulations, we use 3000 channel realizations. The NMSE is defined as $\|\mathbf{h}_1 - \hat{\mathbf{h}}_1\|_2^2 / \|\mathbf{h}_1\|_2^2$.

We present the NMSE assuming low noise levels $\sigma_n^2 \in \{0.01,\ 0.001\}$, $M_T = 64$, and $p_r = 0.1$ in Figure 4.3. The curve interference-free is considered a lower bound of the performance. As we expected, the ST-RPS improves the performance under a scenario with noise. The estimated channel is improved while decreasing the pilot contamination effect as we will show in the next simulation results. Note that for $p_r = 0$ the improvement is low when the noise is decreased.

Figure 4.4 shows the reduction of pilot contamination effect following Equation (4.18), normalized by ρ_d, versus signal-to-interference ratio (SIR) for $M_T \in \{32, 64\}$. Moreover, $p_r = 0$ means that we sent all sequence pilots (full) or without selection, $p_r = \{0.1, 0.2\}$ means that 10%, 20% of the matrix with probability contain entries with zeros, respectively.

Figure 4.5 shows the performance of the proposed scheme with MMSE estimator, for $p_r = \{0,\ 0.25\}$. Note that, when there are more antennas and $p_r = 0$, the effect of *Lemma 1* and Equation (4.17) is confirmed with the reduction of the NMSE. However, notice that for the ST-RPS with $p_r = 0.25$, i.e., 25% of $\mathbf{\Phi}_1$ and $\mathbf{\Phi}_2$, the reduction in the NMSE is larger than $p_r = 0$. At $M_T = 32$, a slight performance improvement is obtained. At $M_T = 64$, the estimated channel is almost-perfect. For $M_T = 96, 128, 256$ the performance improvement continues. Thus, the results corroborate with a *Conjecture* 1.

Figure 4.3 – Comparison assuming low noise variance σ_n^2.

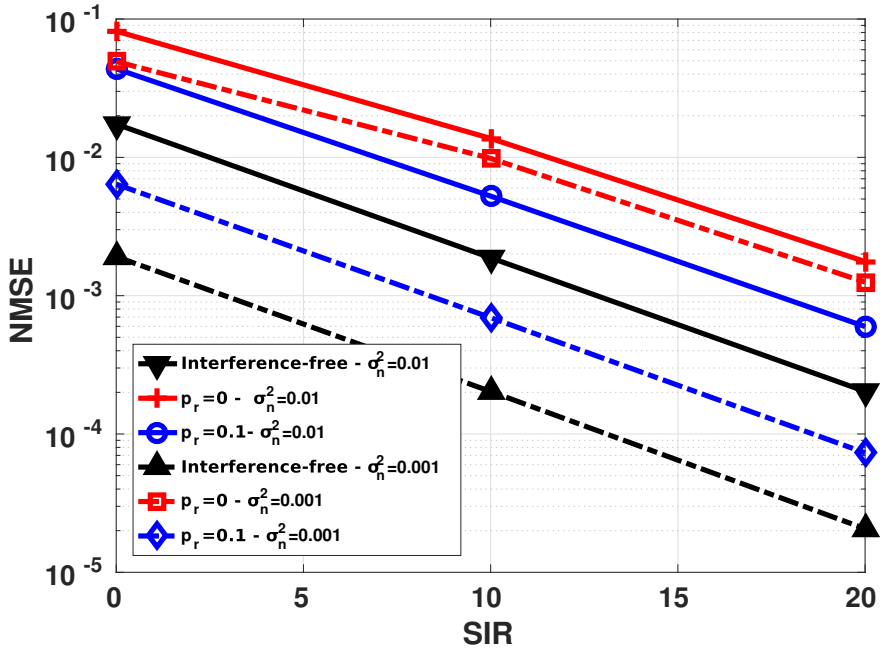

Source: Created by the author.

Figure 4.4 – Performance results for $M_T \in \{32, 64\}$.

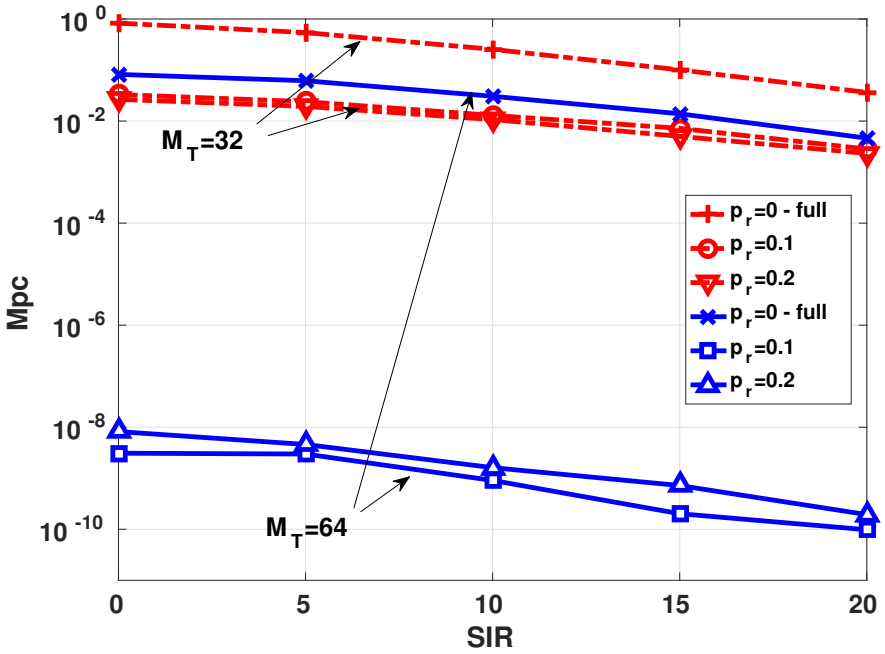

Source: Created by the author.

Figure 4.5 – Performance with different number M_T.

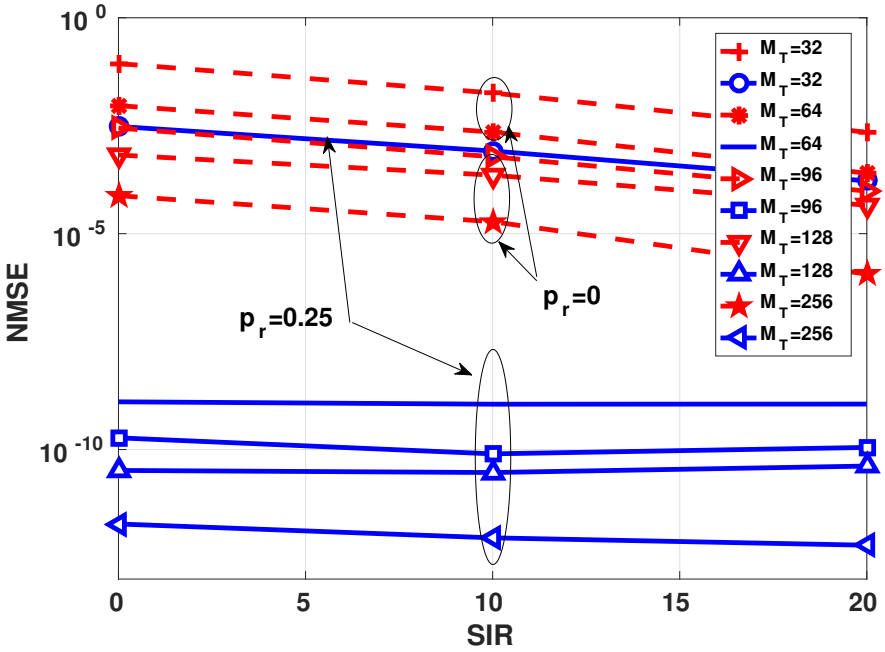

Source: Created by the author.

The *Conjecture* 1 is also supported by the results in Figure 4.6, where we evaluate the NMSE versus the number of antennas with ST-RPS performance ($M_T \in [32, 256]$). Note that $M_T = 40$ is enough to have almost-perfect channel estimation. Otherwise, to achieve the same performance $p_r = 0$ needs more than $M_T = 256$.

Figure 4.6 – Pilot contamination effect for different M_T.

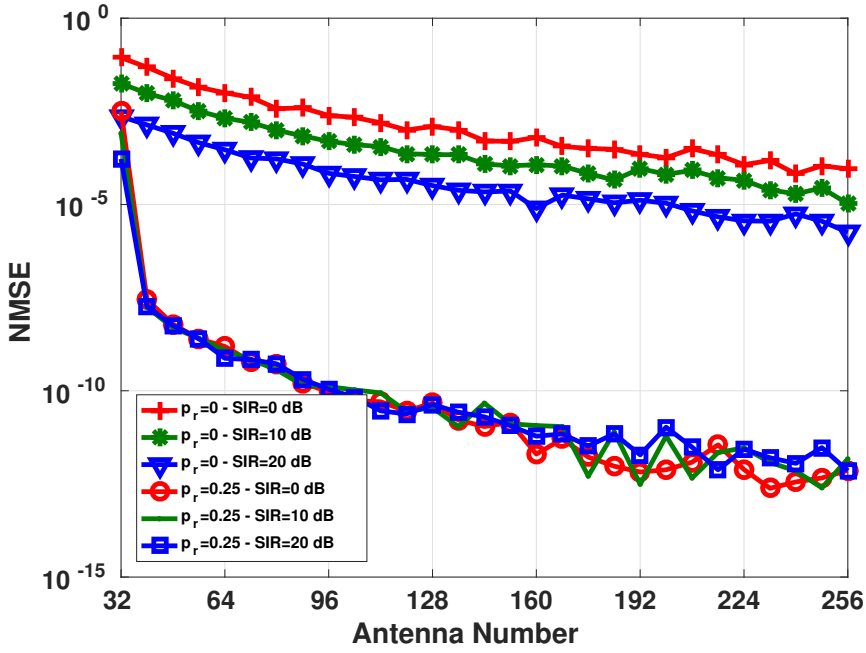

Source: Created by the author.

4.7 Conclusions and Future Works

In this chapter, we have proposed a new training sequence scheme based on ST-RPS method, which avoids coordination between cells. Using computer simulations, it is shown that the interference by pilot contamination between two cells is mitigated and vanished when the number of antennas is increased. The main finding with the ST-RPS is that we can improve the channel estimation, and achieve pilot decontamination with a reduced number of antennas, e.g., 40 for our simulation scenario. For future works, we are planning to investigate the proposed scheme: 1) with more than two cells, 2) uplink case, 3) validate the results mathematically.

5 CONCLUSION

In this thesis, we provided solutions for three problems at the 5G system. The original contributions of this work encompasses three proposed schemes:

- the quantized feedback capitalized by MC technique;
- the beam selection precoder under a beam domain channel representation;
- the ST-RPS to mitigate the pilot contamination.

Also, different scenarios were evaluated, single and multi-cell, millimeter wave, micro-cell backhaul, and a clustered MU one.

The first part of Chapter 2 brought a review into MC technique. It gave the necessary understanding and concepts to apply the MC for the feedback channel problem in FDD. Then, we exploited the low-rank structure in the channel matrix and proposed the general framework which uses completion technique. The proposed framework was evaluated in two application scenarios: wireless backhauling communications and MU. The results showed an accurate CSI estimation with minimal feedback overhead. Thereby, a high energy efficiency and low complexity at the Rx came out. These benefits are possible thanks to the low-rank structure of the channel matrix, which happens in a massive MIMO scenario characterized by finite scattering propagation. Furthermore, a important key points was raised for the extension to the tensor completion.

In Chapter 3, we exploited the MU massive MIMO channel to design precoder. From the CSI at the BS, our formulation exploits the geometric sparsity of the channel considering a practical rate assignment based on the MCS of the LTE table, beam selection, and power optimization. We used the MRT principle combined with beam selection to reduce the complexity of precoder design. An optimal solution to capacity following the MRT principle was shown, and heuristics based on Lagrangean relaxation and greedy assignment were developed. Simulation results showed that our optimal solution could achieve a better performance than the ZFBF scheme. Besides, compared to the linear MRT precoder, the proposed low-complexity heuristics improved the performance under a scenario with channel sparsity.

Note that the reconstructed CSI by the MC framework can be directly used for any precoder design based on full-CSI. Also, the reconstructed CSI can be decomposed in the sparse channel representation at the BS in order to design any precoder used in Chapter 3.

Finally, we proposed a scheme named ST-RPS to minimize the pilot contamination problem in the multi-cell scenario in Chapter 4. The scheme was based on the space-time pattern pilot transmission. The simplicity came from the Bernoulli distribution to decide transmission without coordination among cells. Some simulation results have shown that the ST-RPS scheme leads to a good channel estimation accuracy due the reduced pilot contamination.

5.1 Perspectives

This work has several perspectives, which are discussed as follows:

- In the proposed CSI feedback and reconstruction framework, an extension of the ECU mode is possible by using statistical CSI feedback. In this case, the Rx can estimate and feed the channel covariance matrix back to the BS, which, by its turn, can recover the covariance matrix by using structured MC.

- The extension of the matrix completion framework to tensor completion would be an interesting topic when considering frequency-selective channels for instance. Using MIMO-orthogonal frequency division multiplexing (OFDM), a low-rank channel tensor should be sampled and reconstructed, where the third-dimension is represented by the frequency (subcarriers) dimension. Tensor completion is a generalization of matrix completion of higher order arrays [46]. The motivation for a tensor modeling in signal processing is associated with simultaneous benefits from multiple forms of diversity (space, time, frequency, and/or code) to perform MU signal separation/equalization and channel estimation under model uniqueness conditions and requirements more relaxed than the matrix-based approaches [131, 132]. For example, using the ECU mode, a given undersampled channel tensor can be recovered only with a subset of entries.

- It would worth comparing MC and CS techniques to solve the channel estimation problem. Both MC and CS exploit the sparse structure of the channel in different ways. While MC assumes low-rank property of the channel matrix, CS does not need such an assumption. On the other hand, CS techniques require the knowledge of the sparsifying basis to represent the (sparse) channel, which is not needed with MC techniques. A future work could compare both approaches in the context of this thesis.

- Another interesting point is to compare the latency of the proposed the DDU feedback mode, which assumes an FDD system, with that of a TDD system, to provide instantaneous CSI to the BS.

- Regarding the beam selection and rate adaptation approach, the investigation of other heuristics which are more adapted to low-SNRs values is a topic for future work. To this end, the starting point consists of selecting the beams by taking into account predefined LMUI values.

- In the proposed ST-RPS scheme, we intend to evaluate its performance in a scenario with more than two cells with several UEs. In particular, when considering several UEs, the proposed ST-RPS scheme should instead be applied at the UE side and

the channel estimation is done at the BS. In this case, orthogonality among pilot sequences of in-cell UEs may not hold and co-channel will affect channel estimation at the BS. Hence, a performance evaluation in this scenario is an interesting topic.

- Finally, the development of a mathematical proof of the conjecture presented in Chapter 4 is essential to explain the behavior of the proposed ST-RPS scheme.

BIBLIOGRAPHY

1 METIS project. [S.l.: s.n.], 2017. Available from: <https://metis-ii.5g-ppp.eu/>.

2 DAHLMAN, E.; PARKVALL, S.; SKOLD, J. **4G, LTE-Advanced Pro and The Road to 5G, Third Edition**. 3rd. [S.l.]: Academic Press, 2016. ISBN 0128045752, 9780128045756.

3 CORPORATION, M. E. Mitsubishi Electric's New Multibeam Multiplexing 5G Technology Achieves 20Gbps Throughput. **Public Relations Division**, n. 2984, 2016. Available from: <http://www.mitsubishielectric.com/news/2016/0121.html>.

4 LARSSON, E. G. et al. Massive MIMO for Next Generation Wireless Systems. **IEEE Communications Magazine**, v. 52, n. 2, p. 186–195, Feb. 2014. ISSN 0163-6804. DOI: 10.1109/MCOM.2014.6736761.

5 MARZETTA, T. L. Noncooperative Cellular Wireless with Unlimited Numbers of Base Station Antennas. **IEEE Transactions on Wireless Communications**, v. 9, n. 11, p. 3590–3600, Nov. 2010. ISSN 1536-1276. DOI: 10.1109/TWC.2010.092810.091092.

6 LAMARE, R. C. de. Massive MIMO Systems: Signal Processing Challenges and Research Trends. **CoRR**, abs/1310.7282, 2013. arXiv: 1310.7282. Available from: <http://arxiv.org/abs/1310.7282>.

7 XIE, H. et al. A Unified Transmission Strategy for TDD/FDD Massive MIMO Systems With Spatial Basis Expansion Model. **IEEE Transactions on Vehicular Technology**, v. 66, n. 4, p. 3170–3184, Apr. 2017. ISSN 0018-9545. DOI: 10.1109/TVT.2016.2594706.

8 LOVE, D. J. et al. An Overview of Limited Feedback in Wireless Communication Systems. **IEEE Journal on Selected Areas in Communications**, v. 26, n. 8, p. 1341–1365, Oct. 2008. ISSN 0733-8716. DOI: 10.1109/JSAC.2008.081002.

9 BJÖRNSON, E.; BENGTSSON, M.; OTTERSTEN, B. E. Optimal Multiuser Transmit Beamforming: A Difficult Problem with a Simple Solution Structure [Lecture Notes]. **IEEE Signal Processing Magazine**, v. 31, n. 4, p. 142–148, 2014. DOI: 10.1109/MSP.2014.2312183. Available from: <http://dx.doi.org/10.1109/MSP.2014.2312183>.

10 BJÖRNSON, E.; LARSSON, E. G.; DEBBAH, M. Massive MIMO for Maximal Spectral Efficiency: How Many Users and Pilots Should Be Allocated? **IEEE Transaction Wireless Communications**, v. 15, n. 2, p. 1293–1308, 2016. DOI: 10.1109/TWC.2015.2488634. Available from: <http://dx.doi.org/10.1109/TWC.2015.2488634>.

11 RAPPAPORT, T. S. et al. Millimeter Wave Mobile Communications for 5G Cellular: It Will Work! **IEEE Access**, v. 1, p. 335–349, 2013. ISSN 2169-3536. DOI: 10.1109/ACCESS.2013.2260813.

12 XIE, H.; GAO, F.; JIN, S. An Overview of Low-Rank Channel Estimation for Massive MIMO Systems. **IEEE Access**, v. 4, p. 7313–7321, 2016. ISSN 2169-3536. DOI: 10.1109/ACCESS.2016.2623772.

13 ZHOU, Z. et al. Channel Estimation for Millimeter-Wave Multiuser MIMO Systems via PARAFAC Decomposition. **IEEE Transactions on Wireless Communications**, v. 15, n. 11, p. 7501–7516, Nov. 2016. ISSN 1536-1276. DOI: 10.1109/TWC.2016.2604259.

14 GAO, Z. et al. Spatially Common Sparsity Based Adaptive Channel Estimation and Feedback for FDD Massive MIMO. **IEEE Transactions on Signal Processing**, v. 63, n. 23, p. 6169–6183, Dec. 2015. ISSN 1053-587X. DOI: 10.1109/TSP.2015.2463260.

15 ADHIKARY, A. et al. Joint Spatial Division and Multiplexing - The Large-Scale Array Regime. **IEEE Transaction Information Theory**, v. 59, n. 10, p. 6441–6463, 2013. DOI: 10.1109/TIT.2013.2269476. Available from: <http://dx.doi.org/10.1109/TIT.2013.2269476>.

16 NAM, J. et al. Joint Spatial Division and Multiplexing: Opportunistic Beamforming, User Grouping and Simplified Downlink Scheduling. **IEEE Journal of Selected Topics in Signal Processing**, v. 8, n. 5, p. 876–890, Oct. 2014. ISSN 1932-4553. DOI: 10.1109/JSTSP.2014.2313808.

17 SONG, G. H.; BRADY, J.; SAYEED, A. **Beamspace MIMO Transceivers for Low-Complexity and Near-Optimal Communication at mm-Wave Frequencies**. In: 2013 IEEE International Conference on Acoustics, Speech and Signal Processing. [S.l.: s.n.], May 2013. p. 4394–4398. DOI: 10.1109/ICASSP.2013.6638490.

18 SAYEED, A.; BRADY, J. **Beamspace MIMO for High-Dimensional Multiuser Communication at Millimeter-Wave Frequencies**. In: 2013 IEEE Global Communications Conference (GLOBECOM). [S.l.: s.n.], Dec. 2013. p. 3679–3684. DOI: 10.1109/GLOCOM.2013.6831645.

19 YIN, H. et al. A Coordinated Approach to Channel Estimation in Large-Scale Multiple-Antenna Systems. **IEEE Journal on Selected Areas in Communications**, v. 31, n. 2, p. 264–273, Feb. 2013. ISSN 0733-8716. DOI: 10.1109/JSAC.2013.130214.

20 RAO, X.; LAU, V. K. N.; KONG, X. **CSIT estimation and feedback for FDD multi-user massive MIMO systems**. In: 2014 IEEE International Conference on Acoustics, Speech and Signal Processing (ICASSP). [S.l.: s.n.], May 2014. p. 3157–3161. DOI: 10.1109/ICASSP.2014.6854182.

21 CAI, W. et al. Asymptotic Capacity Analysis for Sparse Multipath Multiple-Input Multiple-Output Channels. **IEEE Communications Letters**, v. 19, n. 12, p. 2262–2265, Dec. 2015. ISSN 1089-7798. DOI: 10.1109/LCOMM.2015.2490069.

22 YU, Y. et al. A Low-Complexity Transceiver Design in Sparse Multipath Massive MIMO Channels. **IEEE Signal Processing Letters**, v. 23, n. 10, p. 1301–1305, Oct. 2016. ISSN 1070-9908. DOI: 10.1109/LSP.2016.2582199.

23 HOGAN, J.; SAYEED, A. **Beam Selection for Performance-Complexity Optimization in High-Dimensional MIMO Systems**. In: 2016 Annual Conference on Information Science and Systems (CISS). [S.l.: s.n.], Mar. 2016. p. 337–342. DOI: 10.1109/CISS.2016.7460525.

24 SAMIMI, M. K.; RAPPAPORT, T. S. **Local multipath model parameters for generating 5G millimeter-wave 3GPP-like channel impulse response**. In: PROC. 10th European Conf. Antennas and Propagation (EuCAP). [S.l.: s.n.], Apr. 2016. p. 1–5. DOI: 10.1109/EuCAP.2016.7481410.

25 SHEN, W. et al. Joint CSIT Acquisition Based on Low-Rank Matrix Completion for FDD Massive MIMO Systems. **IEEE Communications Letters**, v. 19, n. 12, p. 2178–2181, Dec. 2015. ISSN 1089-7798. DOI: 10.1109/LCOMM.2015.2492960.

26 BJÖRNSON, E.; HOYDIS, J.; SANGUINETTI, L., et al. Massive MIMO Networks: Spectral, Energy, and Hardware Efficiency. **Foundations and Trends® in Signal Processing**, Now Publishers, Inc., v. 11, n. 3-4, p. 154–655, 2017.

27 BUZZI, S.; D'ANDREA, C. Massive MIMO 5G Cellular Networks: mm-wave vs. micro-wave Frequencies., 23 Feb. 2017. arXiv: 1702.07187v1 [cs.IT].

28 VALDUGA, S. T.; ALMEIDA, A. L. F. de. **Fourth Technical Report UFC/Ericsson - Channel Estimation in Very-Large Scale MIMO**. GTEL-UFC, July 2014.

29 _____. **First Technical Report UFC/Ericsson - CSI Feedback and Reconstruction Using Matrix Completion for Massive MIMO Systems**. GTEL-UFC, Mar. 2015.

30 _____. **Second Technical Report UFC/Ericsson - Feedback Signaling and CSI Reconstruction Using Completion Techniques**. GTEL-UFC, Oct. 2015.

31 _____. **Third Technical Report UFC/Ericsson - CSI Feedback and Reconstruction Using Matrix Completion and Tensor Completion for FDD Uplink Multi User Massive MIMO**. GTEL-UFC, Feb. 2016.

32 VALDUGA, S. T. et al. Minimization of Pilot Contamination Effect with Space-Time Pilot Transmission Scheme, 2018. To be submitted.

33 VALDUGA, S. T. et al. **Low complexity beam selection for sparse massive MIMO systems**. In: PROC. Int. Symp. Wireless Communication Systems (ISWCS). Italy: [s.n.], Aug. 2017. p. 414–419. DOI: 10.1109/ISWCS.2017.8108150.

34 VALDUGA, S. T. et al. Low-Complexity Heuristics to Beam Selection and Rate Adaptation in Sparse Massive MIMO Systems. **Transactions on Emerging Telecommunications Technologies - ETT**, Feb. 2018. Submitted.

35 VALDUGA, S. T. et al. **Low-Complexity Codebook-Based Beamforming with Four Transmit Antennas and Quantized Feedback Channel**. In: 2014 IEEE Wireless Communications and Networking Conference (WCNC). [S.l.: s.n.], Apr. 2014. p. 1212–1217. DOI: 10.1109/WCNC.2014.6952322.

36 VALDUGA, S. T. et al. **Esquema MIMO Beamforming Otimizado para Canal de Retorno de Baixa Taxa de Transmissão**. In: XXXIII Simpósio Brasileiro de Telecomunicações, 2015, Juiz de Fora, Anais do XXXIII SBrT. [S.l.: s.n.], 2015. p. 1–5.

37 VALDUGA, S. T. et al. Codebook Design and Performance Analysis of Quantized Beamforming under Perfect and Imperfect Channel State Information. **Journal of Communication and Information Systems - JCIS**, v. 32, n. 1, p. 161–171, 2017. DOI: 10.14209/jcis.2017.16.

38 CANDÈS, E. J.; TAO, T. The Power of Convex Relaxation: Near-Optimal Matrix Completion. **IEEE Transactions on Information Theory**, v. 56, n. 5, p. 2053–2080, May 2010. ISSN 0018-9448. DOI: 10.1109/TIT.2010.2044061.

39 KESHAVAN, R. H.; MONTANARI, A.; OH, S. Matrix Completion from Noisy Entries. **Journal of Machine Learning Research,** v. 99, p. 2057–2078, 11 June 2009. arXiv: 0906.2027v2 [cs.LG].

40 CHERNEY, D.; DENTON, T.; WALDRON, A. **Linear Algebra**. [S.l.]: University of California Davis, 2013.

41 NETFLIX. [S.l.: s.n.], 2009. Available at http://www.netflixprize.com.

42 HUANG, L. T. et al. **Truncated nuclear norm minimization for tensor completion**. In: 2014 IEEE 8th Sensor Array and Multichannel Signal Processing Workshop (SAM). [S.l.: s.n.], June 2014. p. 417–420. DOI: 10.1109/SAM.2014.6882431.

43 KESHAVAN, R. H.; OH, S.; MONTANARI, A. **Matrix Completion from a Few Entries**. In: THE IEEE International Symposium on Information Theory, (ISIT'09). [S.l.: s.n.], June 2009. p. 324–328. DOI: 10.1109/ISIT.2009.5205567.

44 CABRAL, R. et al. Matrix Completion for Weakly-Supervised Multi-Label Image Classification. **IEEE Transactions on Pattern Analysis and Machine Intelligence**, v. 37, n. 1, p. 121–135, Jan. 2015. ISSN 0162-8828. DOI: 10.1109/TPAMI.2014.2343234.

45 FAZEL, M.; HINDI, H.; BOYD, S. P. **Log-Det Heuristic for Matrix Rank Minimization with Applications to Hankel and Euclidean Distance Matrices**. In: PROCEEDINGS of the American Control Conference. [S.l.: s.n.], 2003. v. 3, p. 2156–2162. DOI: 10.1109/acc.2003.1243393. Available from: <http://dx.doi.org/10.1109/acc.2003.1243393>.

46 HUANG, L.-.; DE ALMEIDA, A. L.; SO, H. Target Estimation in Bistatic MIMO Radar via Tensor Completion. **Signal Process.**, Elsevier North-Holland, Inc., Amsterdam, The Netherlands, The Netherlands, v. 120, n. 100, p. 654–659, Mar. 2016. ISSN 0165-1684. DOI: 10.1016/j.sigpro.2015.09.036. Available from: <https://doi.org/10.1016/j.sigpro.2015.09.036>.

47 OH, S. **Matrix completion: Fundamental limits and efficient algorithms**. 2011. PhD thesis – Stanford University.

48 LO, T. K. Y. Maximum Ratio Transmission. **IEEE Transactions on Communications**, v. 47, n. 10, p. 1458–1461, 1999. DOI: 10.1109/26.795811. Available from: <http://dx.doi.org/10.1109/26.795811>.

49 RUSEK, F. et al. Scaling Up MIMO: Opportunities and Challenges with Very Large Arrays. **IEEE Signal Processing Magazine**, v. 30, n. 1, p. 40–60, Jan. 2013. ISSN 1053-5888. DOI: 10.1109/MSP.2011.2178495.

50 JINDAL, N. MIMO Broadcast Channels With Finite-Rate Feedback. **IEEE Transactions on Information Theory**, v. 52, n. 11, p. 5045–5060, Nov. 2006. ISSN 0018-9448. DOI: 10.1109/TIT.2006.883550.

51 SANTIPACH, W.; HONIG, M. L. **Asymptotic performance of MIMO wireless channels with limited feedback**. In: IEEE Military Communications Conference, 2003. MILCOM 2003. [S.l.: s.n.], Oct. 2003. v. 1, 141–146 vol.1. DOI: 10.1109/MILCOM.2003.1290092.

52 AU-YEUNG, C. K.; LOVE, D. J. On the performance of random vector quantization limited feedback beamforming in a MISO system. **IEEE Transactions on Wireless Communications**, v. 6, n. 2, p. 458–462, Feb. 2007. ISSN 1536-1276. DOI: 10.1109/TWC.2007.05351.

53 KUO, P. H.; KUNG, H. T.; TING, P. A. **Compressive sensing based channel feedback protocols for spatially-correlated massive antenna arrays**. In: 2012 IEEE Wireless Communications and Networking Conference (WCNC). [S.l.: s.n.], Apr. 2012. p. 492–497. DOI: 10.1109/WCNC.2012.6214417.

54 SHEN, J. C. et al. High-Dimensional CSI Acquisition in Massive MIMO: Sparsity-Inspired Approaches. **Computing Research Repository CoRR**, abs/1505.00426, 2015. Available from: <http://arxiv.org/abs/1505.00426>.

55 SIM, M. S. et al. Compressed Channel Feedback for Correlated Massive MIMO Systems. **Computing Research Repository CoRR**, abs/1503.09002, 2015. Available from: <http://arxiv.org/abs/1503.09002>.

56 WANG, H.; WANG, W.; ZHANG, Z. **On the design of hybrid limited feedback for massive MIMO systems**. In: 2014 IEEE International Conference on Communications (ICC). [S.l.: s.n.], June 2014. p. 4795–4800. DOI: 10.1109/ICC.2014.6884079.

57 HU, R. et al. **Robust channel estimation for switch-based mmWave MIMO systems**. In: PROC. 9th Int. Conf. Wireless Communications and Signal Processing (WCSP). [S.l.: s.n.], Oct. 2017. p. 1–7. DOI: 10.1109/WCSP.2017.8170914.

58 LEE, B. et al. **Antenna grouping based feedback reduction for FDD-based massive MIMO systems**. In: 2014 IEEE International Conference on Communications (ICC). [S.l.: s.n.], June 2014. p. 4477–4482. DOI: 10.1109/ICC.2014.6884026.

59 WUNDER, G.; SCHRECK, J. **Feedback Information Transmission and Scheduling in a Radio Access Network**. [S.l.], May 2011.

60 SUN, S.; PETROPULU, A. P.; BAJWA, W. U. **Target estimation in colocated MIMO radar via matrix completion**. In: 2013 IEEE International Conference on Acoustics, Speech and Signal Processing. [S.l.: s.n.], May 2013. p. 4144–4148. DOI: 10.1109/ICASSP.2013.6638439.

61 MIGLIORE, M. D. et al. MIMO Channel-State Estimation in the Presence of Partial Data and/or Intermittent Measurements. **Electronics**, v. 6, n. 2, 2017. ISSN 2079-9292. DOI: 10.3390/electronics6020033. Available from: <http://www.mdpi.com/2079-9292/6/2/33>.

62 TSAI, J.-.; BUEHRER, R. M.; WOERNER, B. D. **The impact of AOA energy distribution on the spatial fading correlation of linear antenna array**. In: VEHICULAR Technology Conference. IEEE 55th Vehicular Technology Conference. VTC Spring 2002 (Cat. No.02CH37367). [S.l.: s.n.], 2002. v. 2, 933–937 vol.2. DOI: 10.1109/VTC.2002.1002625.

63 CANDÈS, E. J.; RECHT, B. **Exact low-rank Matrix Completion via Convex Optimization**. In: 46TH Annual Allerton Conference on Communication, Control, and Computing. [S.l.: s.n.], Sept. 2008. p. 806–812. DOI: 10.1109/ALLERTON.2008.4797640.

64 RECHT, B. A Simpler Approach to Matrix Completion. **J. Mach. Learn. Res.**, JMLR.org, v. 12, p. 3413–3430, Dec. 2011. ISSN 1532-4435. Available from: <http://dl.acm.org/citation.cfm?id=1953048.2185803>.

65 BOURGAIN, J.; TZAFRIRI, L. Invertibility of 'large' submatrices with applications to the geometry of Banach spaces and harmonic analysis. **Israel Journal of Mathematics**, v. 57, n. 2, p. 137–224, June 1987. ISSN 1565-8511. DOI: 10.1007/BF02772174. Available from: <https://doi.org/10.1007/BF02772174>.

66 FAZEL, M. **Matrix Rank Minimization with Applications**. 2002. PhD thesis – Stanford University.

67 CANDÈS, E. J.; PLAN, Y. Matrix Completion with Noise. **Proceedings of the IEEE**, v. 98, n. 6, p. 925–936, June 2010. ISSN 0018-9219. DOI: 10.1109/JPROC.2009.2035722.

68 RECTH, B.; FAZEL, M.; PARRILO, P. A. Guaranteed Minimum-Rank Solutions of Linear Matrix Equations via Nuclear Norm Minimization. **SIAM Review**, v. 52, n. 3, p. 471–501, 2010. DOI: 10.1137/070697835.

69 LEEUWEN, J. V. **Handbook of Theoretical Computer Science: Algorithms and Complexity**. Ed. by Warwick, A. R. Meyer and M. Nival. Cambridge, MA, USA: MIT Press, 1990. ISBN 0262220385.

70 GRANT, M.; BOYD, S. **CVX: Matlab Software for Disciplined Convex Programming, version 2.1**. [S.l.: s.n.], Mar. 2014. http://cvxr.com/cvx.

71 AYACH, O. E. et al. **The capacity optimality of beam steering in large millimeter wave MIMO systems**. In: PROC. IEEE 13th Int. Workshop Signal Processing Advances in Wireless Communications (SPAWC). [S.l.: s.n.], June 2012. p. 100–104. DOI: 10.1109/SPAWC.2012.6292865.

72 HOLMA, H.; TOSKALA, A. **LTE for UMTS - OFDMA and SC-FDMA Based Radio Access**. [S.l.]: Wiley Publishing, 2009. ISBN 0470994010, 9780470994016.

73 COLDREY, M. et al. Wireless backhaul in future heterogeneous networks. **Ericsson Review**, v. 91, p. 1–11, 2014.

74 HUR, S. et al. **Multilevel millimeter wave beamforming for wireless backhaul**. In: 2011 IEEE GLOBECOM Workshops (GC Wkshps). [S.l.: s.n.], Dec. 2011. p. 253–257. DOI: 10.1109/GLOCOMW.2011.6162448.

75 _____. Millimeter Wave Beamforming for Wireless Backhaul and Access in Small Cell Networks. **IEEE Transactions on Communications**, v. 61, n. 10, p. 4391–4403, Oct. 2013. ISSN 0090-6778. DOI: 10.1109/TCOMM.2013.090513.120848.

76 SWINDLEHURST, A. et al. Millimeter-Wave Massive MIMO: The Next Wireless Revolution? **Communications Magazine, IEEE**, v. 52, n. 9, p. 56–62, Sept. 2014. ISSN 0163-6804. DOI: 10.1109/MCOM.2014.6894453.

77 CASTAÑEDA, E. et al. An Overview on Resource Allocation Techniques for Multi-User MIMO Systems. **IEEE Communications Surveys Tutorials**, v. 19, n. 1, p. 239–284, Firstquarter 2017. ISSN 1553-877X. DOI: 10.1109/COMST.2016.2618870.

78 ADHIKARY, A. et al. Joint Spatial Division and Multiplexing for mm-Wave Channels. **IEEE Journal on Selected Areas in Communications**, v. 32, n. 6, p. 1239–1255, June 2014. ISSN 0733-8716. DOI: 10.1109/JSAC.2014.2328173.

79 HAYKIN, S. **Adaptive Filter Theory (3rd Ed.)** Upper Saddle River, NJ, USA: Prentice-Hall, Inc., 1996. ISBN 0-13-322760-X.

80 CAI, J.-. F.; CANDÈS, E. J.; SHEN, Z. A Singular Value Thresholding Algorithm for Matrix Completion. **SIAM J. on Optimization**, Society for Industrial and Applied Mathematics, Philadelphia, PA, USA, v. 20, n. 4, p. 1956–1982, Mar. 2010. ISSN 1052-6234. DOI: 10.1137/080738970. Available from: <http://dx.doi.org/10.1137/080738970>.

81 KUNZI, H. P. et al. Studies in Linear and Nonlinear Programming. v. 31, p. 611, 1963. ISSN 0012-9682. DOI: 10.2307/1910003.

82 MA, S.; GOLDFARB, D.; CHEN, L. Fixed Point and Bregman Iterative Methods for Matrix Rank Minimization. **Math. Program.**, Springer-Verlag New York, Inc., Secaucus, NJ, USA, v. 128, n. 1-2, p. 321–353, June 2011. ISSN 0025-5610. DOI: 10.1007/s10107-009-0306-5. Available from: <http://dx.doi.org/10.1007/s10107-009-0306-5>.

83 BALZANO, L.; NOWAK, R. D.; RECHT, B. Online Identification and Tracking of Subspaces from Highly Incomplete Information. **Computing Research Repository CoRR**, abs/1006.4046, 2010. Available from: <http://arxiv.org/abs/1006.4046>.

84 JAIN, P.; NETRAPALLI, P.; SANGHAVI, S. **Low-rank Matrix Completion Using Alternating Minimization**. In: PROCEEDINGS of the Forty-fifth Annual ACM Symposium on Theory of Computing. Palo Alto, California, USA: ACM, 2013. (STOC '13), p. 665–674. ISBN 978-1-4503-2029-0. DOI: 10.1145/2488608.2488693. Available from: <http://doi.acm.org/10.1145/2488608.2488693>.

85 LIN, T. T.; HERRMANN, F. J. Compressed wavefield extrapolation. **GEOPHYSICS**, v. 72, sm77–sm93, 2007. ISSN 0016-8033. DOI: 10.1190/1.2750716.

86 PARIKH, N.; BOYD, S. P. Proximal Algorithms. **Foundations and Trends in Optimization**, v. 1, n. 3, p. 127–239, 2014. DOI: 10.1561/2400000003.

87 MAJUMDAR, A.; WARD, R. K. Some Empirical Advances in Matrix Completion. **Signal Processing**, v. 91, n. 5, p. 1334–1338, 2011. ISSN 0165-1684. DOI: http://dx.doi.org/10.1016/j.sigpro.2010.12.005. Available from: <http://www.sciencedirect.com/science/article/pii/S0165168410004196>.

88 MAJUMDAR, A. **Matrix Completion via Thresholding**. Ed. by Non-convex Convex and NP hard matrix completion algorithms. [S.l.: s.n.], 2011. http://www.mathworks.com/matlabcentral/fileexchange/26395-matrix-completion-via-thresholding.

89 CARRON, I. **Welcome to The Advanced Matrix Factorization Jungle**. [S.l.: s.n.], 2014. https://sites.google.com/site/igorcarron2/matrixfactorizations. [Online; accessed 19-July-2017].

90 BARTOLOMÉ, D. **Fairness Analysis of Wireless Beamforming Schedulers**. Jan. 2005. PhD thesis – Universitat Politécnica de Catalunya. Available from: <http://hdl.handle.net/10803/6891>.

91 FREITAS, W. C. et al. **Exploiting Dimensions of the MIMO wireless channel: multidimensional link adaptation**. In: 2005 IEEE 61st Vehicular Technology Conference. [S.l.: s.n.], May 2005. v. 2, 924–928 vol. 2. DOI: 10.1109/VETECS.2005.1543441.

92 CAVALCANTE, D.; CAVALCANTE, C. C. **Channel Estimation in Link Adaptation Strategies for MIMO-OFDM Systems**. In: WORLD Wireless Research Forum. [S.l.: s.n.], 2006.

93 KOLOMVAKIS, N.; MATTHAIOU, M.; COLDREY, M. **Massive MIMO in Sparse Channels**. In: 2014 IEEE SPAWC, Toronto, ON, Canada, June 22-25, 2014. [S.l.: s.n.], 2014. p. 21–25. DOI: 10.1109/SPAWC.2014.6941309. Available from: <http://dx.doi.org/10.1109/SPAWC.2014.6941309>.

94 BARBOTIN, Y. et al. Estimation of Sparse MIMO Channels with Common Support. **IEEE Transactions on Communications**, v. 60, n. 12, p. 3705–3716, 2012. DOI: 10.1109/TCOMM.2012.091112.110439. Available from: <http://dx.doi.org/10.1109/TCOMM.2012.091112.110439>.

95 KERRET, P. de; GESBERT, D. **Sparse Precoding in Multicell MIMO Systems**. In: IEEE WCNC. [S.l.: s.n.], Apr. 2012. p. 958–962. DOI: 10.1109/WCNC.2012.6214513.

96 CORBILLON, X. et al. **Cross-Layer Scheduler for Video Streaming over MPTCP**. In: PROCEEDINGS of the 7th International Conference on Multimedia Systems, MMSys 2016, Klagenfurt, Austria, May 10-13, 2016. [S.l.: s.n.], 2016. 7:1–7:12. DOI: 10.1145/2910017.2910594. Available from: <http://doi.acm.org/10.1145/2910017.2910594>.

97 KUHN, H. W. The Hungarian Method for the Assignment Problem. In: JÜNGER, M. et al. (Eds.). **50 Years of Integer Programming 1958-2008 - From the Early Years to the State-of-the-Art**. [S.l.]: Springer, 2010. p. 29–47. DOI: 10.1007/978-3-540-68279-0_2.

98 GERSHMAN, A. B. et al. Convex Optimization-Based Beamforming. **IEEE Signal Processing Magazine**, v. 27, n. 3, p. 62–75, May 2010. ISSN 1053-5888. DOI: 10.1109/MSP.2010.936015.

99 RASHID-FARROKHI, F.; LIU, K. J. R.; TASSIULAS, L. Transmit amforming and power control for cellular wireless systems. **IEEE Journal on Selected Areas in Communications**, v. 16, n. 8, p. 1437–1450, Oct. 1998. ISSN 0733-8716. DOI: 10.1109/49.730452.

100 BENGTSSON, M.; OTTERSTEN, B. Optimal and suboptimal transmit beamforming. In: HANDBOOK of Antennas in Wireless Communications. [S.l.]: CRC Press, 2001. p. 18–1.

101 SUN, C. et al. Beam Division Multiple Access Transmission for Massive MIMO Communications. **IEEE Transactions on Communications**, v. 63, n. 6, p. 2170–2184, 2015. DOI: 10.1109/TCOMM.2015.2425882. Available from: <http://dx.doi.org/10.1109/TCOMM.2015.2425882>.

102 YU, Y. et al. A Low-Complexity Transceiver Design in Sparse Multipath Massive MIMO Channels. **IEEE Signal Processing Letters**, v. 23, n. 10, p. 1301–1305, Oct. 2016. ISSN 1070-9908. DOI: 10.1109/LSP.2016.2582199.

103 LI, L.; ASHIKHMIN, A. E.; MARZETTA, T. L. Interference Reduction in Multi-Cell Massive MIMO Systems II: Downlink Analysis for a Finite Number of Antennas. **CoRR**, abs/1411.4183, 2014. Available from: <http://arxiv.org/abs/1411.4183>.

104 CHENG, Y.; PESAVENTO, M. Joint Discrete Rate Adaptation and Downlink Beamforming Using Mixed Integer Conic Programming. **IEEE Transaction Signal Processing**, v. 63, n. 7, p. 1750–1764, 2015. DOI: 10.1109/TSP.2015.2393837. Available from: <http://dx.doi.org/10.1109/TSP.2015.2393837>.

105 WEICHSELBERGER, W. et al. A Stochastic MIMO Channel Model with Joint Correlation of Both Link Ends. **IEEE Transactions Wireless Communications**, IEEE Press, Piscataway, NJ, USA, v. 5, n. 1, p. 90–100, Nov. 2006. ISSN 1536-1276. DOI: 10.1109/TWC.2006.1576533. Available from: <http://dx.doi.org/10.1109/TWC.2006.1576533>.

106 BAJWA, W.; SAYEED, A.; NOWAK, R. **Sparse Multipath Channels: Modeling and Estimation**. In: DIGITAL Signal Processing Workshop and 5th IEEE Signal Processing Education Workshop, 2009. DSP/SPE 2009. [S.l.: s.n.], Jan. 2009. p. 320–325. DOI: 10.1109/DSP.2009.4785942.

107 CHENG, Y. **Joint Downlink Beamforming and Discrete Resource Allocation Using Mixed-Integer Programming**. Jan. 2014. PhD thesis – Technische Universitält, Darmstadt. Available from: <http://tuprints.ulb.tu-darmstadt.de/3741/>.

108 BAJWA, W. U. et al. Compressed Channel Sensing: A New Approach to Estimating Sparse Multipath Channels. **Proceedings of the IEEE**, v. 98, n. 6, p. 1058–1076, June 2010. ISSN 0018-9219. DOI: 10.1109/JPROC.2010.2042415.

109 BRADY, J.; SAYEED, A. **Beamspace MU-MIMO for high-density gigabit small cell access at millimeter-wave frequencies**. In: 2014 IEEE 15th International Workshop on Signal Processing Advances in Wireless Communications (SPAWC). [S.l.: s.n.], June 2014. p. 80–84. DOI: 10.1109/SPAWC.2014.6941321.

110 KOLOMVAKIS, N.; MATTHAIOU, M.; COLDREY, M. **Massive MIMO in sparse channels**. In: 2014 IEEE 15th International Workshop on Signal Processing Advances in Wireless Communications (SPAWC). [S.l.: s.n.], June 2014. p. 21–25. DOI: 10.1109/SPAWC.2014.6941309.

111 BJÖRNSON, E.; JORSWIECK, E. A. Optimal Resource Allocation in Coordinated Multi-Cell Systems. **Foundations and Trends in Communications and Information Theory**, v. 9, n. 2-3, p. 113–381, 2013. DOI: 10.1561/0100000069. Available from: <http://dx.doi.org/10.1561/0100000069>.

112 LIU, Y.; DAI, Y.; LUO, Z. Coordinated Beamforming for MISO Interference Channel: Complexity Analysis and Efficient Algorithms. **IEEE Transaction on Signal Processing**, Institute of Electrical and Electronics Engineers Inc., v. 59, n. 3, p. 1142–1157, Mar. 2011. ISSN 1053-587X. DOI: 10.1109/TSP.2010.2092772.

113 YANG, H.; MARZETTA, T. L. Performance of Conjugate and Zero-Forcing Beamforming in Large-Scale Antenna Systems. **IEEE Journal on Selected Areas in Communications**, v. 31, n. 2, p. 172–179, Feb. 2013. ISSN 0733-8716. DOI: 10.1109/JSAC.2013.130206.

114 ASHIKHMIN, A. E.; MARZETTA, T. L.; LI, L. Interference Reduction in Multi-Cell Massive MIMO Systems I: Large-Scale Fading Precoding and Decoding. **CoRR**, abs/1411.4182, 2014. Available from: <http://arxiv.org/abs/1411.4182>.

115 RUSEK, F. et al. Scaling Up MIMO: Opportunities and Challenges with Very Large Arrays. **IEEE Signal Processing Magazine**, v. 30, n. 1, p. 40–60, Jan. 2013. ISSN 1053-5888. DOI: 10.1109/MSP.2011.2178495.

116 WAI, H. T.; LI, Q.; MA, W. K. **A convex Approximation Method for Multiuser MISO Sum Rate Maximization under Discrete Rate Constraints**. In: 2013 IEEE International Conference on Acoustics, Speech and Signal Processing. [S.l.: s.n.], May 2013. p. 4759–4763. DOI: 10.1109/ICASSP.2013.6638564.

117 PANG, J. et al. Design of Cognitive Radio Systems under Temperature-Interference Constraints: A Variational Inequality Approach. **IEEE Transactions on Signal Processing**, Institute of Electrical and Electronics Engineers Inc., v. 58, n. 6, p. 3251–3271, June 2010. ISSN 1053-587X. DOI: 10.1109/TSP.2010.2043138.

118 SIERKSMA, G. **Linear and Integer Programming: Theory and Practice;** 2nd. London: CRC Press, 2001. (Advances in applied mathematics). Available from: <http://cds.cern.ch/record/2136135>.

119 PALOMAR, D. P.; CHIANG, M. A Tutorial on Decomposition Methods for Network Utility Maximization. **IEEE Journal on Selected Areas in Communications**, v. 24, n. 8, p. 1439–1451, Aug. 2006. ISSN 0733-8716. DOI: 10.1109/JSAC.2006.879350.

120 MEREDITH, J. M.; KRAUSE, J. **Technical report (TR): Study on channel model for frequencies from 0.5 to 100 GHz**. 3GPP, Mar. 2017.

121 IBM ILOG CPLEX Optimize. [S.l.: s.n.], Last 2017. http://www-01.ibm.com/software/integration/optimization/cplex-optimizer/.

122 GONDZIO, J. Interior Point Methods 25 Years Later. **European Journal of Operational Research**, v. 218, n. 3, p. 587–601, 2012. DOI: 10.1016/j.ejor.2011.09.017.

123 MEGIDDO, N. Linear Programming in Linear Time When the Dimension Is Fixed. **J. ACM**, v. 31, n. 1, p. 114–127, 1984. DOI: 10.1145/2422.322418.

124 RINNOOYKAN, A.; TELGEN, J. The Complexity of Linear Programming. **Statistica Neerlandica**, Wiley Online Library, v. 35, n. 2, p. 91–107, 1981.

125 SHOR, N. Z.; KIWIEL, K. C.; RUSZCAYÜSKI, A. **Minimization Methods for Non-differentiable Functions**. New York, NY, USA: Springer-Verlag New York, Inc., 1985. ISBN 0-387-12763-1.

126 ASHIKHMIN, A. E.; MARZETTA, T. L. **Pilot contamination precoding in multi-cell large scale antenna systems.** In: ISIT. [S.l.]: IEEE, 2012. p. 1137–1141. ISBN 978-1-4673-2580-6. Available from: <http://dblp.uni-trier.de/db/conf/isit/isit2012.html#AshikhminM12>.

127 SØRENSEN, J. H.; CARVALHO, E. de. **Pilot decontamination through pilot sequence hopping in massive MIMO systems**. In: PROC. IEEE Global Communications Conf. [S.l.: s.n.], Dec. 2014. p. 3285–3290. DOI: 10.1109/GLOCOM.2014.7037313.

128 YIN, H. et al. Robust Pilot Decontamination Based on Joint Angle and Power Domain Discrimination. **IEEE Transactions on Signal Processing**, v. 64, n. 11, p. 2990–3003, June 2016. ISSN 1053-587X. DOI: 10.1109/TSP.2016.2535204.

129 MÜLLER, R. R.; COTTATELLUCCI, L.; VEHKAPERÄ, M. Blind Pilot Decontamination. **IEEE Journal of Selected Topics in Signal Processing**, v. 8, n. 5, p. 773–786, Oct. 2014. ISSN 1932-4553. DOI: 10.1109/JSTSP.2014.2310053.

130 BRANDT, K.; SYSKING, M. The matrix cookbook. **Tech. Univ. Denmark, Lyngby, Denmark**, 2008.

131 ALMEIDA, A. L. F. d.; FAVIER, G.; MOTA, J. C. M. PARAFAC-based unified tensor modeling for wireless communication systems with application to blind multiuser equalization. **Signal Processing**, v. 87, n. 2, p. 337–351, 2007. Tensor Signal Processing. ISSN 0165-1684. Available from: <http://www.sciencedirect.com/science/article/pii/S0165168406001757>.

132 ALMEIDA, A. L. F. d. **Tensor modeling and signal processing for wireless communication systems**. Nov. 2007. Thesis – Université de Nice Sophia Antipolis. Available from: <https://tel.archives-ouvertes.fr/tel-00460157>.